

WL-TR-97-1191

CONTINUOUS WAVE SINGLY RESONANT  
INTRACAVITY OPTICAL PARAMETRIC OSCILLATORS  
USING PERIODICALLY POLED LiNbO<sub>3</sub>



LEONEL P. GONZALEZ

UNIVERSITY OF DAYTON  
CENTER FOR ELECTRO-OPTICS  
300 COLLEGE PARK  
DAYTON OH 45469-0245

OCTOBER 1997

FINAL REPORT FOR 05/01/96-08/31/97

APPROVED FOR PUBLIC RELEASE; DISTRIBUTION IS UNLIMITED

19980805 017

AVIONICS DIRECTORATE  
WRIGHT LABORATORY  
AIR FORCE MATERIAL COMMAND  
WRIGHT PATTERSON AFB OH 45433-7623

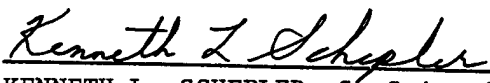
DTIC QUALITY INSPECTED 1

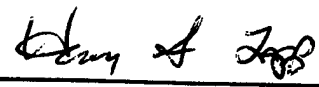
## NOTICE


USING GOVERNMENT DRAWINGS, SPECIFICATIONS, OR OTHER DATA INCLUDED IN THIS DOCUMENT FOR ANY PURPOSE OTHER THAN GOVERNMENT PROCUREMENT DOES NOT IN ANY WAY OBLIGATE THE US GOVERNMENT. THE FACT THAT THE GOVERNMENT FORMULATED OR SUPPLIED THE DRAWINGS, SPECIFICATIONS, OR OTHER DATA DOES NOT LICENSE THE HOLDER OR ANY OTHER PERSON OR CORPORATION; OR CONVEY ANY RIGHTS OR PERMISSION TO MANUFACTURE, USE, OR SELL ANY PATENTED INVENTION THAT MAY RELATE TO THEM.

THIS REPORT IS RELEASABLE TO THE NATIONAL TECHNICAL INFORMATION SERVICE (NTIS). AT NTIS, IT WILL BE AVAILABLE TO THE GENERAL PUBLIC, INCLUDING FOREIGN NATIONS.

THIS TECHNICAL REPORT HAS BEEN REVIEWED AND IS APPROVED FOR PUBLICATION.

  
KENNETH L. SCHEPLER, Sr Scientist  
EO Targeting Branch  
EO Sensor Technology Div

  
HENRY S. LAPP, Chief  
EO Targeting Branch  
EO Sensor Technology Div

  
RICHARD D. HUNZIKER, Chief  
EO Sensor Technology Division  
Sensors Directorate

IF YOUR ADDRESS HAS CHANGED, IF YOU WISH TO BE REMOVED FROM OUR MAILING LIST, OR IF THE ADDRESSEE IS NO LONGER EMPLOYED BY YOUR ORGANIZATION PLEASE NOTIFY AFRL/SNJT WRIGHT-PATTERSON AFB OH 45433 -7405 TO HELP MAINTAIN A CURRENT MAILING LIST.

Do not return copies of this report unless contractual obligations or notice on a specific document requires its return.

REPORT DOCUMENTATION PAGE			Form Approved OMB No. 0704-0188	
Public reporting burden for this collection of information is estimated to average 1 hour per response, including the time for reviewing instructions, searching existing data sources, gathering and maintaining the data needed, and completing and reviewing the collection of information. Send comments regarding this burden estimate or any other aspect of this collection of information, including suggestions for reducing this burden, to Washington Headquarters Services, Directorate for Information Operations and Reports, 1215 Jefferson Davis Highway, Suite 1204, Arlington, VA 22202-4302, and to the Office of Management and Budget, Paperwork Reduction Project (0704-0188), Washington, DC 20503.				
1. AGENCY USE ONLY (Leave blank)		2. REPORT DATE 7 Oct 1997		3. REPORT TYPE AND DATES COVERED Final, 1 May 96 - 31 Aug 97
4. TITLE AND SUBTITLE Continuous Wave Singly Resonant Intracavity Optical Parametric Oscillators Using Periodically Poled LiNbO3			5. FUNDING NUMBERS PE61102F PR - 2300 TA - AA WU - 17	
6. AUTHOR(S) Leonel P. Gonzalez				
7. PERFORMING ORGANIZATION NAME(S) AND ADDRESS(ES) University of Dayton Center for Electro-Optics 300 College Park Dayton OH 45469-0245			8. PERFORMING ORGANIZATION REPORT NUMBER	
9. SPONSORING/MONITORING AGENCY NAME(S) AND ADDRESS(ES) Wright Laboratory 2700 D Street, Suite 2 Wright-Patterson AFB OH 45433-7405			10. SPONSORING/MONITORING AGENCY REPORT NUMBER  WL-TR-97-1191	
11. SUPPLEMENTARY NOTES				
12a. DISTRIBUTION AVAILABILITY STATEMENT Approved for public release; distribution is unlimited.			12b. DISTRIBUTION CODE	
13. ABSTRACT (Maximum 200 words) The use of continuous wave singly resonant optical parametric oscillators (CW SROs) has been limited in the past mainly because of the high threshold powers necessary. Thresholds of SROs are orders of magnitude greater than doubly resonant oscillators. While lithium niobate has long been in use as a nonlinear material, periodically poled lithium niobate (PPLN) recently emerged as an excellent source for CW SROs. Quasi-phase matching with PPLN has allowed access to the higher nonlinear coefficients of lithium niobate permitting construction of CW SROs. By placing the OPO within the laser resonator, threshold should be significantly reduced. We have designed, built, and investigated an optical parametric oscillator within a laser cavity to access the high circulating fields within the resonator. The intracavity OPO acted as the output coupler for the laser and ideally the total down converted power from the OPO should approach the maximum output power available from the pump laser under optimal output coupling. PPLN OPOs were built within the resonators of a lamp-pumped Nd:YAG laser and a diode-pumped Nd:YVO4 laser. Combined idler output at 3.3 microns from both ends of an intracavity 50-mm PPLN OPO was 1.15 W. Output of the Nd:YVO4 laser optimized for 1.064-micron output with the same resonator was 5 W. The entire device, except for power supply and cooler, fit on a 1' x 2' breadboard.				
14. SUBJECT TERMS nonlinear optics, periodically poled lithium niobate, intracavity optical parametric oscillator, lasers, infrared			15. NUMBER OF PAGES 120	
			16. PRICE CODE	
17. SECURITY CLASSIFICATION OF REPORT UNCLASSIFIED	18. SECURITY CLASSIFICATION OF THIS PAGE UNCLASSIFIED	19. SECURITY CLASSIFICATION OF ABSTRACT UNCLASSIFIED	20. LIMITATION OF ABSTRACT SAR	

# TABLE OF CONTENTS

TABLE OF CONTENTS .....	iii
LIST OF FIGURES .....	v
LIST OF TABLES .....	vii
ACKNOWLEDGMENTS .....	viii
INTRODUCTION .....	1
<b>1: Theory of Optical Parametric Oscillators .....</b>	<b>4</b>
Optical Parametric Oscillators Using Periodically Poled LiNbO <sub>3</sub> .....	4
Self Consistency Analysis of Double Pump Pass OPO .....	9
Manley Rowe Relations and Clamping of the Pump Beam .....	12
Temperature Tuning .....	13
Conclusions .....	15
<b>2: Double Pump Passing OPO Experiment .....</b>	<b>16</b>
Experimental Layout: Pump Laser and optics .....	16
Mode Matching Between Pump Beam and OPO Cavity .....	20
Results .....	23
Conclusions .....	29
<b>3: Intracavity OPO Experiment with Nd:YAG Laser .....</b>	<b>32</b>
Thermal Lensing of Nd:YAG Rod .....	32
Early Intracavity Attempts .....	35
Modified Intracavity Layout .....	37
Results .....	41
Remarks .....	46
Conclusions .....	47

<b>4: Intracavity OPO Experiment with Nd:YVO<sub>4</sub> Laser</b>	<b>49</b>
Nd:YVO <sub>4</sub> Laser	49
Results	52
Signal Investigation	66
Pump Clamping	71
Optimum Output Power from the Laser	74
Intracavity OPO Experiment with 50 mm PPLN	78
Conclusion	83
<b>5: Conclusion and Future Research</b>	<b>84</b>
<b>APPENDIX A: Design, set-up and alignment of an intracavity OPO</b>	<b>89</b>
A.1 Design	89
A.2 Cavity set-up	92
A.3 Alignment	94
<b>APPENDIX B: Transmission Curves of Dual High Reflecting OPO Mirror</b>	<b>99</b>
<b>APPENDIX C: Intracavity OPO Layouts</b>	<b>101</b>
<b>REFERENCES</b>	<b>106</b>

## LIST OF FIGURES

1. Round Trip Through SRO Cavity .....	10
2. Theoretical Temperature Tuning Curves of PPLN .....	14
3. Nd:YAG Laser Layout .....	17
4. External Cavity, Double Pass OPO Experimental Layout .....	18
5. Signal and Idler Powers vs. Pump Power .....	25
6. Temperature Tuning Curve of Double Pass OPO .....	28
7. Stability of Double Pass OPO .....	29
8. Thermal Lensing of Nd:YAG vs. Current .....	34
9. Initial Layout of Intracavity OPO .....	35
10. General Intracavity Layout with Beamsplitter and Double HR Mirror .....	38
11. Linear Intracavity Setup (Cavity I) .....	39
12. OPO with Beamsplitter and IC (Cavity III) .....	40
13. Signal and Idler vs. Current (Cavity II) .....	41
14. Pump Power with OPO On and Off (Cavity II) .....	43
15. Best Signal and Idler from the Nd:YAG Setup (Cavity III) .....	45
16. Thermal Lensing of Nd:YVO <sub>4</sub> .....	51
17. Idler and Signal vs. Diode Current .....	52
18. Intracavity Pump Power with OPO On/Off .....	55
19. Idler Stability .....	58
20. Intracavity Temperature Tuning Curve .....	59
21. Signal and Idler Powers #1 .....	61
22. Intracavity Pump Power .....	62
23. Signal and Idler Power #2 .....	64
24. Intracavity Signal Power vs. Current .....	67
25. Optimum and Displaced Overlap Between Pump (Dashed) and Signal (Solid) Beams .....	72

26. Transverse and Angular Overlap Misalignment Between Pump (Dashed) and Signal (Solid) Beams .....	73
27. Loss Due to Attenuators vs. Angle .....	75
28. Typical Power Out vs. Intracavity Attenuator Angle .....	77
29. Optimum Output Power and Total Down Converted Power vs. Current .....	79
30. Idler Power from 50 mm PPLN .....	80
31. Signal Powers from 50 mm PPLN .....	81
32. Intracavity Pump Power and Depletion .....	82
B.1 Broadband Transmission Spectra of Double HR OPO End Mirrors .....	100
B.2 Expanded Plot of HR Region .....	98
Cavity I: Linear Intracavity OPO Cavity (Nd:YAG) .....	101
Cavity II: Intracavity (Nd:YAG) with Beamsplitter and IC .....	102
Cavity III: Intracavity (Nd:YAG) with Beamsplitter and IC (modified Cavity II) .....	103
Cavity IV: Intracavity (Nd:YVO <sub>4</sub> ) with Beamsplitter .....	104
Cavity V: Intracavity (Nd:YVO <sub>4</sub> ) with Beamsplitter and 50 mm PPLN .....	105

## LIST OF TABLES

1. HWP and Polarizer Specifications .....	19
2. Input Coupler Specifications .....	21
3. Double HR OC Specifications .....	23
4. Material properties of Nd:YAG and Nd:YVO <sub>4</sub> .....	50
5. % Transmission of beamsplitter at 1.064 and 1.57 $\mu\text{m}$ for incidence angles of 55, 57 and 60 deg .....	66
6. Signal, idler and pump beam profiles at 28.0 amps (clamped) .....	69
7. Signal, idler and pump beam profiles at 24.0 amps (unclamped) .....	70
8. Results of intracavity loss fit .....	77

## ACKNOWLEDGMENTS

This work would not have been possible without the help and support of numerous people. Vince Dominic has been my advisor for this thesis and has always kept me pointed in the right direction whether I realized it or not and always suggested options I had never considered. Larry Myers was around early on for a large part of this work and to him I am greatly indebted for his enthusiasm and counseling when things appeared as if they'd never work. It's been a pleasure bouncing ideas off of Bob Eckardt; he is one of the most organized people I've ever met. I'd like to thank Leno Pedrotti for being on my committee and teaching me about lasers in general. I am indebted to Ken Schepler and the people at AAJL and AAJT for providing the funding, support and resources for this work. Without them this project would not have been possible. I'd like to thank Ph.D. student Mark Missey for not only sharing an office with me for the last year but for many enlightening conversations and a steady supply of PPLN samples at the end. I'd like to thank Andy Zakel and Chris Brewer; we began our graduate work together and have been house mates for the last year. I thank them for the times we've spent together and wish them luck on their paths to Ph.D.'s. Finally, I'd like to thank my family for supporting me in everything I have done, regardless of where I've been or where I'm going, *gracias para todo*.

This work was funded through AFOSR, DARPA and Wright Laboratory

## INTRODUCTION

Although lasers have been in use for over 30 years, they do not cover the entire electro-magnetic spectrum, especially in the near to mid infrared. Since the development of the first laser, nonlinear optics has evolved as a method to fill in the wavelength gaps not accessible by ordinary lasers. One particular nonlinear device, the optical parametric oscillator (OPO), has become a standard method of converting a stock laser wavelength (i.e., 1.06  $\mu\text{m}$  for Nd:YAG, YLF, YVO<sub>4</sub>) to two lower energy but longer wavelength photons known as the signal and idler. Operation of the first OPO was demonstrated by Giordmaine and Miller in 1965, using a lithium niobate (LiNbO<sub>3</sub>) crystal as the medium, coupling the pump beam to the signal and idler[1]. One of the problems for most of these 30 years was that the conversion efficiency of this process has been extremely low. Conversion efficiency has been hampered by the quality and availability of the nonlinear crystals. Also, the pump lasers used in these processes have been limited in available continuous wave (CW) power and spatial quality.

Many of the early OPOs were doubly resonant oscillators (DROs). In DROs, both the signal and idler wavelengths are resonated within the parametric oscillator. While resonating both wavelengths lowers the oscillation threshold, it also increases the complexity of the cavity. In order to resonate both waves, tight tolerances must be placed on the cavity dimensions such that both waves constructively interfere after one round trip. The advantage of a singly resonant oscillator (SRO) is that only one of the wavelengths, either the signal or the idler, is resonated. While this leads to a higher threshold, the restrictions on cavity tolerances are not as severe. The first CW SRO was demonstrated by Yang *et al.*, [2] using potassium titanyl phosphate (KTP). Since then,

many advances in CW SROs have been made, especially with the use of periodically poled  $\text{LiNbO}_3$ .

In the last few years, periodically poled  $\text{LiNbO}_3$  (PPLN) has emerged as an excellent source of nonlinear frequency conversion. Lithium niobate is a well characterized commercially available material. It has been used in the past for nonlinear frequency conversion but as a bulk, single-domain material. In these cases, the full potential of  $\text{LiNbO}_3$  was not used since experimenters were limited to the nonlinear coefficient that could be accessed in a birefringently phase matched interaction. Satisfying the phase matching requirements via the birefringence of the material restricts the propagation directions and polarizations of the interacting light beams and thus limits the nonlinearity that can be accessed.

Using PPLN to do quasi-phase matching (QPM), researchers have demonstrated very efficient external optical parametric oscillators. External OPOs have operated with pump depletions in excess of 90% [3]. These OPOs generally have grating periods near 30  $\mu\text{m}$  yielding signal and idler wavelengths in the vicinity of 1.5 and 3.3  $\mu\text{m}$ , respectively.

The theory of intracavity OPOs was first presented by Oshman and Harris [4]. Pulsed intracavity DROs have been previously demonstrated using single-domain  $\text{LiNbO}_3$  crystals [5]. In a pulsed DRO threshold, levels are easily met. In order for an OPO to run efficiently, it must be pumped above threshold with operating efficiency increasing as threshold is exceeded. In the case of a CW singly resonant oscillator, the pump thresholds can be on the order of a few watts of pump power. In order to pump several times above threshold, a high power pump source is necessary. Pump powers greater than 10 W may be needed and these power levels may not be easily available in a compact laser source.

By building the OPO inside the laser cavity, one immediately gains access to higher pump powers than would be available externally from a given laser. In this case, a

lower power, less expensive laser can suffice. The drawback is now in the added restrictions on the necessary cavity optics. If the pump wavelength is not used externally, there is no need to couple any of the pump beam out of the laser since the OPO is within the laser cavity. Both laser cavity end mirrors can then be highly reflecting. The OPO mirrors have to be specified to handle two wavelengths, signal and idler, and possibly the pump as well. We may also need an optic within the cavity which decouples the pump and OPO cavities.

This thesis presents the first demonstration of an intracavity OPO using periodically poled  $\text{LiNbO}_3$ . Chapter 1 deals with general OPO theory and the requirements and effects on the pump beam. Chapter 2 discusses the results from an external CW singly resonant OPO in which the pump beam was double passed through the OPO cavity. Chapter 3 explains the early intracavity OPO work done with a lamp-pumped Nd:YAG laser. Chapter 4 discusses the results of an intracavity OPO which used a diode-pumped Nd:YVO<sub>4</sub> laser. Lastly, Chapter 5 discusses conclusions and possible directions for future research with an intracavity system.

# CHAPTER 1

## 1. Theory of Optical Parametric Oscillators

Optical parametric oscillation is a method of converting photons at one frequency to two lower energy, longer wavelength photons via a process known as difference frequency generation (DFG). This process can occur in a material which lacks inversion symmetry and therefore has a second-order nonlinear susceptibility. In order for this process to occur efficiently the conditions of conservation of energy and momentum must be satisfied. This chapter discusses the basic theory behind OPOs and the corresponding requirements and effects on the pump beam. It also discusses quasi-phase matching (QPM) and temperature tuning of the OPO.

### Optical Parametric Oscillators Using Periodically Poled LiNbO<sub>3</sub>

A parametric process is one in which the initial and final quantum mechanical states of a system are identical. Another feature of a parametric process is that the photon energy is always conserved [6]. Optical parametric oscillation is a three-wave mixing process similar to parametric amplification. In the former, mirrors are used to resonate either one or both of the generated waves. When both waves are resonated, the system is known as a doubly resonant oscillator (DRO). In the case of only one beam resonated, the system is called a singly resonant oscillator (SRO).

The three waves in an OPO are referred to as the pump, signal, and idler where the pump beam is supplied and the signal and idler are generated within the OPO. In a parametric oscillator there is no dependence on resonant transitions as in a laser [7], this

allows the signal and idler of the OPO to be tuned over a wide range of frequencies as long as the following conditions are met. The first of these is conservation of energy:

$$\hbar\omega_p = \hbar\omega_s + \hbar\omega_i \quad (1.1.1)$$

where the subscripts  $p$ ,  $s$  and  $i$  refer to the pump, signal, and idler,  $\omega$  is the angular frequency and  $\hbar$  is Planck's constant. Equation 1.1.1 states that the energy from a pump photon must be simultaneously broken down to two lower energy signal and idler photons. The second requirement is conservation of momentum.

$$\vec{k}_p = \vec{k}_s + \vec{k}_i \quad (1.1.2)$$

and the wave vector  $\vec{k}$  can be written as

$$\vec{k}_j = \vec{n}_j\omega_j \quad (1.1.3)$$

where the subscript  $j$  refers to the pump, signal, or idler beams. For a colinearly phase matched interaction Eqn. 1.1.2 can be rewritten as

$$n_p\omega_p = n_s\omega_s + n_i\omega_i \quad (1.1.4)$$

where  $n$  is the respective index of refraction. Equations 1.1.1 and 1.1.4 must be simultaneously satisfied in order for the parametric oscillator to work properly.

In addition to the conservation laws, all three waves must satisfy the Maxwell equations:

$$\vec{\nabla} \times \vec{H} = \vec{\sigma}\vec{E} + \frac{\partial}{\partial t}(\epsilon_0\vec{E} + \vec{P}) \quad (1.1.5)$$

and

$$\vec{\nabla} \times \vec{E} = -\frac{\partial}{\partial t}(\mu_0\vec{H}) \quad (1.1.6)$$

where  $\vec{H}$ ,  $\vec{E}$  and  $\vec{P}$  are the magnetic, electric and polarization field vectors respectively. Terms  $\epsilon_0$  and  $\mu_0$  are the electric and magnetic permeabilities and  $\vec{\sigma}$  is the conductivity tensor. The polarization vector consists of linear and nonlinear components. Assuming a lossless medium allows the  $\vec{\sigma}\vec{E}$  term can be set to zero.

Using a vector identity and the fact that  $\bar{\nabla} \cdot \bar{E}$  vanishes if  $\bar{E}$  represents a plane wave then Eqn. 1.1.6 can be rewritten as:

$$\nabla^2 \bar{E} = \mu_0 \frac{\partial^2}{\partial t^2} [\epsilon_0 (\bar{I} + \bar{\chi}_L) \bar{E} + \mu_0 \bar{P}_{NL}] \quad (1.1.7)$$

where  $\bar{\chi}_L$  is the linear susceptibility tensor and  $\bar{P}_{NL}$  is the nonlinear polarization density. The  $\bar{P}_{NL}$  contains the higher order nonlinear polarization terms and can be expressed as:

$$\bar{P}_{NL} = \epsilon_0 \bar{\chi}^{(2)} : \bar{E} \bar{E} + \epsilon_0 \bar{\chi}^{(3)} : \bar{E} \bar{E} \bar{E} + \dots \quad (1.1.8)$$

and in our case the  $\bar{\chi}^{(3)}$  and higher terms are omitted since they are much weaker than the second order term.

The electric fields can be written as

$$\bar{E}_j(z, t) = \frac{1}{2} \hat{e}_j A_j(z) e^{i(k_j z - \omega_j t)} + \text{c.c.} \quad (1.1.9)$$

where  $A_j(z)$  is the spatially varying amplitude and the subscript  $j$  refers to pump, signal, or idler. By taking the second spatial derivative of Eqn. 1.1.9 and equating it to Eqn. 1.1.7 and using the slowly varying envelope approximation, the following coupled wave equations result:

$$\frac{\partial A_p}{\partial z} = -\frac{1}{2} \alpha_p A_p + \frac{i\omega_p}{2n_{pc}} A_s A_i e^{-i\Delta k z} \chi_{eff}^{(2)} \quad (1.1.10a)$$

$$\frac{\partial A_s}{\partial z} = -\frac{1}{2} \alpha_s A_s + \frac{i\omega_s}{2n_{sc}} A_p A_i^* e^{+i\Delta k z} \chi_{eff}^{(2)} \quad (1.1.10b)$$

$$\frac{\partial A_i}{\partial z} = -\frac{1}{2} \alpha_i A_i + \frac{i\omega_i}{2n_{ic}} A_p A_s^* e^{+i\Delta k z} \chi_{eff}^{(2)} \quad (1.1.10c)$$

where  $\alpha$  represents loss and  $\Delta k$  is the phase mismatch between the waves given as:

$$\Delta k = k_p - k_s - k_i \quad (1.1.11)$$

The second order effective nonlinear susceptibility,  $\chi_{eff}^{(2)}$ , couples the three equations and is a material property whose value is dependent on the propagation direction, polarization

and frequency of incident fields. The effective susceptibility is defined as:

$$\chi_{\text{eff}}^{(2)} = 2d_{\text{eff}} \quad (1.1.12)$$

where  $d_{\text{eff}}$  is the nonlinear coefficient[6]. The units of  $\chi_{\text{eff}}^{(2)}$  are inverse electric field, m/V.

In the case of PPLN, all the fields are linearly polarized along the c-axis of the crystal allowing use of the larger  $d_{33}$  coefficient of LiNbO<sub>3</sub>. Quasi phase matching allows access to the  $d_{33}$  coefficient (22.06 pm/V for  $1.064 \rightarrow 1.57 + 3.3 \mu\text{m}$ ) while still achieving phase matching. The phase matched condition is when Eqn. 1.1.11 equals zero. In non-QPM, Type I and II phase matching, this condition is satisfied using birefringence to compensate for the phase velocity dispersion. One of the waves is polarized orthogonal to the other two waves to satisfy the birefringence requirement [8]. In QPM, all three waves can have the same polarization, and thus access the larger  $d$  coefficient, while still satisfying the phase matching requirement.

Since QPM has altered the nonlinear coefficient,  $d_{33}$  is modified by [9]:

$$d_{\text{qpm}} = \frac{2}{\pi} d_{33} e^{-ik_g z} \quad (1.1.13)$$

The  $2/\pi$  and exponential terms arise from a Fourier series representation of the square-wave modulated nonlinear coefficient. In this expression,  $k_g$  is the grating wave vector and is given as  $2\pi/\Lambda$  where  $\Lambda$  is the length of one grating period. The exponential term in Eqn. 1.1.11 can be included in the coupled wave equations such that Eqn 1.1.9 becomes:

$$\Delta k = k_p - k_s - k_i - k_g = 0 \quad (1.1.14)$$

where the phase matching requirement now includes the additional variable of the grating period which is independent of the wavelengths. This grating can be engineered to satisfy Eqn. 1.1.12. Grating periods in use range from sub-10  $\mu\text{m}$  periods to beyond 30  $\mu\text{m}$ .

Assuming that the pump beam is undepleted by the interaction in the nonlinear media, Eqn. 1.1.10a can be written as:

$$\frac{\partial A_p}{\partial z} = 0 \quad (1.1.15)$$

and assuming the loss is small and phase matching is satisfied,  $\Delta k = 0$ , the coupled wave equations for the signal and idler become:

$$\frac{dA_s}{dz} = \frac{i\omega_s}{2n_s c} A_p A_i^* \chi_{eff}^{(2)} \quad (1.1.16a)$$

and

$$\frac{dA_i}{dz} = \frac{i\omega_i}{2n_i c} A_p A_s^* \chi_{eff}^{(2)} \quad (1.1.16b)$$

To uncouple Eqns. 1.1.16, a second derivative with respect to  $z$  is taken, keeping in mind that the amplitudes have spatial dependence. In the resulting equations, the first order derivatives of the amplitudes are substituted with Eqns 1.1.15 and 1.1.16 yielding:

$$\frac{d^2 A_s}{dz^2} = \Gamma^2 A_s \quad (1.1.17a)$$

and

$$\frac{d^2 A_i}{dz^2} = \Gamma^2 A_i \quad (1.1.17b)$$

where

$$\Gamma^2 = \frac{\omega_s \omega_i}{4n_s n_i} |\chi_{eff}^{(2)}|^2 |A_p|^2 \quad (1.1.18)$$

and  $\Gamma$  can be considered as the nonlinear gain. The intensity of the pump beam is related to the amplitude by

$$I_p = \frac{1}{2} \epsilon_0 n_p c |A_p|^2 \quad (1.1.19)$$

The solutions to Eqns. 1.1.17 are of the form:

$$A_s(z) = C_1 \cosh(\Gamma z) + C_2 \sinh(\Gamma z) \quad (1.1.20a)$$

$$A_i(z) = C_3 \cosh(\Gamma z) + C_4 \sinh(\Gamma z) \quad (1.1.20b)$$

Using the boundary conditions that at  $z = 0$ ,  $A_s(0)$  and  $A_i(0)$  are the inputs and that the first derivatives at  $z = 0$  are 0 gives solutions of:

$$A_s(z) = A_s(0) \cosh(\Gamma z) + i \sqrt{\frac{n_i \omega_s}{n_s \omega_i}} \frac{\chi_{\text{eff}}^{(2)} A_p}{[\chi_{\text{eff}}^{(2)} A_p]} A_i^*(0) \sinh(\Gamma z) \quad (1.1.21a)$$

and

$$A_i(z) = A_i(0) \cosh(\Gamma z) + i \sqrt{\frac{n_s \omega_i}{n_i \omega_s}} \frac{\chi_{\text{eff}}^{(2)} A_p}{[\chi_{\text{eff}}^{(2)} A_p]} A_s^*(0) \sinh(\Gamma z) \quad (1.1.21b)$$

Assuming there is no idler input,  $A_i(0) = 0 = A_i(0)^*$ , which holds in the case of a singly resonant oscillator where the idler is not resonated Eqns. 1.1.21 become

$$A_s(z) = A_s(0) \cosh(\Gamma z) \quad (1.1.22a)$$

$$A_i(z) = i \sqrt{\frac{n_s \omega_i}{n_i \omega_s}} \frac{\chi_{\text{eff}}^{(2)} A_p}{[\chi_{\text{eff}}^{(2)} A_p]} A_s^*(0) \sinh(\Gamma z) \quad (1.1.22b)$$

Equations 1.1.22 describe how the amplitudes of the signal and idler waves grow via propagation through the nonlinear media. The signal phase has no dependence on the pump, it retains its phase as it propagates through the cavity. The phase of the idler wave is determined by both the signal and pump beams. However, since this is an SRO resonating only the signal, the idler leaves the cavity after being generated within the crystal. Each pass of the signal through the crystal generates a new idler beam and this beam is free to take on a phase predetermined by the pump and signal beams. This is one of the advantages of an SRO over a doubly-resonant oscillator. In a DRO where both the signal and idler are resonated, the phase of both beams is critical and this places tighter tolerances on the layout and stability of the cavity.

## Self Consistency Analysis of Double Pump Pass OPO

In analyzing the threshold behavior of an OPO a self-consistency analysis can be done. In this method, a column vector representing the fields is sent through one round trip (1RT) of the cavity and forced to reproduce itself once it returns to its starting point. The field column vectors is written as:

$$A(z) = \begin{bmatrix} A_s(z)e^{ik_s z} \\ A_i^*(z)e^{ik_i z} \end{bmatrix} \quad (1.2.1)$$

The matrix for propagation through a nonlinear crystal of length  $L$  is given as [6]:

$$[\text{crystal}] = \begin{bmatrix} \text{Cosh}(\Gamma L)e^{ik_s L} & i\sqrt{\frac{n_i \omega_s}{n_s \omega_i}} \text{Sinh}(\Gamma L)e^{ik_s L} K \\ -i\sqrt{\frac{n_s \omega_i}{n_i \omega_s}} \text{Sinh}(\Gamma L)e^{-ik_i L} K^* & \text{Cosh}(\Gamma L)e^{-ik_i L} \end{bmatrix} \quad (1.2.2)$$

where  $K$  is

$$\frac{\chi_{\text{eff}}^2 A_p}{|\chi_{\text{eff}}^2 A_p|} \quad (1.2.3)$$

$A(z)$  must reproduce itself after 1RT through the cavity shown in Figure 1 which is a simple two mirror SRO cavity.

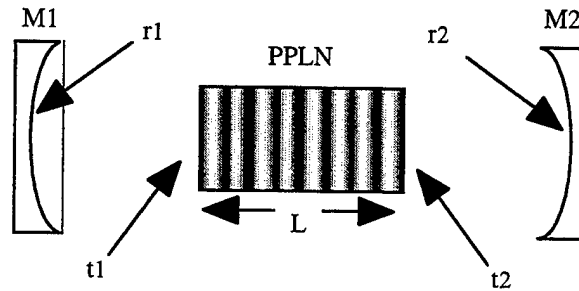


**Figure 1. Round Trip Through the SRO Cavity.** This shows a two-mirror SRO cavity. The  $r_i$ 's are the mirror reflectivities and the  $t_i$ 's are the transmission at the PPLN faces. The length of the PPLN is  $L$ . Mirror M1 is the input coupler with the curved surface reflective at the signal. Mirror M2 for a pump double pass OPO reflects both the pump and signal. Both mirrors are highly transmitting at the idler

The  $r_i$ 's represent the reflection coefficient of the mirrors for each wavelength and  $t_i$  is the transmission coefficient at the faces of the crystal. Both mirrors are highly reflecting at the signal and M2 is also highly reflecting at the pump wavelength. Both mirrors are also highly transmitting at the idler. The end faces of the PPLN are antireflection (AR) coated for all three wavelengths.

Propagation through one round trip of the cavity is given as

$$A(1RT) = TA_{\text{input}} \quad (1.2.4)$$

where  $T$  is the matrix multiplication of the cavity. For a round trip beginning immediately after the first surface of the PPLN, the matrix multiplication can be written as:

$$T = \begin{bmatrix} t_{s1} & 0 \\ 0 & t_{i1}^* \end{bmatrix} \begin{bmatrix} r_{s1} & 0 \\ 0 & r_{i1}^* \end{bmatrix} \begin{bmatrix} t_{s1} & 0 \\ 0 & t_{i1}^* \end{bmatrix} [\text{crystal}] \begin{bmatrix} t_{s2} & 0 \\ 0 & t_{s2}^* \end{bmatrix} \begin{bmatrix} r_{s2} & 0 \\ 0 & r_{i2}^* \end{bmatrix} \begin{bmatrix} t_{s2} & 0 \\ 0 & t_{s1} \end{bmatrix} [\text{crystal}] \quad (1.2.5)$$

The distances traveled in air are not included since these do not affect the calculations. In this case, the crystal matrix is included twice since the end mirror, M2, of the OPO is highly reflecting at the pump. This allows the pump to be reflected back through the crystal providing gain in both passes. For self-consistency  $A(1RT) = A_{\text{input}}$  and in order to have a nontrivial solution ( $A \neq 0$ ) the determinant of  $[T - I]$ , where  $I$  is the identity matrix, must be zero. This solution is

$$1 - e^{2ik_s L} r_s^2 t_s^2 \cosh^2(\Gamma L) = 0 \quad (1.2.6)$$

where the assumptions that the transmission at both crystal faces and reflection at the mirrors are identical. The reflection coefficient  $r_i$  can be replaced by

$$r_{s1} = r_{s2} = |r_s| e^{i\phi_s} = \sqrt{R_s} e^{i\phi_s}$$

A similar substitution can be made for the transmission coefficient assuming the end faces of the PPLN are identical. These terms can be included in Eqn. 1.2.6 to yield:

$$1 - T_s^2 R_s \cosh(\Gamma L) = 0 \quad (1.2.7)$$

where the exponential terms have been grouped and set as:

$$2\phi_s + 2k_s L + 2\theta_s = 2m\pi \quad (1.2.8)$$

forcing the signal to constructively interfere with itself after a cavity round trip.

Solving Eqn. 1.2.7 for  $\Gamma^2$  and setting it equal to Eqn. 1.1.18 gives

$$I_{p,threshold} = \frac{(1 - T_s^2 R_s) 2n_s n_i n_p \epsilon_0 c^3}{L^2 T_s^2 R_s \omega_s \omega_i |\chi_{QPM}^{(2)}|^2} \quad (1.2.9)$$

This equation holds only for the nonphysical case of plane waves. The complications to this formula arising from the Gaussian profiles of the actual beams is discussed in Sect. 2.3. Equation 1.2.9 is the minimum intensity of the pump beam, which is double passed through the crystal, for the SRO to reach threshold. In the case where the pump is only allowed one pass through the crystal, the threshold result is the same as equation 1.2.9 except it is larger by a factor of 2. This idea of nonresonantly reflecting the pump beam back through the OPO was originally discussed by Bjorkholm [11].

### Manley Rowe Relations and Clamping of the Pump Beam

Ideally, once the intensity of the pump beam reaches the threshold level of the OPO, the pump will stay clamped at this level and any pump above this value will be converted into signal and idler photons. This is discussed by Yariv and Louisell in reference [12] and recently demonstrated in an intracavity OPO by Colville *et al.* [13].

The intensity of the pump, signal or idler beams can be written as

$$I_j = \frac{1}{2} \epsilon_0 n_j c |A_j|^2 \quad (1.3.1)$$

where the subscript  $j$  refers to the pump, signal or idler beam. Taking the spatial derivative of Eqn. 1.3.1 yields:

$$\frac{dI_p}{dz} = \frac{1}{2} \epsilon_0 n_p c \left[ A_p \frac{dA_p^*}{dz} + A_p^* \frac{dA_p}{dz} \right] \quad (1.3.2a)$$

$$\frac{dI_s}{dz} = \frac{1}{2} \epsilon_0 n_s c \left[ A_s \frac{dA_s^*}{dz} + A_s^* \frac{dA_s}{dz} \right] \quad (1.3.2b)$$

$$\frac{dI_i}{dz} = \frac{1}{2} \epsilon_0 n_i c \left[ A_i \frac{dA_i^*}{dz} + A_i^* \frac{dA_i}{dz} \right] \quad (1.3.2c)$$

The lossless case of Eqns. 1.1.10 can be substituted into Eqns. 1.3.2. The resulting three equations are similar and can be expressed as:

$$\frac{d}{dz} \left( \frac{I_s}{\omega_s} \right) = \frac{d}{dz} \left( \frac{I_i}{\omega_i} \right) = \frac{d}{dz} \left( -\frac{I_p}{\omega_p} \right) \quad (1.3.3)$$

Equation 1.3.3 is known as the Manley-Rowe relationship. It states that the rate of photons created at the signal frequency is equal to the rate at the idler. Both of these are equal to the rate at which photons at the pump wavelength are destroyed [6].

Once the OPO turns on and signal and idler photons are generated, the pump intensity must clamp at this threshold level. Pump power above threshold is converted to signal and idler photons [14]. This effect has been seen in both pulsed and CW intracavity OPOs [4, 13]. Rewriting the intensities in terms of powers as in Ref. 7, Eqn. 1.3.3 can be expressed as:

$$\frac{P_s}{\omega_s} = \frac{P_i}{\omega_i} = -\frac{(P_p)_{\text{thresh}}}{\omega_p} \left[ \frac{P_p}{(P_p)_{\text{thresh}}} - 1 \right] \quad (1.3.4)$$

where the powers are measured within the OPO cavity. High efficiency operation can be achieved for pump powers beyond threshold,  $P > P_{\text{threshold}}$ .

### Temperature Tuning

In the case of QPM using PPLN, tuning of the signal and idler beams can be accomplished over the transparency range of the  $\text{LiNbO}_3$  by temperature tuning. Varying the temperature of  $\text{LiNbO}_3$  changes the index of refraction [15]. Temperature also affects

the crystal length which modifies the grating period [16]. Due to these considerations, Eqn. 1.1.14 should be written as

$$\frac{n(\lambda_p, T)}{\lambda_p} - \frac{n(\lambda_s, T)}{\lambda_s} - \frac{n(\lambda_i, T)}{\lambda_i} - \frac{1}{\Lambda(T)} = 0 \quad (1.4.1)$$

Solutions to this equation can be found analytically by specifying either wavelength or temperature and solving for the other variable given a fixed grating period. Figure 2 shows typical tuning curves as a function of temperature for three different grating periods. The pump wavelength is 1.064  $\mu\text{m}$ .

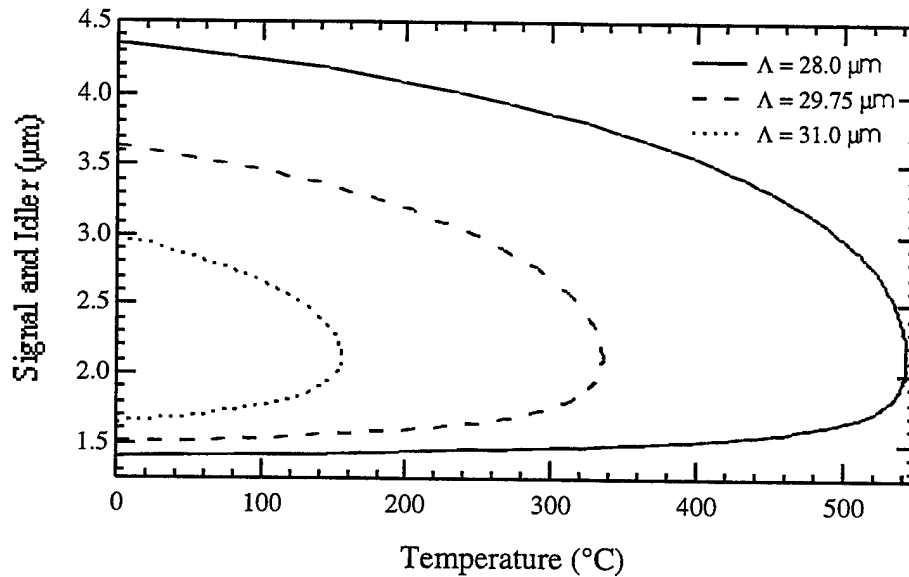


**Figure 2. Theoretical Temperature Tuning Curves of PPLN.** Tuning ranges as a function of temperature for a pump wavelength of 1.064  $\mu\text{m}$ . Grating periods are 28.0, 29.75 and 31.0  $\mu\text{m}$ .

At a fixed temperature, an increase in grating period yields longer wavelength signals and shorter wavelength idlers.

## Conclusions

This chapter has discussed the basic equations relating to the theory and operation of an OPO. First the coupled wave equations were solved using the undepleted pump approximation. Next, a self consistency analysis of the OPO cavity was done, which led to a threshold intensity for the pump beam. Afterwards, the Manly-Rowe relation was shown, as well as clamping of the pump and the potential for a highly efficient operation. Lastly, the temperature tuning of a QPM OPO using PPLN was discussed and a theoretical plot of the tuning curves for different gratings was shown.

Quasi phase matching has many benefits over traditional birefringent phase matching. In birefringent phase matching, tuning can be done by adjustment of either angle or temperature. With angular tuning, some of the problems encountered are restricted angular acceptance and Poynting vector walk-off limiting the interaction length [8]. Temperature tuning is dependent on how the indices change with temperature. Another drawback of birefringent phase matching is that one of the waves is polarized orthogonal to the other two, limiting the usage of the larger nonlinear coefficients. In QPM, all waves can be polarized in the same direction, allowing access to the largest  $d$  components. Also QPM has the advantage of being temperature tuned over the entire transmission band of the nonlinear material. In  $\text{LiNbO}_3$ , tuning can be done over the range of visible wavelengths and out to approximately  $4\text{ }\mu\text{m}$  [8].

## 2. Double Pump Passing OPO Experiment

The double pump pass OPO experiments were done to obtain experience in the construction and alignment of an OPO external to the laser and to observe any phenomena associated with the pump being double passed. Double passing of the pump beam reduces the OPO threshold by half, compared to the case where the pump beam is singly passed. Threshold reduction arises since the pump beam makes two passes through the nonlinear crystal during one round trip of the resonated wave, providing gain during both passes. Double pump passing will also be experienced during the intracavity OPO experiments since linear cavity lasers are inherently double passed.

### Experimental Layout: Pump Laser and Optics

The pump laser used for the first part of this experiment was a continuous wave (CW) Nd:YAG (neodymium-doped yttrium aluminum garnet) Spectra Physics Series 3000 laser (serial number 248). This laser was originally intended for use in the intracavity experiment. Early attempts at an intracavity OPO were done within the housing of this laser. It soon became apparent that a bread board type platform would be needed for the experiment, so the laser head containing the rod and arc lamp were removed from the original housing and mounted on an external platform. The cavity end mirrors were also removed and mounted on Oriel fine adjustment mounts. This laser was then reassembled and aligned on one end of an optical table per the method described in Appendix A.

The layout of the laser is shown in Fig. 3. The length of the cylindrical Nd:YAG rod is 80 mm with a diameter of 4 mm. The distance from the rod face to each end mirror was  $882 \pm 1$  mm. The distance from the rod end to the aperture was  $87 \pm 1$  mm. The aperture had a diameter of 0.059" (1.5 mm). The overall cavity dimensions were the same as when the laser was in its housing.

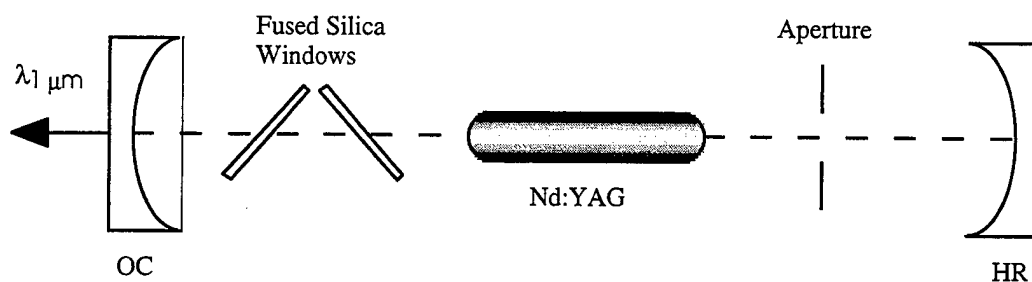


**Figure 3. Nd:YAG Laser Layout.** The end mirrors are 600 mm ROC and are 882 mm from the faces of the Nd:YAG rod. The aperture diameter was 1.5 mm and was located 87 mm from the rod. The fused silica windows acted as Brewster plates.

The radius of curvature (ROC) of each of the end mirrors was 600 mm. The high reflector (HR) was  $R > 99\%$  at  $1.06 \mu\text{m}$  and the output coupler (OC) was  $R = 85\%$ . The fused silica windows within the cavity had a dual purpose. In this setup, they were used as Brewster plates to polarize the laser. Polarization of the output was vertical with respect to the table and the polarization purity was better than 100:1. They were later used as an intracavity attenuator to vary the loss within the cavity. This will be discussed in Chapter 4. The laser was labeled as having a maximum output of 10W and the arc lamp could be driven from 10 to 19.9 amps.

Figure 4 on the following page shows the table layout from the laser to the OPO cavity. After the beam left the laser, it was guided toward the other end of the table. A Faraday isolator was inserted in the beam path to prevent any back reflections from entering the laser cavity and possibly disrupting the laser. A variable attenuator consisting of a half wave plate (HWP) and polarizing cube were then added to the beam path. The HWP and polarizer allowed external adjustment of the laser power while allowing the laser to operate at a constant current, in this case maximum current of 19.9 amps. Keeping the laser at a constant current maintains a fixed divergence from the laser since the thermal lensing of the rod is held constant.



Before these optics were inserted into the beam path, the beam size at the input surfaces of these optics was measured to ensure that the damage threshold of the optics was not exceeded. At the HWP, the beam radius was  $1.57 \pm 0.01$  mm. Assuming the worst case that the maximum power from the laser, 11W, was reaching the HWP, the intensity would be  $142 \text{ W/cm}^2$ , which is below the safe level from Table 1. Similarly, the beam radius at the location of the polarizer was  $1.65 \pm 0.01$  mm, giving a maximum intensity of  $129 \text{ W/cm}^2$ , also below the safe level. The polarizer was mounted such that the transmitted beam was vertically polarized and any s-polarization was reflected up towards a beam dump located directly above the polarizer.

Once past the variable attenuator, the beam was sent through the mode matching optics. These were -100 mm and +90 mm focal length lenses on BK7 substrates. The lenses were AR coated for  $1.064 \mu\text{m}$  with a damage specification of  $35\text{-}37 \text{ J/cm}^2$  @ 532 nm, 10 ns pulse, 10 Hz with a  $500 \mu\text{m}$  beam size. This corresponds to about  $3.5 \text{ MW/cm}^2$  damage threshold with a  $500 \mu\text{m}$  beam size, parameters well above the intensities in this set up.

Using two mode matching lenses allows greater flexibility in adjusting the waist size and location of the focused beam. If just one mode matching lens is used then its position is governed by the divergence of the laser beam after the OC. Two lenses allow independent adjustment of the beam regardless of its divergence. After the lenses were positioned the beam was profiled.

### **Mode Matching Between Pump Beam and OPO Cavity**

To optimize use of the PPLN crystal, the pump and signal beams must be mode matched. Mode matching is determined by the length of crystal used. This is done by setting  $L/b$ , the ratio of the crystal length  $L$  to twice the confocal parameter of the beam  $b$ ,

equal to one [10]. This forces the collimated portion of the beam to be equal to the length of the crystal. This equation can be written as:

$$\frac{L_c}{b_j} = 1 = \frac{L_c}{\frac{2\pi n_j w_{0j}^2}{\lambda_j}} \quad 2.2.1$$

where the subscript j refers to either the pump or the signal beam,  $L_c$  is the length of the crystal,  $n_j$  is the index of refraction of the crystal,  $\lambda_j$  is the wavelength of interest and  $w_{0j}$  is the minimum spot size (waist) of the beam. Equation 2.1 can be solved for  $w_{0j}$  such that:

$$w_{0j} = \sqrt{\frac{\lambda_j L_c}{2\pi n_j}} \quad 2.2.2$$

For a pump wavelength of 1.064  $\mu\text{m}$ ,  $L_c$  of 50 mm,  $n_p$  of 2.16319 at 165 °C ,  $w_{0p}$  is 63  $\mu\text{m}$  and  $w_{0s}$  is 76  $\mu\text{m}$  with  $n_s$  of 2.14467 and  $\lambda_s$  of 1.55  $\mu\text{m}$ . At the same temperature and pump and signal wavelengths, an  $L_c$  of 25 mm yields  $w_{0p}$  of 44  $\mu\text{m}$  and  $w_{0s}$  of 54  $\mu\text{m}$ .

Once the necessary spot size of the pump beam is determined, the propagation through the input coupler (IC) must be considered. Propagation through the IC expands the pump beam since the IC acts as a negative lens. For the double pump pass experiment, the specifications of the IC are given in Table 2.

**Table 2: Input Coupler Specifications.** The center thickness was measured. Coating specifications were supplied by the manufacturer.

<u>Input Coupler Specifications:</u>		
manufacturer	Quality Thin Films	
substrate	CaF <sub>2</sub>	
n	1.428 @ 1.064 $\mu\text{m}$	
diameter	1"	
$t_c$	3.69 mm	
coatings:	S1 (plano)	HT 1.06, 3.4 - 4.6 $\mu\text{m}$
	S2 (37.5 mm ROC)	HR 1.38 - 1.55 $\mu\text{m}$
		HT 3.4 - 4.6 $\mu\text{m}$

The transmission curve of the IC was supplied by the manufacturer. The transmission at 1.064  $\mu\text{m}$  was given as 92 %. The region of high reflectivity ( $R \sim 99 \%$ ) was from 1.275 to 1.580  $\mu\text{m}$ . Reflectivity quickly decreases outside this range. There was no data supplied giving transmission at the idler.

We measured the focal spot and divergence behavior of the pump beam using the knife edge technique. This technique involves scanning a knife edge across the beam and noting the distance traveled between the points where the power drops to 84% and 16% of its value when the knife edge is not in the beam. The distance between these points gives the  $1/e^2$  beam radius at that point,  $w(z)$ .

For each measurement position along the  $z$  axis, the beam was measured in two orthogonal directions. Measurements were done symmetrically about the waist with measurements near the waist more closely spaced, about 2 mm apart. Beyond the waist, measurements were further spaced, about 10 to 20 mm apart. None of the measurements involved a beam waist larger than 1 mm. Once this data was collected, it was fit to the beam propagation equation:

$$w(z) = w_0 \sqrt{1 + \left( \frac{z - z_0}{z_R} \right)^2} \quad 2.2.3$$

where  $z_0$  is the location of the minimum waist,  $z_R$  is the Rayleigh range of the beam and  $w_0$  is the minimum waist. By simultaneously fitting to these three parameters, the  $M^2$  value of the beam can be found [17]. The  $M^2$  determines how many times,  $M$ , above diffraction limited is the beam and is determined by:

$$M^2 = \frac{\pi w_0^2}{\lambda z_R} \quad 2.2.4$$

A value of 1 indicates a diffraction-limited beam while values greater than one indicate a nonideal beam. Values less than one are nonphysical since a beam cannot be better than diffraction limited.

The  $M^2$  value for the beam was found using a radial average of the waists in the x and y planes [17]. The radial values of the waist are determined by:

$$w_r(z) = \sqrt{\frac{w_x^2(z) + w_y^2(z)}{2}} \quad 2.2.5$$

Using these values, the  $M^2$  of the pump beam was calculated to be  $1.05 \pm 0.03$ . The radial values were used because of the idea of an embedded Gaussian. This idea states that any beam has “embedded” within it a perfect TEM<sub>00</sub> beam.

After profiling the pump beam focused by the mode matching lenses, the location of the minimum waist in air is noted. This waist should be smaller than the required waist for modematching since this IC acts as a negative lens, plano concave, which will magnify and translate the waist. For an  $L_c$  of 25 mm, the size of the pump beam for proper modematching is 44  $\mu\text{m}$ . Since the IC is a negative lens, we must compensate its effect on the beam. If the pump beam is focused to a size of  $\sim 30 \mu\text{m}$  in air and this IC is inserted in the path, the new waist size will be 44  $\mu\text{m}$  displaced 12 mm back towards the IC from its original position. Insertion of the PPLN will also displace the waist location but will not affect the waist size.

For the cavity built in this experiment, a 50 mm PPLN crystal was used first and later replaced with a 25 mm crystal. The distance from the inner surface of the IC to the face of the 50 mm long PPLN was  $26.0 \pm 0.1$  mm. The grating period of the PPLN was 29.75  $\mu\text{m}$ . The distance from the back face of the PPLN to the 50-mm ROC output coupler was  $30.4 \pm 0.1$  mm.

The OC used in this experiment allowed double passing of the pump. The OC has a dual HR coating on the curved surface. This coating reflects both the pump and signal wavelengths. The plano surface is AR coated at the idler wavelength. Table 3 gives the specifications for the double HR OC and the transmission curves are given in Appendix B.

**Table 3: Double HR OC Specifications.** The coating values given were specified to the manufacturer.

<u>Double HR OC Specifications</u>	
manufacturer	CVI Laser Corporation
PO#	201C-023-171
substrate	CaF <sub>2</sub>
diameter	1"
coatings:	S1 (curved)    HR 1.064 & 1.57 $\mu\text{m}$
	S2 (plano)     HT 3.3 $\mu\text{m}$

The double HR OCs were originally purchased for the intracavity experiment as well as to have OPO mirrors readily available. With this in mind, three different plano/concave combinations were purchased in addition to plano/plano mirrors which could be used as filters for the idler. The different curvatures purchased were 50, 100 and 150 mm ROCs.

## Results

With the laser off, the IC was inserted and aligned using the alignment HeNe laser. Next, the laser power was brought up and the new beam waist was measured after the IC. Next, the laser was shut off and the PPLN and OC were added again using the HeNe for alignment. After inserting all of the components, the laser was slowly brought up in power and the OPO cavity alignment was optimized using the green light (532 nm) due to frequency doubling from the PPLN.

Alignment of the OPO was completed by first intentionally misaligning the IC. Next the OC was adjusted such that the green light reflected from the OC was sent back through the PPLN and superimposed on the pump beam before the IC. This was accomplished by inserting an aperture prior to the IC aligned to the pump beam and then adjusting the OC until the green light was also centered on the aperture. Next, the IC was aligned such that the green light reflected from the IC was superimposed on the green light generated from a single pass through the PPLN. This was accomplished by observing both green spots beyond the OC.

After initial attempts at alignment, damage appeared on one PPLN end. After noticing this, the laser was shuttered and the oven was allowed to cool down from its operating temperature of 175 °C. Once the oven had cooled, the PPLN was removed and examined. A corner of the crystal had broken off leaving the PPLN unusable since there was a previous crack on the other side of the crystal thus leaving no clear aperture. Since there were no other 50 mm long samples on hand, a 25 mm sample of the same period was put in its place. The mode matching optics were not changed, therefore the pump waist within the new sample was still 66  $\mu\text{m}$  after repositioning the IC and oven locations.

After realignment with the new crystal, the OPO operated sporadically, flashing on and off. The OPO cavity mirrors were translated to vary the length of the cavity but this had no observable effect on the operation. Power measurements of the pump beam were done before the IC, yielding a lower value than expected. An inspection before each component in the beam path showed that the power through the isolator had decreased. Alignment through the isolator appeared fine so a decision was made to remove it from the beam path. Once the isolator was removed, the OPO ran robustly.

After adjusting the cavity for best overall performance by adjusting the end mirrors angularly and longitudinally, the pump power was slowly decreased while maintaining OPO operation by slight alignment adjustment of the end mirrors. Closer to threshold, the OPO cavity is much more sensitive to misalignment. Through this manner, the OPO threshold was reduced to below 2W. The dimensions of the OPO cavity were  $26.97 \pm 0.01$  mm from the 37.5 mm ROC input coupler to the front face of the PPLN. The distance from the back face of the PPLN to the 50 mm ROC output coupler was  $40.87 \pm 0.01$  mm. This cavity produces a signal waist of 79  $\mu\text{m}$  at the center of the PPLN and an  $L/b_s$  of 0.47.

Figure 5 shows signal and idler powers measured after the OC as a function of pump power present before the IC. These measurements were done at an oven temperature of 175 °C.

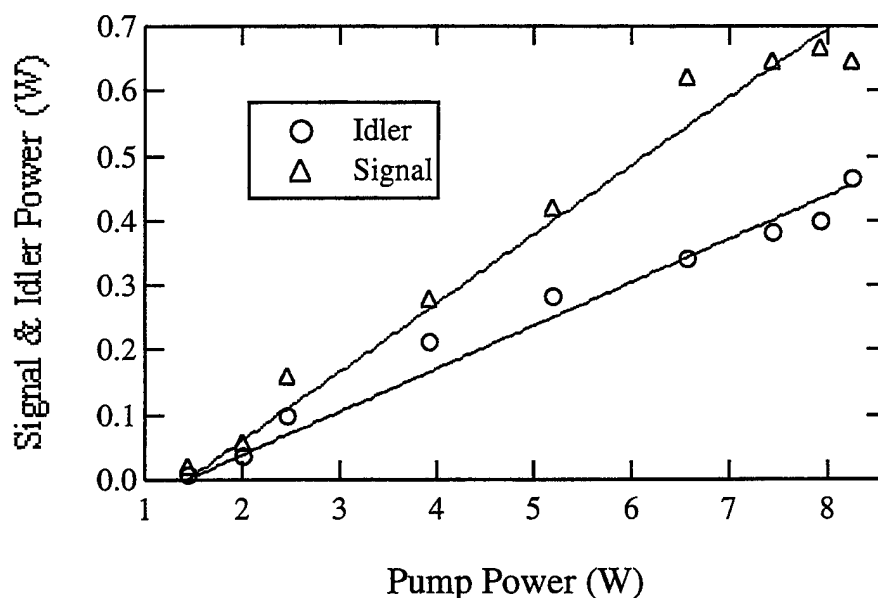


**Figure 5. Signal and Idler Powers vs. Pump Power.** These were signal and idler values measured after the double HR end mirror. The plot shows an OPO threshold of about 1.5 W incident on the IC. The PPLN used was 25 mm long.

Note, although it wasn't measured, there is also idler and signal leaking from the other end of the OPO, from the IC. The powers from the other end should be comparable to those shown in Fig. 5. At the operating temperature of 175 °C, the signal wavelength was  $1.5852 \pm 0.0002 \mu\text{m}$  and the corresponding idler was  $3.2388 \pm 0.0004 \mu\text{m}$ . Maximum signal power was ~650 mW with a maximum idler of ~450 mW. Threshold as determined by the power at which the SFG (red) was first visible was approximately 1.5 W of pump measured before the IC.

Rewriting Eqn. 1.2.9 in terms of the threshold pump power is given as:

$$P_{th} = \frac{1}{2} \frac{2(1-R_s)}{R_s} \left\{ \frac{\lambda_p \lambda_s \lambda_l n_s n_l \epsilon_0 c}{32\pi^2 d_{eff_{QPM}}^2 L} \right\} \left\{ \frac{\left(1 + \frac{w_s^2}{w_p^2}\right)}{h_{sm}} \right\} \quad (2.3.1)$$

where  $w_p$  and  $w_s$  are the minimum pump and signal waists within the PPLN. Note that Eqn. 2.3.1 assumes that  $L/b_p = L/b_s$ . The average value of  $L/b_p$  (measured value for the pump waist was 66  $\mu\text{m}$ ) and  $L/b_s$  (PARAXIA predicts a signal waist of 79  $\mu\text{m}$ ) is 0.46. For this value the  $L/b$  factor  $h_{SM} = 0.38$  [Refs. 10, 29, 30] and the waist values used in computing  $P_{th}$  are 65.3  $\mu\text{m}$  and 79.7  $\mu\text{m}$  for the pump and signal respectively. The mirror reflectivity,  $R_s$ , was taken as 99 % and the faces of the PPLN crystal were assumed to have perfect transmission at the signal. The value of  $d_{eff_{QPM}}$  in bulk  $\text{LiNbO}_3$  for an interaction between 1.064 generating 1.57 and 3.3  $\mu\text{m}$  is  $2/\pi * 22.06 \text{ pm/V}$ . Equation 2.3.1 yields a theoretical pump threshold of 2.77 W.

A few months later, this experiment was repeated to collect additional data, namely temperature tuning and idler stability data. The overall setup was the same as before except for a few changes. The pump laser was now a Nd:YVO<sub>4</sub> (neodymium-doped yttrium orthovanadate) which operated CW and was diode pumped. This laser emitted a maximum of 8 W at wavelength of 1.0643  $\mu\text{m}$ , very close to the Nd:YAG wavelength of 1.0642  $\mu\text{m}$  ( $\Delta\lambda = 0.1 \text{ nm}$ ). This laser was used as the pump because the beam quality and power of the Nd:YAG used previously had been deteriorating. Another change was the sample of PPLN used. The sample used in the first setup was supplied by Dr. Larry Myers and was sample # 625-2 (0.5 x 16 x 25 mm<sup>3</sup>). This was a sample Dr. Myers had poled at Stanford University. Unfortunately, this crystal had a fatal encounter with the floor in the period before rebuilding the double pass experiment for a second time. The new crystal used was poled by Mark Missey, in-house, at WPAFB. This crystal had the same period as the previous one,  $\Lambda = 29.75 \mu\text{m}$ , with the same length of poled region, 25 mm. The new crystal had an overall length of 25.5 mm with 0.25 mm

of unpoled LiNbO<sub>3</sub> divided between the two end faces. The thickness was 0.5 mm and the width was 5 mm. This crystal was labeled as number 29.75-1 #10.

After setting up the experiment as in Fig. 4, the pump beam radial waist was measured to be  $26 \pm 9 \mu\text{m}$  before insertion of the IC. The  $M^2$  of the pump beam was  $2 \pm 1$ . The large  $M^2$  uncertainty of the pump beam may be due to an insufficient number of measurements done near the beam waist. Due to deadlines, the mode matching of the pump beam was not optimized. After aligning the OPO, the new threshold was 3 W of pump measured before the IC. This is a factor of 2 greater than the previous setup and may be due to the combination of changes stated earlier as well as the change in beam quality,  $M^2$ . The main goal in redoing the experiment was not to reproduce the low threshold results but to evaluate the temperature tunability and stability of this OPO.

Wavelength measurements were done using the Acton Research Corp. Spectra Pro 750 monochromator. It utilizes a Czerny-Turner design and the diffraction grating used had 600 grooves/mm blazed for  $1.0 \mu\text{m}$ . A Thorlabs Ge photodiode was used to measure the signal wavelengths. The PMT supplied with the monochromator cut off shortly after  $1.0 \mu\text{m}$  and the signal wavelengths measured were in the vicinity of  $1.5 \mu\text{m}$ . From the measurements of the signal wavelengths, we were able to calculate the idler wavelengths via energy conservation, Eqn. 1.1.1. An initial attempt with the PMT was made to measure the red light due to sum frequency generation (SFG) between the pump and signal. This corresponded to a wavelength of about 634 nm for a signal of  $1.57 \mu\text{m}$ . Although we were able to detect this with the PMT, this signal did not have a cleanly defined wavelength peak. The wavelength also appeared to randomly hop a few nanometers during the spectral scans. Due to this uncertainty in the location of the center and the fact that there would be less error in a direct measurement of the signal wavelength, we used the Ge detector. The bandgap wavelength of Ge is  $1.88 \mu\text{m}$  and it is sensitive over a range of roughly 800 to 1850 nm [18].

Figure 6 shows the temperature tuning curve of the double pass OPO experiment. The uncertainty in the wavelength measurements are less than the size of the markers and the data is within the uncertainty of the Sellmeier equation [15].

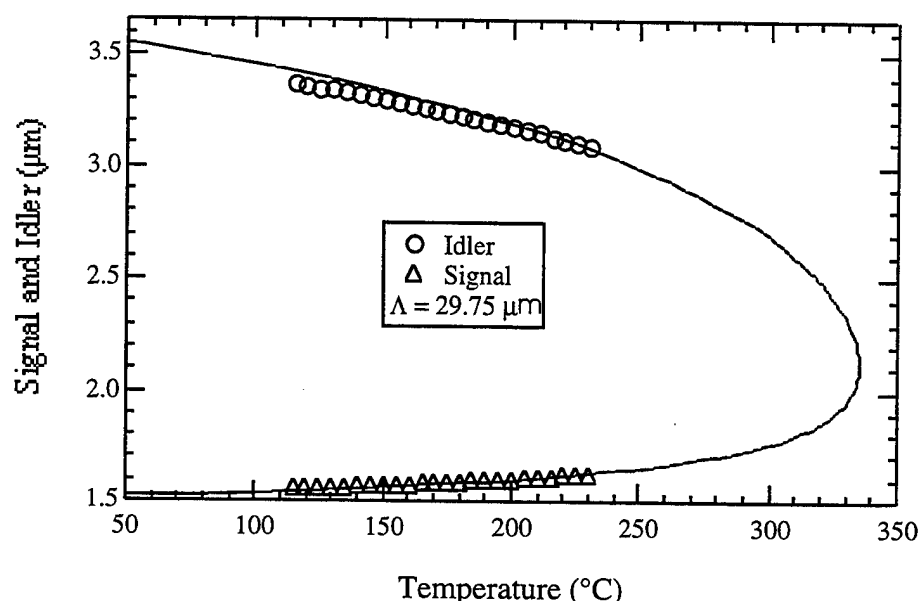


**Figure 6. Temperature Tuning Curve of the Double Pass OPO.** Measurements of the signal were done with a monochromator using a Ge detector. Idler values were calculated from the measured signal. The grating period of the PPLN was 29.75  $\mu\text{m}$ .

The OPO ran over a temperature range of 115 to 230  $^{\circ}\text{C}$  ( $\Delta T = 115^{\circ}\text{C}$ ). The signal varied from  $1.5555 \pm 0.0002 \mu\text{m}$  to  $1.6201 \pm 0.0002 \mu\text{m}$  ( $\Delta\lambda_s = 65 \text{ nm}$ ) and the idler tuned from  $3.3704 \pm 0.0004 \mu\text{m}$  to  $3.0881 \pm 0.0004 \mu\text{m}$  ( $\Delta\lambda_i = 282 \text{ nm}$ ).

Next, the stability of the OPO was examined by observing the idler output over time. The analog output of a Newport Multifunction Optical Power Meter (model 1835c) was sent to a LeCroy 9310 (300 MHz) oscilloscope. The information from the oscilloscope was then downloaded and is plotted in Fig. 7. Note, the detector was a thermal head with a relatively slow response time such that any short, pulsing transients of the idler power may not have been detected.

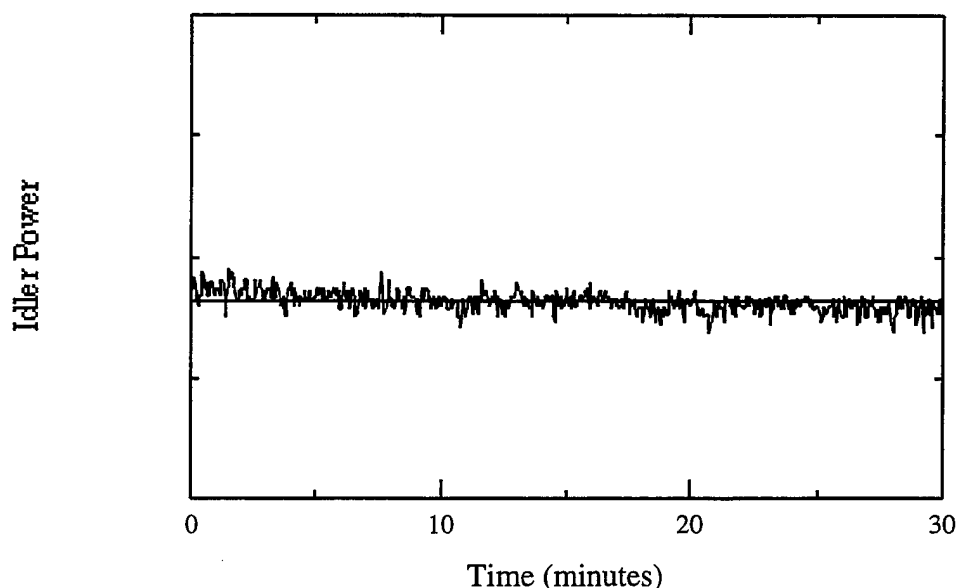


**Figure 7. Stability of Double Pass OPO.** Idler power over this period was 82 mW with a stability of  $\pm 5\%$ .

This plot is a 30 minute trace of the idler power measured after M1 with a Ge filter. The OPO had been running for over 1 hour before this data was taken.. The average idler power over this period was  $82 \pm 4$  mW or  $\pm 5\%$  stability. The OPO was operated at a pump level of about 2 times threshold.

Over the period shown in Fig. 7, the idler power shows a downward trend. An observation of the idler power over a few hours showed a slow oscillation of the idler power. The data of the idler power stability over a few hours was not collected. A possible explanation of the slow power variance could be the air temperature in the lab changing throughout the day.

## Conclusions

The double pass pumping experiments were conducted to evaluate the possibility of low thresholds from nonresonant pump reflection while awaiting the arrival of the beamsplitters for the intracavity OPO. With the double HR as the end mirror of the OPO, the double pass experiments were conducted giving low thresholds (1.5 W) and good

conversion efficiency (~30% pump depletion). Even lower thresholds for PPLN based CW OPOs have recently been reported. D. Chen [21] of The Aerospace Corporation has recently demonstrated a threshold below 1 W using a 25 mm long PPLN crystal in a 4 mirror ring OPO similar to Reference 3. The difference between Chen's cavity and the one presented here is that he used a cavity that is actively locked for resonance of both the signal and pump waves.

In the double pass experiment, the OPO cavity has a low Q at the pump. The pump enters through the IC, is reflected at the OC and exits the OPO cavity through the IC. The signal within the OPO cavity sees gain due to both passes of the pump through the PPLN. In D. Chen's experiment, both the signal and pump waves are resonated within the OPO cavity. In order to accomplish this, the cavity is much more complex, needing the use of a cavity locking scheme to keep the finesse of the cavity at the pump wavelength high.

One of the questions from this experiment is why removal of the isolator improved the OPO performance. The isolator was in place to prevent the reflected pump beam from interfering with the stability of the laser. After its removal there was no obvious change in the operation of the pump laser. Removal of the isolator increased the pump power available at the OPO. This may indicate that the isolator was not properly aligned to the polarization of the pump beam.

At pump levels below OPO threshold ( $< 1.5$  W), the OPO could be made to flash on by lightly tapping on the setup or on certain parts of the table. By tapping, a flash of red could be seen from the OPO, the red being due to the pump and signal experiencing sum-frequency generation. This tapping was eventually attributed to spiking of the laser. Later during the intracavity experiment with the Nd:YAG laser, the same effect was seen. A fast detector was used to observe the pump and then the table was tapped. The pump power was seen to suddenly spike up and quickly oscillate down to its steady state value. This spiking momentarily raised the OPO above threshold causing it to briefly turn on.

The tuning curve shown in Fig. 6 ranges from a signal value of  $1.5555 \pm 0.0002$   $\mu\text{m}$  to  $1.6201 \pm 0.0002$   $\mu\text{m}$ . This tuning range is limited by the mirror coating bandwidths of the IC and possibly photorefractive distortion. The transmission curve of the double HR mirror is constant over this wavelength range ( $R = 99\%$ ). The transmission curve of the IC begins to significantly increase after 1.62  $\mu\text{m}$ . The phase-matched signal wavelength becomes longer and the threshold increases drastically as the IC reflectivity drops. However, no measurements were done to measure threshold as a function of mirror reflectivity.

At 115  $^{\circ}\text{C}$ , the signal was  $1.5555 \pm 0.0002$   $\mu\text{m}$ . The reflectivities of both end mirrors at this wavelength are sufficient to sustain oscillation, as well as the transmission at the PPLN faces. At this temperature, the OPO may have ceased to run due to photorefractive distortion of the beams within the PPLN. This has been seen by other experimenters at a similar operating temperature (110  $^{\circ}\text{C}$ ) [20].

### 3. Intracavity OPO Experiment with Nd:YAG Laser

This chapter deals with our first intracavity OPO experiments using an Nd:YAG laser. This was the same laser used in the previous chapter to pump the external double pass OPO. Building the OPO within the laser cavity gives the OPO access to higher pump powers than would be available externally from the same laser. In addition to the higher pump powers, the OPO also has the benefit of a double passed pump beam which aides in lowering the threshold.

#### Thermal Lensing of Nd:YAG

Before we could design a stable cavity configuration for both the laser and the intracavity OPO, we needed to carefully characterize the thermal lensing properties of the Nd:YAG rod. Cavity layout and stability are dependent on the fact that the Nd:YAG rod within the laser acts as a current-dependent positive focal length lens.

The Nd:YAG rod is pumped by a Krypton ( $Kr^+$ ) arc lamp with the rod and lamp located at the foci of a gold plated elliptical cavity. Since the light emitted from the lamp is broad band, not all of it goes towards pumping the laser transition, the excess goes into heating the rod via UV absorption and  $Nd^{3+}$  nonradiative relaxation. With the lamp and rod at the foci of the ellipse, the rod can be treated as being uniformly heated by the lamp. Since a temperature gradient between the surface and center of the rod is created, a change in the refractive index occurs as well. The change in the refractive index is along both the radial and tangential directions of the rod, causing a thermally induced birefringence within the rod [22].

One effect of the thermal birefringence is in the polarization of the beam. Nd:YAG will naturally lase unpolarized. Insertion of a Brewster plate within the cavity increases the losses to the  $s$ -polarized light allowing only the  $p$ -polarized light to lase.

Due to the index variation within the rod, the polarization is not uniform. The thermal birefringence leads to a spatial variation of the polarization.

Thermal lensing of the rod is mainly a result of the radial change in the refractive index [19]. The radially dependent refractive index change across the rod can be modeled as a quadratic variation which can be written as [23]:

$$n(r) = n_0 - \frac{1}{2} n_2 r^2 \quad 3.1.1$$

where  $n_0$  is the index of refraction of Nd:YAG which is 1.81633 @ 1.064  $\mu\text{m}$ . The  $n_2$  term corresponds to a spatial rate of change of the refractive index. This term is dependent on the optical pumping power incident on the rod and has units of inverse length squared. The coefficient  $n_2$  can be experimentally determined by sending a probe beam through the rod and measuring the probe beam behavior after the rod as a function of the  $\text{Kr}^+$  lamp current.

An HeNe laser was collimated, apertured to the rod diameter of 4 mm and then sent through the rod. Next the  $\text{Kr}^+$  lamp was turned on and the temperature was allowed to stabilize. With the rod now acting as a lens, the HeNe laser came to a focus after passing through the rod. The beam emerging from the rod was profiled via the knife edge technique to determine the location of the minimum waist (focus). These measurements were done at five currents and the results are shown in Fig. 8 below:

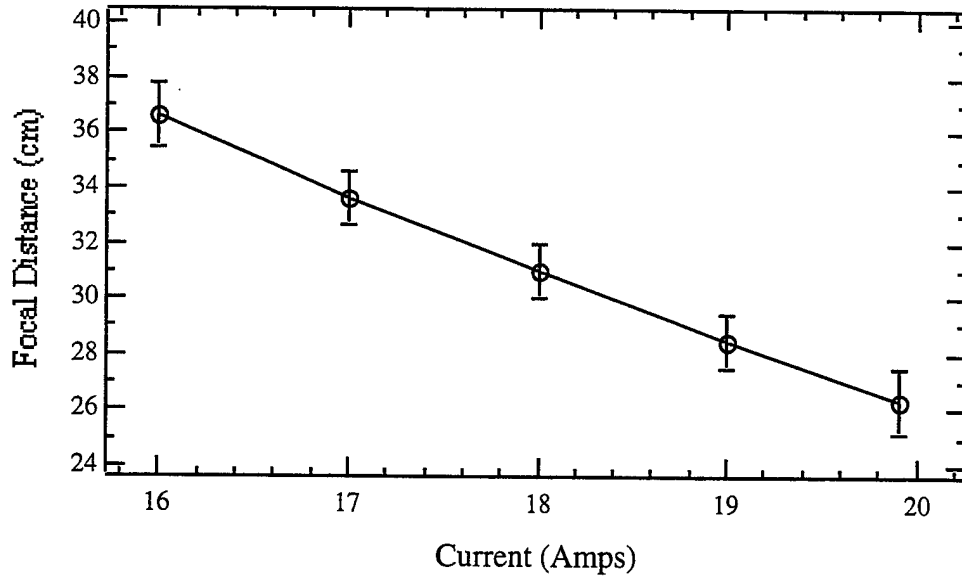


**Figure 8. Thermal Lensing of Nd:YAG vs. Current.** Focal distances were determined by doing a knife-edge scan of a HeNe laser after passing through the Nd:YAG rod and locating the minimum waist at each current.

The focal distance values are the distances from the end of the rod to the location of the minimum waist. Note, the voltage across the arc lamp is ~8 kV therefore the current values can be replaced by a pumping power in watts. At 19.9 amps, the power pumping the rod is ~160 kW.

From this data,  $n_2$  can be determined using the approximation from reference [23] that:

$$n_2 \approx \frac{1}{Lz_f} \quad (3.1.2)$$

where  $L$  is the length of the Nd:YAG rod and  $z_f$  is the focal distance from the end of the rod. The approximation involves the fact that the HeNe laser is collimated and that  $z_f > L$ , the focal distance being greater than the length of the rod.

With this information, the rod can now be modeled at different pumping levels, or currents. The Nd:YAG rod was modeled within PARAXIA as a Gaussian duct, a radially varying index. The procedure in Appendix A describes the steps taken to design the OPO cavity.

### Early Intracavity Attempts

With an understanding of the thermal lensing of the rod, a cavity design was proposed. This design was built within the housing of the Spectra Physics laser. The design used two lenses placed in one leg of the cavity. These lenses were used for mode matching between the pump and OPO cavities. The BK7 lenses had the same coatings and damage specifications as the mode matching lenses used in the double pass experiment. Two ZnS meniscus lenses were then placed between the mode matching lenses to define the OPO cavity. The ZnS lenses had an HR coating on the concave surface for the signal and an AR coating on both surfaces for the pump and idler wavelengths.

A stable cavity with these elements was designed using PARAXIA. Figure 9 shows the layout of this cavity:

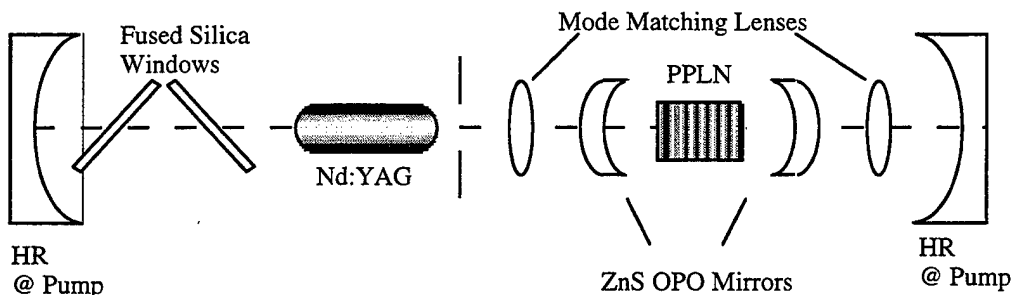


**Figure 9. Initial Layout of Intracavity OPO.** This was the cavity design for the first attempt at an intracavity OPO. The OC of the Nd:YAG laser has been replaced by a HR mirror. The OPO cavity is defined by the ZnS meniscus mirrors.

With this setup, the PPLN was never inserted because after all the elements were in place and the laser was running, intracavity power was only a few watts, barely at threshold for the OPO. The main problem was that there were too many elements within the cavity, each contributing to the overall loss and complicating the alignment. The ZnS optics were also found to have a centration problem. The center of curvature of the faces were not coaligned to the center of the substrate. Another difficulty was that since the laser

was still within its original housing, there was no convenient method of mounting optics within the laser cavity.

One method we used to simplify mounting of the extra OPO optics was to insert a 45 degree mirror within the laser cavity and have one leg of the laser accessible outside the housing. This worked but now the main problem was instability in the laser power level. Some of the components were not well stabilized allowing any external vibrations to be coupled into the laser. This was clearly evident when the Photon Inc. BeamScan device (model 1180-NIR) was used to observe the beam profile. The BeamScan essentially uses a slit on a rotating collar and a fast silicon photodiode to give a spatial profile of the beam in one axis. The head of the BeamScan unit can then be rotated to observe the beam in the other axis.

Sending the output of the BeamScan to an oscilloscope we were able to observe noise ripples on the beam. These ripples were constantly in motion. The source of the noise was traced to the hardware used to mount the turning mirror and mode matching lenses. They were coupling vibrations from the water pump and hoses to the laser beam. By applying pressure on these mounts, the amount of noise in the beam could be made to change.

A decision was made to start over on the intracavity experiment. The laser would be removed from its housing and directly setup on an optics table. It was also decided that better optics would be needed. The ZnS meniscus lenses were available at the time but were inadequate as input couplers. During the double pass experiment from the last chapter, a ZnS mirror was tried as an input coupler but the OPO never ran in this configuration. As a check, the ZnS mirror was used as an OC. The green due to doubling from the PPLN was severely scattered by the OC. These optics appeared to give excessive scatter to a beam transmitted through them. When a green beam was transmitted through them, a bright center spot was visible but around this spot was

scattered green light. Scattering was not seen when a  $\text{CaF}_2$  substrate optic was used as an OC. We believe that the coating on the ZnS optic was of poor optical quality.

It was decided to purchase two sets of optics for the intracavity experiment. One was the double HRs already described in the double pass experiment. The second was a dichroic beamsplitter to allow the pump and OPO cavities to be separated. For the layout shown in Fig. 9, the OPO cavity would be directly coupled to the laser cavity. There was no easy method of extracting the signal and idler or turning the OPO cavity off without affecting the laser. The beamsplitter ordered was a  $\text{CaF}_2$  substrate window, 4 mm thickness, inserted near Brewster's angle for the signal wavelength of  $1.57\text{ }\mu\text{m}$ . This optic had an HR coating on one surface to reflect the  $p$ -polarized pump as well as transmit the  $p$ -polarized signal and idler beams. The second surface was uncoated. Since we were worried about losses at the pump wavelength, this optic was ordered with the main specification being high reflectivity at the pump followed by high transmission at the signal. The double HR mirrors arrived before the beamsplitters and because of this we conducted the double passing pump experiments first. Once the beamsplitters arrived, work was again undertaken on the intracavity experiment.

### **Modified Intracavity Layout**

The general design of the intracavity OPO with the new optics is shown in Fig. 10. The overall number of optics has been reduced, compared to Fig. 9 and the OPO can be turned off by either misalignment of mirror M2 or physically blocking the path between M2 and the beamsplitter.

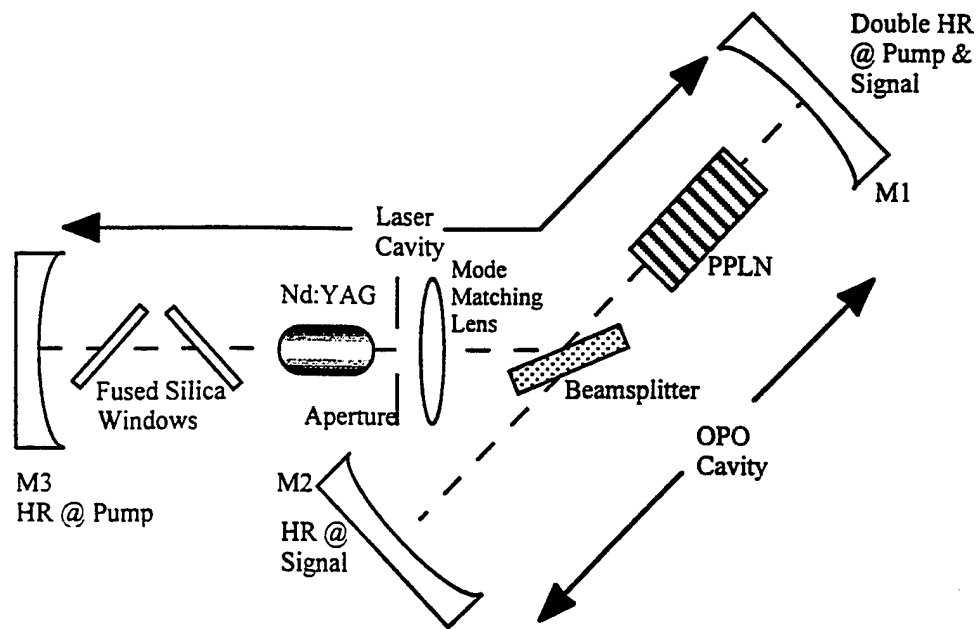


**Figure 10. General Intracavity Layout with Beamsplitter and Double HR Mirror.** The pump laser cavity is defined by M3, the beamsplitter and M1. The OPO cavity is defined by M1 and M2. The OPO can be turned off by blocking M2 without affecting the pump laser alignment.

The pump laser cavity is defined by the path from M3, through the Nd:YAG rod and mode matching lens, reflected off the beamsplitter, through the PPLN and reflected off the double HR (M1). Mirror M3 can be either the OC for the Nd:YAG laser or another HR mirror. The OPO cavity is defined by mirrors M1 and M2. To ease mounting of the components the polarization of the pump beam was horizontal. Since the beamsplitter transmits only *p*-polarized light at the signal, the PPLN is mounted on its side. If the pump laser was polarized vertically, then due to the beamsplitter, the OPO cavity would have to be mounted at an angle above the table. Horizontal polarization of the pump beam allows all the components to be in a plane parallel to the table top.

After designing and setting up a cavity per Appendix A, the pump laser was turned on and aligned for power. Next, the PPLN was inserted and adjusted until the laser was running again. For the first few weeks in which this setup was tried, the OPO never ran CW. It could be made to run by tapping either on the optical table or one of the

mounts holding an optical component. This tapping phenomena was seen during the double pass experiment and was attributed to spiking of the laser as mentioned earlier.

With no success running the OPO in this setup, the cavity was reconfigured without the beamsplitter. This was done to minimize the number of components within the OPO cavity. The layout is shown in Fig. 11 (Cavity I, Appendix C) and is essentially the double pass experiment within the laser cavity, the other leg of the laser was kept the same. The IC was the same optic used for the double pass OPO experiment.

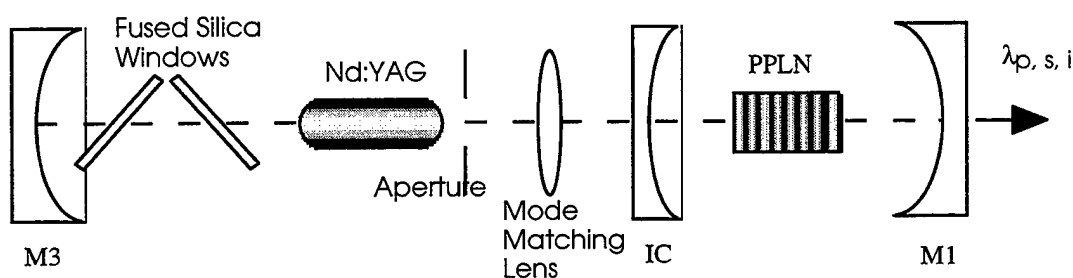


**Figure 11. Linear Intracavity Setup (Cavity I).** This is the intracavity set-up using the double pass OPO cavity within the Nd:YAG cavity.

In this arrangement, the intracavity OPO ran for the first time. Idler power from the OPO was ~100 mW.

With an OPO running, and having wavelengths at ~1.5  $\mu\text{m}$  and ~3.3  $\mu\text{m}$  available, these were used to test the transmission of the beamsplitter. An attempt was made to test the transmission of the beamsplitter using a Perkin Elmer Lambda9 Spectrophotometer. The beamsplitter was inserted at 55 degrees but this translated the beam in one leg of the spectrophotometer giving a false reading. Two beamsplitters at opposite angles could be inserted such that any translation by one is compensated for by the second but there was not sufficient room in the sample holder to place two optics in this manner.

Conversations with the coating engineers at Coherent who fabricated the beamsplitters suggested that the optimum transmission angle for the signal may not be exactly 55 degrees. This is Brewster's angle for the signal wavelength incident on  $\text{CaF}_2$  from air but the coating on one surface of the beamsplitter appears to change the angle of

optimum transmission. Using the signal from the OPO, transmission through the beamsplitter was measured as the incidence angle was varied. Care was taken to capture all of the transmitted beam with the power meter. These results indicated that the optimum transmission angle was not 55 but between 56 and 57 degrees.

The intracavity OPO was rebuilt with the beamsplitter now placed in the cavity at an incidence angle of 56 degrees; unfortunately, the OPO was still only flashing on. Since there was now a better incidence angle on the beamsplitter, the next approach was to optimize the alignment of the OPO cavity independent of the pump cavity. Although adjustment of M2 allows control of the OPO, true alignment of the OPO involves use of both M1 and M2 simultaneously. Unfortunately, adjustment of M1 also affects the alignment of the pump laser cavity. To avoid this problem, the input coupler from the double pass experiment was again utilized. Figure 12 shows the new setup for the OPO end of the laser cavity (Cavity II, Appendix C).

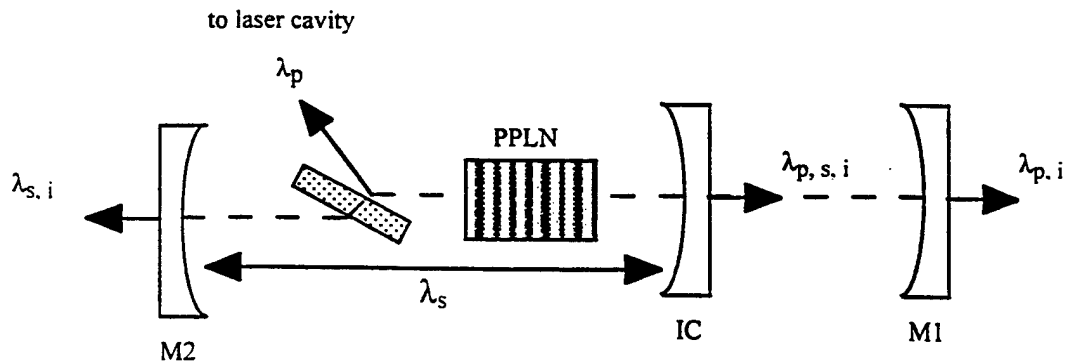


**Figure 12. Intracavity OPO with Beamsplitter and IC (Cavity III).** This is the intracavity layout using the IC from the double pass OPO experiment as well as the beamsplitter.

The signal beam now resonated between M2 and the IC. Mirror M1 was the same double HR as before but now it was used to reflect only the pump beam. It also blocked any signal leaking past the IC so that power measurements after M1 only contained pump and idler.

In this setup (Cavity II), the OPO could be aligned with little, albeit some, affect to the pump cavity by the IC. In this method, the intracavity OPO ran for the first time with the beamsplitter in, allowing the OPO to be turned on and off without any physical adjustments to the pump cavity. It was realized that alignment of the intracavity OPO was much more difficult than originally anticipated.

## Results

Figure 13 shows signal and idler powers measured after M1. The beam emerging from M1 has a mixture of the pump, signal and idler as well as green and red all superimposed on one another. Although mirror M1 has an HR coating at the pump and signal wavelengths, the reflectivity is not 100%. The magnitudes of the pump and signal beams are on the order of a few watts within the cavity such that the transmitted beam is on the order of milliwatts, comparable to the power of the idler beam.

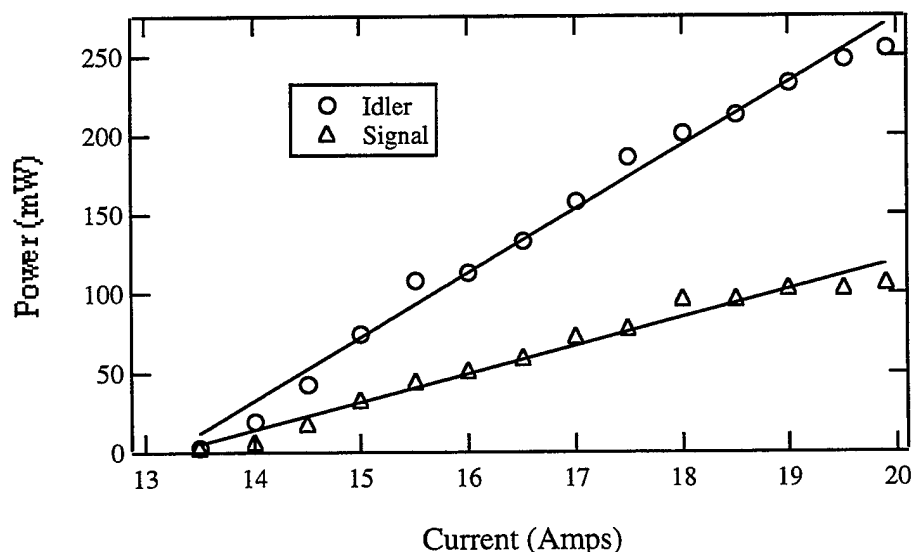


**Figure 13. Signal and Idler vs. Current (Cavity II).** Signal and idler powers as a function of lamp current for the Nd:YAG laser. Measurements were made after M1. Peak idler power was 255 mW, peak signal was 107 mW.

The idler powers were determined by insertion of a Ge filter before the power meter. The bandgap wavelength of Ge is  $1.88 \mu\text{m}$ , effectively blocking the signal and lower

wavelengths and transmitting solely the idler. The Ge is AR coated for the longer wavelengths and its transmission at the idler wavelength was measured to be  $92 \pm 1 \%$ . To separate the signal from the pump and idler beams a  $1.0 \mu\text{m}$  HR mirror was used. This mirror was also coated to transmit  $\sim 30\%$  of the signal beam. No pump was transmitted and the idler was absorbed by the substrate.

Threshold from Fig. 13 was at 13.5 amps and the OPO ran until the current limit was reached at 19.9 amps. Maximum idler power was about 250 mW and the maximum signal was just over 100 mW. These measurements include only the power emanating from one end of the OPO, after M1. Similar power levels can be expected from the other end, although these will be slightly less due to losses from the beamsplitter, but the power emerging from M2 was not measured at this time.

The slope efficiency of the idler is  $40 \pm 1 \text{ mW/Amps}$  or 0.0005% overall wallplug efficiency taking into account the 8 kV across the arc lamp. The signal slope efficiency is  $17.6 \pm 0.8 \text{ mW/Amp}$  or 0.00022% overall wallplug efficiency. The wallplug efficiency of the signal is low since the signal was not intended to be coupled out of the cavity, the OPO end mirrors are both intentionally HR at the signal.

Figure 14 shows the pump power measured external to the cavity (Cavity II). These values were measured after M3, where both signal and pump were present. To separate out the pump a prism was used to disperse the beams. A calibration to intracavity power was not done for this measurement so the pump power values indicate the trend of the circulating intracavity power.

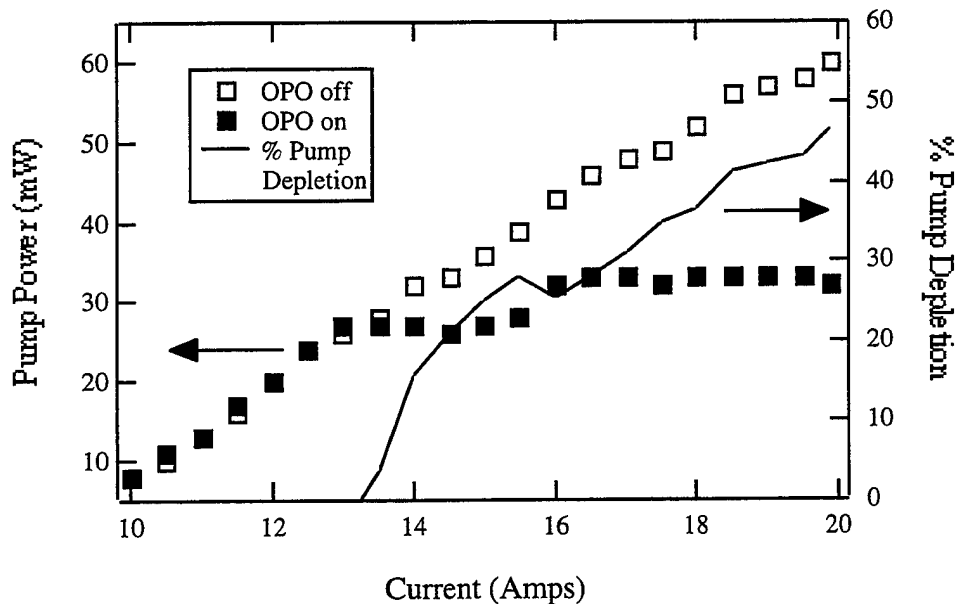


**Figure 14. Pump Power with OPO On and Off (Cavity II).** Pump power measured after a prism to separate the wavelengths. The plot shows the trend of the intracavity power. Pump depletion is 47% at 19.9 amps.

Significant clamping of the pump is observed once the OPO reaches threshold at 13.5 amps. The pump depletion after the OPO turns on quickly, rises and reaches a maximum of 47% at 19.9 amps. This was at about 1.5 times above threshold.

For this cavity (Cavity II), the distance from M3 (600 mm ROC) to the rod face was 375 mm, from the rod face to the lens was 215 mm. The BK7 lens was plano concave with the plano surface towards the rod. The lens was 5.1 mm thick and the ROC of the second surface was 25.8 mm. The distance from the second surface of the lens to the first surface of the PPLN was 77 mm and from the second PPLN surface to the curved surface of the IC was 31 mm. The distance from the plano surface of the IC to the double HR end mirror (100 mm ROC) was 71 mm. The uncertainties in all the distance measurements were  $\pm 1$  mm. At 19.9 amps this cavity produced a pump beam waist of 59  $\mu\text{m}$  at the center of the PPLN. This gives an  $L/b_p = 0.56$ . The signal waist produced by the OPO cavity was 54  $\mu\text{m}$  ( $L/b_s = 1.0$ ).

The beamsplitter was located 47 mm from the second surface of the lens. This distance is only important to allow enough room to mount the beamsplitter close to the

PPLN to keep the OPO cavity short. The distance from M2 to the uncoated surface of the beamsplitter was 72 mm and the mirror was 100 mm ROC.

Within the cavity there was a 0.065" (1.65 mm) diameter pinhole located between the rod and the lens. With the pinhole in the cavity, the pump laser operated single transverse mode (multilongitudinal mode). Removal of the pinhole increased the intracavity power but the pump would operate with multiple spatial modes. With the pump laser operating in multiple transverse modes, the OPO would not run. As the intracavity apertures were increased, the spatial modes of the pump beam increased and the OPO power quickly decreased and would cease operating.

There was also noise on the pump beam with the OPO on. Blocking M2 and observing the pump beam with the BeamScan showed a clean Gaussian with very little noise, although there was still some noise evident, mainly due to mechanical vibrations. When the OPO was allowed to run, there was significant noise in the beam. This was probably due to vibrations in the M2 mirror since the rest of the OPO is contained within the pump cavity and mounted on the same breadboard. M2 was mounted independently of the OPO cavity.

Figure 15 below shows signal and idler powers vs. current for Cavity III in Appendix C. This data was collected about 2 weeks after the data in Figs. 13 & 14. The overall cavity layout was similar but some distances were changed in an effort to improve the stability of the pump laser. Cavity stability was determined by calculating the overall ABCD matrix of the cavity and using the stability criteria of  $(A+D+2)/4$ . A stable cavity has a value between 0 and 1. The stability of the pump laser from the previous data (Cavity II) was 0.57 at 16.0 amps and 0.84 at 19.9 amps. In the following cavity (Cavity III), the stability was 0.51 at 18.0 amps and 0.63 at 19.9 amps.

In Fig. 15, the first instance of signal clamping is observed in the intracavity OPO (Cavity III). Idlers 1 and 2 correspond to idler power measured after mirrors M1 and M2, respectively. The cavity setup for this was 365 mm from M3 to the face of the rod, 450

mm from the opposite rod end to the lens. The same lens was used as before. The distance from the second surface of the lens to the PPLN was 49.5 mm. The distance from the second face of the PPLN to the IC was 31 mm and from the IC to the M1 was 71.3 mm. Mirror M2 was the same as before. The layout of the OPO cavity remained the same.

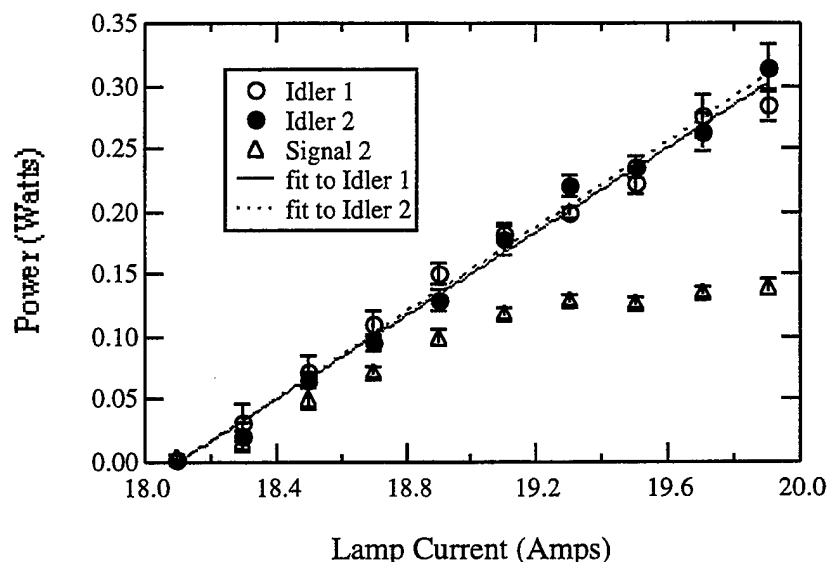


**Figure 15. Best Signal and Idler Power from the Nd:YAG Setup (Cavity III).** This is the most idler and signal power measured from the intracavity OPO using the Nd:YAG laser. Significant clamping of the signal is observed.

The greater idler powers compared to Fig. 13 may be due to better mode matching between the pump and signal beams. From 18.0 to 19.9 amps, the pump waist went from 42 to 47  $\mu\text{m}$ . ( $L/b_p$  of 0.91 and 1.1, respectively). In the previous cavity corresponding to Fig. 13,  $L/b_p$  was 0.32 at 16.0 amps and 0.56 at 19.9 amps.

The higher threshold, 18.0 vs. 13.5 amps (Cavity III vs. Cavity II), may be due to usage of the Nd:YAG rod. In this cavity, the mode size of the pump beam was cylindrical throughout the rod. The radius of the pump beam was  $\sim 300 \mu\text{m}$  at both ends of the Nd:YAG rod. In the previous cavity, the pump beam was not uniformly shaped throughout the rod. At one end of the rod, the beam radius was  $\sim 510 \mu\text{m}$  and at the other end the beam was  $\sim 380 \mu\text{m}$ . About twice as much volume of the Nd:YAG rod was used

in the first layout (Cavity II) indicating more intracavity power for a given current in this setup. This may explain the lower threshold in Fig. 13 (Cavity II) compared to Fig. 15 (Cavity III).

The slope efficiency of idler 1 was  $167 \pm 3$  mW/Amp or 0.002% wallplug efficiency. Idler 2 slope efficiency was  $171 \pm 3$  mW/Amp or 0.002% wallplug efficiency as well. These efficiencies are an order of magnitude greater than the results from Fig. 13 mainly due to greater output power over a shorter current range.

Pump powers with the OPO on and off were recorded as well but the values with the OPO on were much more erratic compared to the results in Fig. 14. The pump powers in this case were measured after M1, where there is also signal and idler present and these probably interfered with the pump measurements. Pump clamping similar to the previous plot was not seen.

### Remarks

The main problem with this OPO was lack of day to day reproducibility. The data shown in Figs. 13 and 14 was taken in one day. After the data was taken, none of the optical components were touched, the laser was shut off by first turning the lamp off and allowing the water to run for a few minutes to gradually cool down the rod and then the water and PPLN oven were shut off. The next day, without making any adjustments, the oven was turned on and allowed to reach temperature. Next, the laser was powered on and allowed to reach operating temperature, but the OPO did not come on. This was a regular occurrence with this laser in that the operation of the OPO was not reproducible. The pump laser regularly came on but the OPO usually had to be readjusted through alignment of either M1, M2 or the PPLN, in order to turn on.

There were many things done to try and stabilize the system. One significant contribution was the mounting of the PPLN. The oven in which the PPLN was held was never intended to be mounted on its side. Since the depth of the oven was greater than

the thickness of the PPLN, mounting the oven on its side allowed some freedom of movement in the PPLN. Although this movement was slight, within a laser cavity it is enough to throw off the alignment. This problem was overcome by inserting a thin strip of aluminum foil between the PPLN and the oven lid, making sure that the aluminum foil was not too thick to stress the crystal.

Another mechanical problem was the 3-axis positioner holding the oven. This was a Newport Corp. fiber positioner unit which works very well in aligning the crystal. This unit has translational adjustment in 3-axes and angular adjustment in 2-axes. The problem was that the unit was also mounted on its side which it was not originally intended to do. Due to this some of the translational adjustments were not repeatable. This unit was later mounted correctly on its base and improvement was immediately seen in the PPLN adjustments.

## Conclusions

The best idler powers recorded in this setup are shown in Fig. 15 (Cavity III). Maximum idler output was  $310 \pm 20$  mW, recorded after mirror M2. All of the data displayed in this chapter was acquired with the cavity shown in Fig. 12 (Cavities II and III). This cavity was a modified version of the general intracavity layout of Fig. 10 with the addition of the IC from the double pass OPO experiment. Addition of this optic allowed a somewhat independent alignment of the OPO cavity relative to the pump laser. The main drawback was the additional loss due to an extra element in the cavity. The IC transmitted about 92% of the pump, causing 8% loss per pass by being inserted within the pump cavity. By inserting IC into the system, it demonstrated the alignment required to turn on the OPO within the laser cavity.

Although the intracavity OPO was made to run with this laser, there were definite concerns as to the reproducibility of any results that were obtained. On many instances, the OPO would run one day, not the next, and then operate the following day. By the

end, the mounting and positioning of most of the components had been reconsidered, but the main problem was the overall length of the laser and having components on separate bases. In the next chapter, many of these problems are overcome with the Nd:YVO<sub>4</sub> laser where the entire intracavity experiment now fits on a 1' x 2' breadboard. The Nd:YVO<sub>4</sub> was a definite improvement over the Nd:YAG laser in performance and day to day operation. While there were some issues with the Nd:YAG, laser there were many techniques learned which later sped the process of constructing the intracavity OPO with the Nd:YVO<sub>4</sub> laser.

#### 4. Intracavity OPO Experiment with Nd:YVO<sub>4</sub> Laser

This chapter continues the discussion of PPLN intracavity OPO experiments with the primary difference that we replaced the Nd:YAG pump laser with a neodymium doped yttrium orthovanadate, Nd:YVO<sub>4</sub> laser. Going to the diode pumped Nd:YVO<sub>4</sub> laser decreased the overall size of the experiment and improved the stability and reproducibility of the OPO.

##### Nd:YVO<sub>4</sub> Laser

The Nd:YVO<sub>4</sub> laser was purchased from Light Solutions Corp. in Mountain View, CA as a breadboard system (model # ORION-8CW-VB, serial # 96129). The 8W CW laser was initially a two mirror linear cavity with 150 mm ROC end mirrors. The Nd:YVO<sub>4</sub> crystal is a cube 4 mm per side and the distance from each crystal face to an end mirror was  $134 \pm 1$  mm. Beam diameter after the OC was  $0.6 \times 0.6$  mm with a divergence of  $5.9 \times 5.9$  mrad. The entire laser, and eventually the entire intracavity experiment, would be mounted on a 1' x 2' breadboard.

The laser is operated by first turning on the Neslab RTE Series Refrigerated Bath/Circulator (serial # 197053137-M983510). The set point is 10.5 °C so that the temperature of the laser diodes does not exceed 19° C. Next, the DC power supply is turned on. At present, the power supply in use is a Sorensen DCS 33-33 power supply. The laser is brought up by increasing the current to the diodes. Maximum current is 30.0 amps and the corresponding voltage is 5.5 V DC.

Another feature of Nd:YVO<sub>4</sub> is that it lases polarized without the use of a Brewster plate, eliminating any thermal birefringence problems. Lasing, as well as maximum absorption, occurs along the c-axis of the crystal. The absorption peak is at approximately 809 nm with a useful range of 801 to 821 nm ( $\Delta\lambda \sim 20$  nm). The degree of polarization was measured by setting this laser at 1W output and using a cube polarizer to

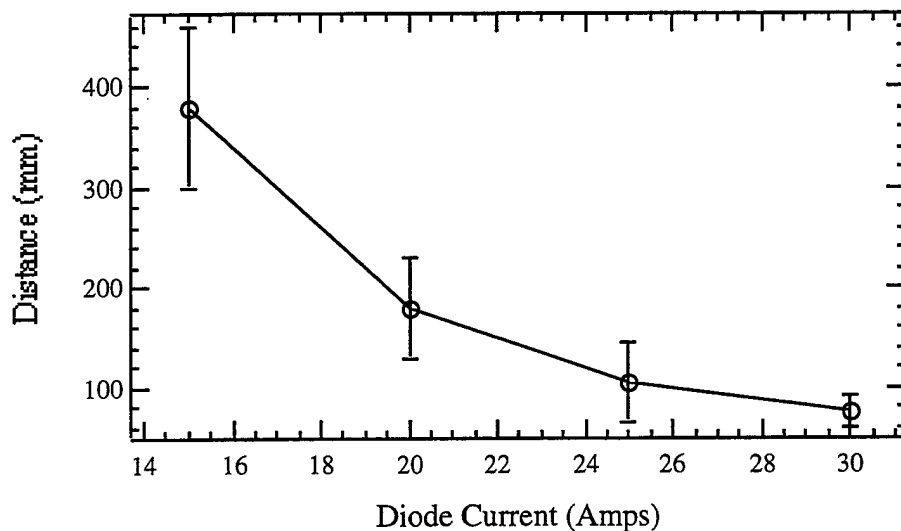
discriminate between the two orthogonal directions. By this method an extinction of  $90 \pm 10:1$  was measured. The setup in which this was measured was similar to Fig. 10 with M3 replaced by a  $1.06 \mu\text{m}$  partial high reflector, 80% R

Table 4 gives a comparison of the properties between Nd:YAG and Nd:YVO<sub>4</sub>. This table is a collection of the information found in References 24 and 25.

**Table 4. Material Properties of Nd:YAG and Nd:YVO<sub>4</sub>.** The pump bandwidth (75%) value describes the wavelength range over which at least 75% of the diode light is absorbed in a 5 mm path through the crystal.

	<u>Nd:YAG</u>	<u>Nd:YVO<sub>4</sub></u>
crystal class	cubic	tetragonal
laser $\lambda$ (nm)	1064.2	1064.3
linewidth (nm)	0.6	0.8
polarization	none	c
radiative lifetime ( $\mu\text{s}$ )	255	115
lifetime at 1 % atomic doping	220	100
peak pump $\lambda$ (nm)	807.5	808.5
pump bandwidth* (75%)	2.5	15.7
Thermal conductivity (W/m-K)	10.3	5.14
Knoop hardness ( $\text{kg mm}^{-2}$ )	1320	480
refractive index @ $1.064 \mu\text{m}$	1.81633	2.168

Figure 16 shows the thermal lensing of the Nd:YVO<sub>4</sub> as a function of diode current. These measurements were done similar to the thermal lensing measurements for the Nd:YAG, using an HeNe laser. At low currents there is little thermal lensing, but once above 15 amps the lensing quickly gains strength.



**Figure 16. Thermal Lensing of Nd:YVO<sub>4</sub>.** Thermal lensing measurements were done by measuring the location where the HeNe laser came to focus after passing through the Nd:YVO<sub>4</sub> crystal.

The data points are connected to show the trend in the data. The large uncertainties arise from multiple reflections due to the pumping optics at the HeNe wavelength (632.8 nm). These interfered in determining the exact position of the focus, especially at the lower currents. Later a CW Nd:YAG laser was made available to measure the thermal lensing. This laser was quickly set up and the output was collimated and sent through the crystal. Due to time constraints, the measurement was done quickly and only at 30 amps. This gave a focus of ~63 mm, within the uncertainty of the previous measurement of  $74 \pm 15$  mm.

Before operating the OPO, the polarization of the pump beam at the PPLN had to be corrected. Since Nd:YVO<sub>4</sub> lases polarized and due to the thermal contacts on the crystal and the method it was mounted within the heatsink, the polarization of the pump beam was vertical throughout the cavity. The polarization required at the OPO was horizontal due to how the PPLN and beamsplitter were mounted, as discussed in the last chapter. To correct the polarization, an HWP was inserted within the cavity between the mode matching lens and the beamsplitter. This allowed the correct polarization at both the OPO,  $\parallel$  to PPLN z-axis, and at the Nd:YVO<sub>4</sub>,  $\parallel$  c-axis. The HWP was AR coated for

1.06  $\mu\text{m}$  and introduced minimal loss to the cavity. Correct polarization at the OPO was verified by using the polarizing beamsplitter used in the external attenuator in Chapter 2. The cube was placed after M1 so that horizontal polarization would pass through. A power meter was then placed after the cube. Power transmitted as a function of HWP angle was observed and the HWP was left at a maximum transmission. Later when the OPO was running, the HWP angle was reverified by observing the change in idler power and the HWP was set to give maximum idler power.

## Results

The arrival of the Nd:YVO<sub>4</sub> laser coincided with the arrival of new PPLN samples. These samples were poled in-house but sent out for polishing and coating. These were the same samples described earlier in chapter 2. The following data, Fig. 17, was taken with sample 29.75-1 # 10.

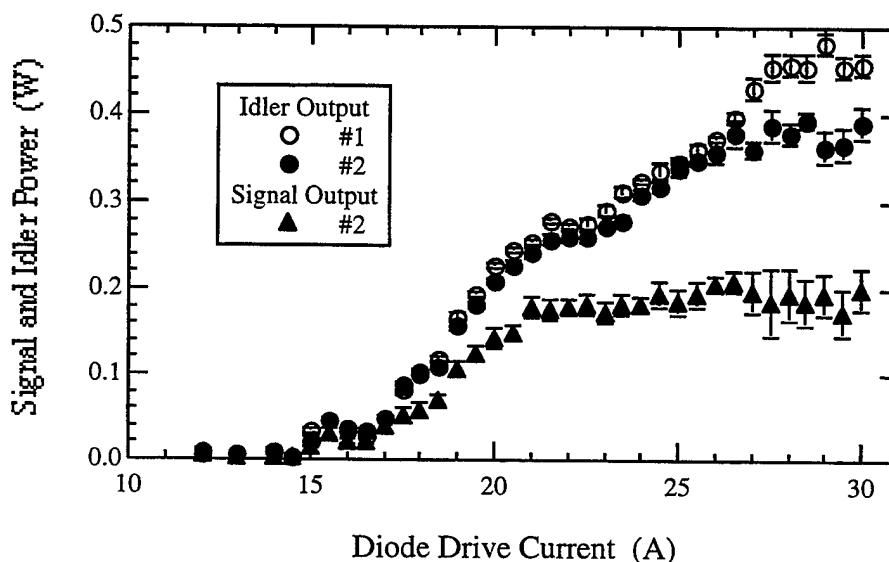


**Figure 17. Idler and Signal vs. Diode Current.** Maximum idler power was  $480 \pm 11$  mW, maximum signal was  $210 \pm 13$  mW. Signal clamping begins at 21 amps and idler clamping begins at 27.5 amps.

With this crystal, we have seen the most idler power produced in the intracavity experiment to date from a 25 mm long sample of PPLN. Maximum idler power was  $480 \pm 11$  mW from one end of the OPO. The oven temperature during this data collection was  $155.0^\circ\text{C}$  stable within  $\pm 0.3^\circ\text{C}$ . Outputs 1 and 2 correspond to signal and idler powers measured after mirrors M1 and M2, respectively. The signal powers at position 2 were determined by measuring the idler at M2, then removing the Ge filter and measuring the total power, which is composed only of signal and idler. The idler values are then subtracted from the filterless readings to give the signal value. Note, there is no pump leaking from M2. This has been verified by misaligning the OPO cavity with M2 and measuring the power after M2, which was below the detector noise level.

The cavity used for all of the results in this section is Cavity IV in Appendix C. Overall cavity dimensions are as follows: the distance from M3 to the face of the Nd:YVO<sub>4</sub> crystal was 70 mm. M3 was a double HR mirror with a 150 mm ROC. From the second Nd:YVO<sub>4</sub> face to the plano surface of the lens was 150 mm. This was the same mode matching lens used in the previous chapter (+50 mm focal length). The distance from the convex lens surface to the first face of the PPLN was 65 mm. The crystal length was 25.5 mm and the distance from the back PPLN surface to M1 was 19 mm. Mirror M1 had a 50 mm ROC. The exact location of the HWP is not critical for mode size as long as it gives the proper pump polarization at the OPO. All distances have an uncertainty of  $\pm 1$  mm. The other leg of the OPO was 25 mm from the front of the PPLN to the beamsplitter and 62 mm from the back of the beamsplitter to M2 which was 100 mm ROC.

Once the OPO was operating, the position of M2 was varied until the maximum idler output was found. Mirror M2 was then left at this position. With this cavity, the calculated sizes of the pump beam were  $80\text{ }\mu\text{m}$  over the length of the PPLN crystal and  $185\text{ }\mu\text{m}$  at the center of the Nd:YVO<sub>4</sub>. The signal waist was  $107\text{ }\mu\text{m}$ , located approximately 2.5 mm from the end of the PPLN closer to mirror M1.

The signal power is only shown from one end of the OPO cavity because of the filter used. After mirror M2 there is only signal and idler present, so by just measuring the idler using the Ge filter and then the power without any filter, the signal power can be determined. Measurement of the signal after M1 is more difficult because there is also pump interfering with the measurement. The idler is still easily measured by using the Ge filter. The pump and signal measurements are more difficult since they are only separated by  $\sim 500$  nm and few filters were available to separate to two wavelengths. A measurement of the signal after M1 was attempted, using the dielectric  $1\ \mu\text{m}$  HR mentioned earlier, which has partial transmission at the signal. While collecting the signal data after M1, it was discovered that the transmission across the mirror surface was not uniform.

To take the measurement, the dielectric mirror was slid into place before the power meter. After measurements at a few currents were done, the signal power readings appeared very erratic. At the next current, the mirror was inserted and a measurement was taken. Next, the mirror was moved such that the beam was incident on a different part of the surface and the power was remeasured. The two values did not coincide and the measurements with this mirror were disregarded. This problem was later corrected in Figs. 21 & 23 by ensuring that the positioning of the mirror was the same for all measurements.

In Fig. 17, the power in idler 1 is slightly higher than idler 2 because it sees less loss. After idler 1 is generated within the crystal, it immediately passes through mirror M1. Idler 2, after being generated within the crystal, passes through the beamsplitter and then through M2. The beamsplitter is inserted near Brewster's angle for the signal wavelength yet the difference in refractive index between the signal and idler, in  $\text{CaF}_2$ , is only  $\Delta n \sim 0.01$ . The difference in Brewster's angle between the signal and idler is minimal, 0.2 degrees. Loss at the idler may be due to the coating on the beamsplitter.

Another characteristic of Fig. 17 is the clamping of the powers. This is evident in the idler beginning at 27 amps and in the signal at 21 amps. The clamping of the signal was also observed in the Nd:YAG setup earlier, Fig. 15, but at the time it was attributed to a possible error in the data collection. Since then it has been verified that the signal is indeed clamping. The signal clamps in almost every instance of the intracavity OPO regardless of the laser or sample of PPLN used. What is perplexing is that even though the signal is clamping the idler power continues to increase.

Figure 18 below shows intracavity pump power with the OPO on and off (Cavity IV). The OPO was turned off by blocking mirror M2.

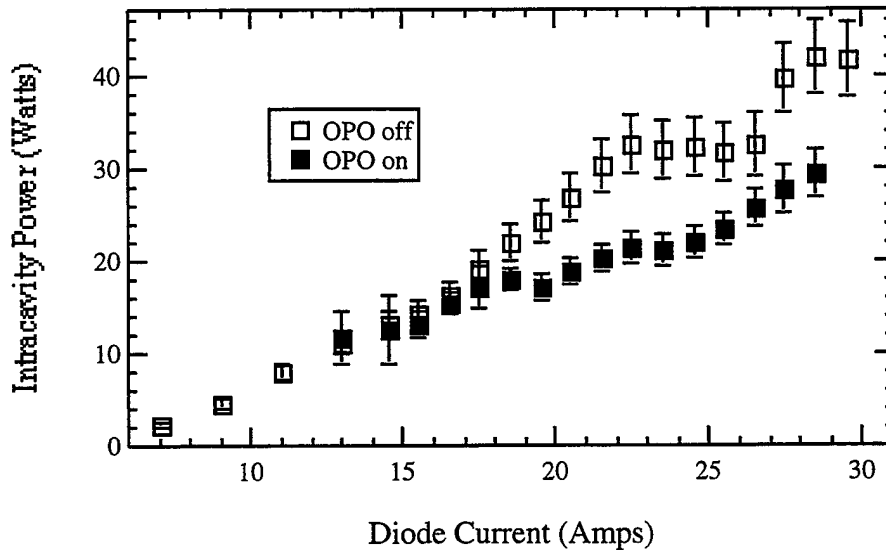


**Figure 18. Intracavity Pump Power with OPO On/Off.** Intracavity pump power measured after M3. Transmission of M3 was  $0.22 \pm 0.01$  % at the pump.

Threshold of the OPO is at ~11 W of intracavity pump power. Equation 4.2.1 is a modification of Eqn. 2.3.1 with the addition of the beamsplitter transmission at the signal

$$P_{th} = \frac{1}{2} \frac{2(1 - T_{B/S}^2 R_S)}{T_{B/S}^2 R_S} \left\{ \frac{\lambda_p \lambda_s \lambda_i n_s n_i \epsilon_0 c}{32\pi^2 d_{eff}^2 L} \right\} \left\{ \frac{\left(1 + \frac{w_s^2}{w_p^2}\right)}{h_{sm}} \right\} \quad (4.2.1)$$

Using Eqn. 4.2.1 and taking the beamsplitter transmission as 96%, the calculated threshold is 40.1 W. Here we used the average value 0.28 of  $L/b_p$  and  $L/b_s$  (using the PARAXIA calculated waists of  $w_p = 80 \mu\text{m}$  and  $w_s = 107 \mu\text{m}$ ). At this value of  $L/b$  the average value of  $h_{SM}$  was 0.25 [Refs. 10, 29, 30] and the waists used in Eqn. 4.2.1 are  $w_p = 83.6 \mu\text{m}$  and  $w_s = 102 \mu\text{m}$ .

The data in the above figure was collected by measuring the pump power leaking through M3. This mirror was identical to M1, double HR but with a different ROC. The transmission value was determined earlier by replacing M3 with an OC and recording the pump power after the OC and M1 as a function of current with the OPO off. The OC was labeled as 20% T so from these values the intracavity power could be determined and a comparison made to the powers measured after M1. The transmission of the double HR mirror was found to be  $0.22 \pm 0.01 \%$  at the pump wavelength (or  $R \sim 99.8\%$ ). The measurement at M3 is solely the pump, the Ge filter was used to check for any idler and the dielectric mirror mentioned earlier was used to check for any signal, neither of which were present.

With the OPO off the intracavity power in Fig. 18 seems to clamp from 22.0 to 27.0 amps and then continue to rise. What is happening is that the cavity (Cavity III) is going through a region of instability when the power clamps and the instability is being countered by greater pumping from the diodes. When this cavity was designed, only two regions of thermal lensing of the Nd:YVO<sub>4</sub> crystal were considered, the maximum and minimum. It was assumed that since the cavity was stable at these two points it would be stable at all points in-between. This was later discovered to not be true. Modeling the thermal lens between these two points shows a region of currents/focal lengths where the cavity goes unstable. The reason why the laser does not completely shut off is that the thermal lensing of the Nd:YVO<sub>4</sub> is astigmatic and because of the spatially localized gain in the laser-diode pumped Nd:YVO<sub>4</sub>.

The astigmatism arises from the Nd:YVO<sub>4</sub> crystal not being uniformly cooled in the horizontal and vertical directions. This leads to different horizontal and vertical thermal gradients causing different thermal lensing properties. Since the crystal acts as a different lens in the two axes, it may go unstable in one axis yet remain stable in the other.

It should be noted that in taking the data for the previous two graphs, the following was done. First the laser was turned on and the current was raised until the OPO came on. The system was allowed to stabilize for about 1 hour at 25 amps. Next an overall alignment was accomplished to optimize the output from the OPO. Next the current was raised to 30 amps and the alignment was checked to see if the idler output could be improved. Once the power was at a maximum, the system was allowed to stabilize for a few minutes. Data was taken first at M1 with the Ge filter. The dielectric mirror was inserted and the Ge filter removed, and finally data was taken with no filters in place. Next the meter was moved to M2 and the same three data sets were taken. Each data entry was an average of 500 points using the Newport Multifunction Meter (1835c). Finally, the power meter was positioned after M3 and the final measurement was done. Once all of these measurements were taken, the current was reduced by 0.5 amps and the system was allowed to stabilize before the next data run began. After all the OPO measurements were done M2 was blocked, OPO off, and the pump power after M3 was measured as a function of diode drive current.

The stability of the idler power is shown in Fig. 19 below (Cavity IV). This measurement was done at diode current of 30.0 amps corresponding to over 3 times OPO threshold. Idler power was measured after mirror M1 and the signal from the Newport power meter was sent to an oscilloscope. Idler power over this period was  $430 \pm 22$  mW or  $\pm 5\%$  stability. The y-axis is arbitrarily scaled below.

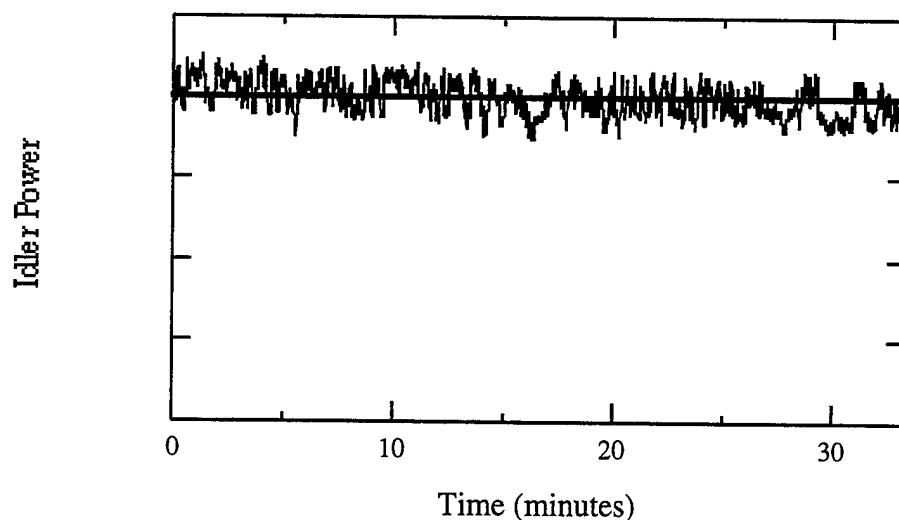


**Figure 19. Idler Stability.** Half-hour trace of the idler power measured at 30.0 amps. Average idler power over this period was  $430 \pm 22$  mW or  $\pm 5\%$  stability.

Figure 19 shows idler power over a half hour period. The OPO had been operating for  $\sim 1.5$  hours before collection of this data. A major improvement in using the Nd:YVO<sub>4</sub> laser over the Nd:YAG is overall stability and reproducibility. Having the entire intracavity OPO setup on a single breadboard is very advantageous. Another change from the Nd:YAG experiments is that the PPLN oven was left continuously on. This also appears to improve overall system stability. Once the OPO was aligned and running, it consistently came on day to day, perhaps not to the power of the previous day but having the OPO consistently turn on by only increasing the current was a major improvement over operation with the Nd:YAG setup. With the OPO running daily, changes made one day could easily be improved upon the next day.

After the power and stability measurements were done, a temperature tuning curve was generated for this OPO (Cavity III). The results are shown in Fig. 20 below:

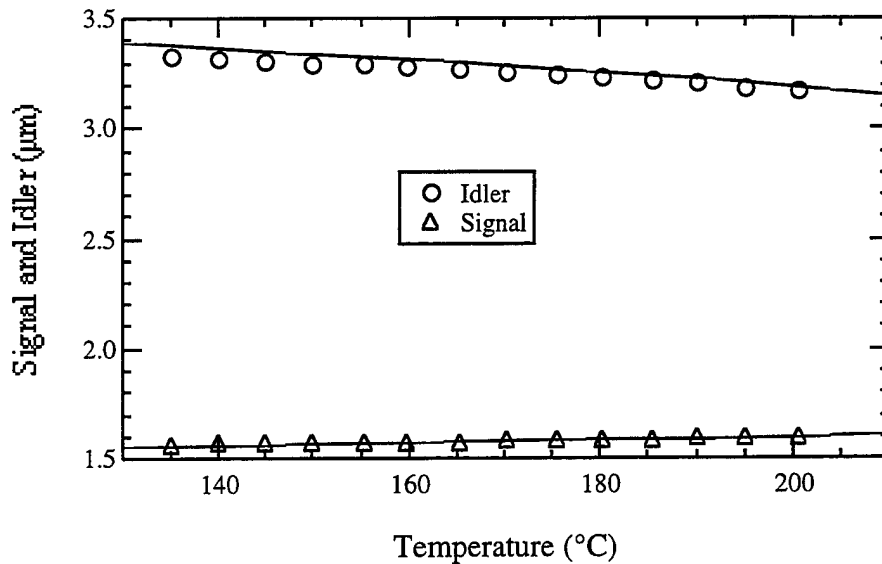


**Figure 20. Intracavity Temperature Tuning Curve.** Signal wavelengths were measured with a monochromator and a Ge detector. Idler wavelengths were calculated from the signal measurements.

The signal wavelengths were measured with a Ge detector and the corresponding idler values were calculated. The uncertainties in the measurements are within the markers and the overall measurements are within the uncertainties in the Sellmeier equation [15]. The OPO operated from 135 to 200 °C (  $\Delta T = 65$  °C). Over this range, the signal tuned from  $1.5639 \pm 0.0001$  μm to  $1.6008 \pm 0.0001$  μm (  $\Delta \lambda_s = 37$  nm) and the idler went from  $3.3316 \pm 0.0002$  μm to  $3.1756 \pm 0.0002$  μm (  $\Delta \lambda_i = 156$  nm).

The tuning range in Fig. 20 is not as large compared to the double pass OPO, Fig. 6. Additional losses from the beamsplitter limit the tunability range. The beamsplitter transmission curve is peaked at a single signal wavelength. On either side of the peak the transmission quickly falls off, increasing the losses at the adjacent wavelengths. The location of the transmission peak can be adjusted by varying the incidence angle upon the beamsplitter.

The PPLN coatings are high performance low loss coatings which are also considered a “soft” coating and somewhat more easily damaged. The cavity was originally set up with crystal 29.75-1 #8. After setting up and aligning the laser, the

power from the OPO would slowly decrease and eventually shut itself off. The oven temperature was varied in a search for a better operating wavelength but eventually the OPO stopped operating. The problem was determined to be the coatings on the crystal faces which had seriously deteriorated. There were burn spots on the end faces and the coatings around the edges of the crystal appeared chipped away. This sample of PPLN was replaced with sample 29.75-1 #10. This is the PPLN sample used for all of the 25-mm data presented in this chapter.

When this crystal was inserted into the cavity an effort was made to use the crystal starting at one end and propagating along the crystal face when necessary. As the temperature tuning data was taken, the OPO power would decrease for each temperature change. No alignment of the cavity would bring the power back up, only translation to a new spot on the crystal would increase the power. It was determined that changing the crystal temperature while keeping the pump beam incident on the crystal was detrimental to the coatings. Later this same crystal was used in the double pass OPO experiment and again the OPO was temperature tuned. The crystal was inserted so that the pump beam was incident on an unused portion of the PPLN face. In this instance the pump beam was blocked while the oven temperature was varied and the temperature was allowed to stabilize before the pump was allowed to reach the crystal again. This method did not seem to damage the coatings.

After the data in Figs. 17 through 20 was taken, the intracavity experiment had to be disassembled and the pump laser rebuilt in its original configuration. A pump laser was needed to redo the double pass OPO experiment. Afterwards, the intracavity OPO was rebuilt and data on two subsequent days was taken to examine the reproducibility of the laser.

Figure 21 shows signal and idler powers from the intracavity OPO operating at 155 °C. The cavity was rebuilt to the same dimensions as the previous cavity (Cavity IV), Fig. 17, in an effort to produce comparable results.

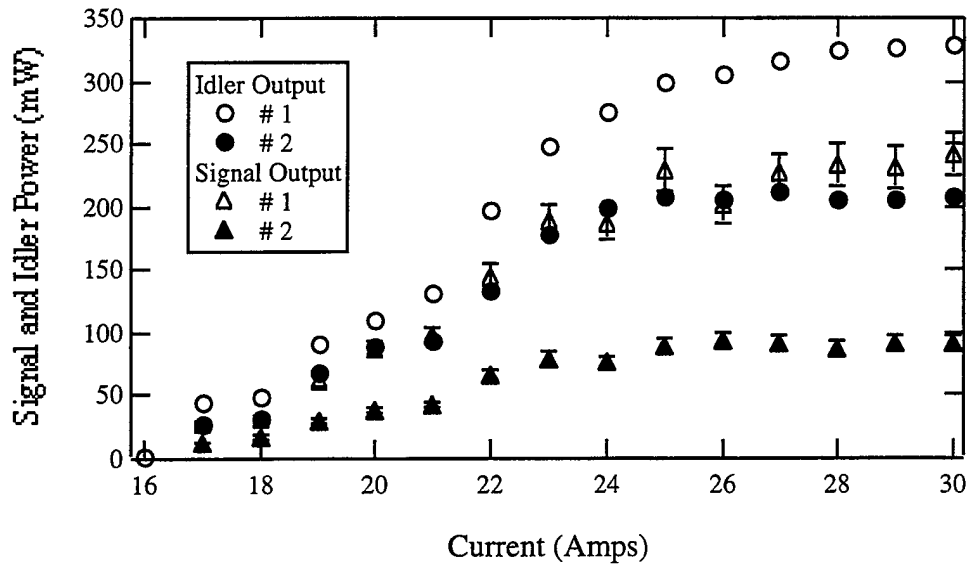


**Figure 21. Signal and Idler Powers #1.** This plot shows signal and idler powers measured from both ends of the OPO cavity.

The error bars for the idler measurements are within the circles. At 30.0 amps the powers were: idler 1 was  $328 \pm 8$  mW, idler 2 was  $208 \pm 6$  mW, signal 1 was  $240 \pm 17$  and signal 2 was  $91 \pm 6$  mW. In this data, the signal at M1 was found using the dielectric mirror mentioned earlier. This mirror was calibrated by finding the signal values at M2, as explained previously, and comparing those values to the ones measured using the dielectric mirror after M2. The transmission of the mirror at the signal was found to be  $28 \pm 2\%$ . The position of the dielectric mirror after M1 and M2 was fixed so that the beam emanating from each end of the OPO was incident on the same part of the dielectric mirror.

Figure 22 shows the intracavity power of this setup (Cavity IV). These measurements were done analogous to the previous intracavity power measurements and show an intracavity threshold of about 11W. The error bars are mainly due to the uncertainty in the transmission of mirror M3,  $\pm 5\%$ . Maximum pump depletion is 35% at 28.0 amps.

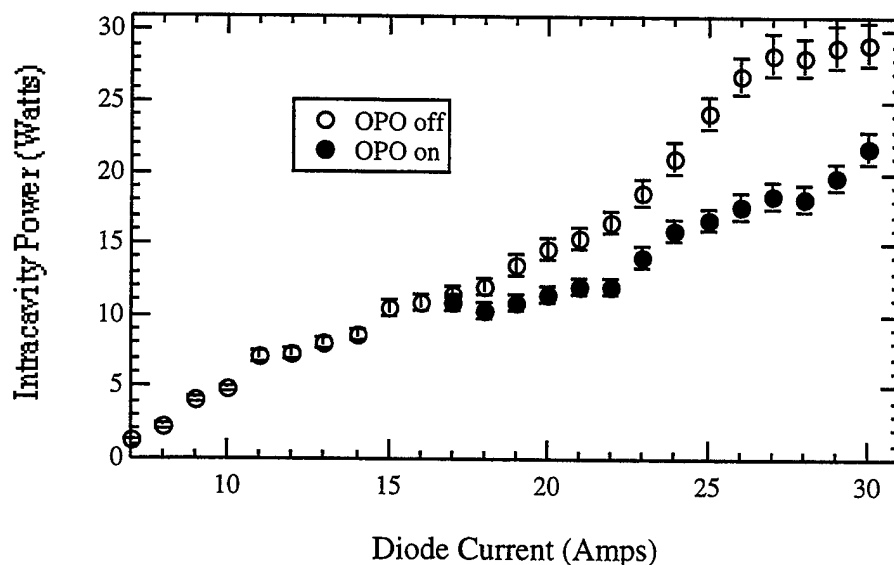


**Figure 22. Intracavity Pump Power.** This is the intracavity pump power corresponding the signal and idler power from Fig. 21.

The OPO turns on in both of these plots, Figs. 18 and 22, at about 11 W of circulating intracavity power but the intracavity power with the OPO off is not identical. This may be explained by an increase in losses within the cavity. When the cavity was built for the second time, care was taken to keep the distances between the cavity elements the same as before. Assuming the cavities are identical, then the decrease in pump power can be explained by an increase in losses due to degradation of the PPLN coatings.

Another difference between Figs. 18 and 22 is that with the OPO off, the pump power does not behave identically. In Fig. 18, the pump power clamps, with the OPO off, from 22.0 to 27.0 amps and then increases from 27.0 to 30.0 amps. Under the same circumstances, the pump power in Fig. 22 clamps from 27.0 to 30.0 amps. While both cavities were built to the same dimensions, Cavity IV, distance differences of a millimeter, especially between the lens and the Nd:YVO<sub>4</sub> crystal, affect the cavity stability with regards to thermal lensing.

During the period between the two cavities, Figs. 17 and 21, the double pass OPO experiment was rebuilt. The same PPLN, 29.75-1 #10, was also used in the double pass

setup. Once the temperature tuning and stability data for the double pass experiment had been collected and before rebuilding the intracavity OPO, the PPLN was cooled down and examined under a microscope. Damage to the coatings had increased since this sample was first used. There were some burn spots evident and the coating near the edges of the PPLN had degraded. Although the coatings had deteriorated, there remained a usable amount of undamaged area on the faces.

As seen previously in the intracavity experiments with the Nd:YAG, the pump power should clamp at the OPO threshold value but it doesn't in either of the setups with this laser. In Fig. 18 once the OPO turns on, the intracavity power continues to rise, goes flat from 17 to 20 amps and then continues to rise again. In Fig. 22 the pump appears to initially clamp when the OPO turns on at 17.0 out to 22.0 amps but at 23.0 amps it begins to rise again. The pump appears to clamp again from 25.0 to 28.0 amps. The different clamping regions may be due to a change in the pump mode requiring a higher threshold as the pump goes to a higher order transverse mode.

Figure 23 is a data set similar to Fig. 21 but taken 6 days later. Measurements were done in the same method as Fig. 21. The idler error bars are within the circles. At 30.0 amps the powers were: idler 1 was  $324 \pm 4$  mW, idler 2 was  $229 \pm 4$  mW, signal 1 was  $163 \pm 11$  and signal 2 was  $89 \pm 6$  mW.

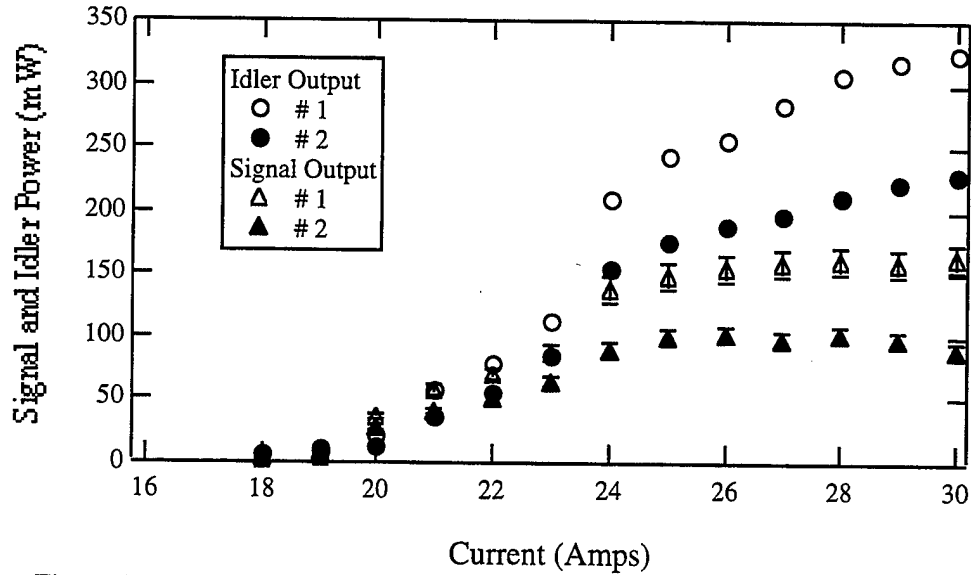


**Figure 23. Signal and Idler Power #2.** Measurements of signal and idler powers from both ends of the OPO cavity. These measurements were done analogous to the method used to generate figure 21.

In the period between data collections, Figs. 21 and 23, the following changes to the cavity (Cavity IV) were made. Mirror M3 was replaced with an OC. The mirrors had the same ROCs and were swapped by just removing the optic from the mount without loosening the base so that the distances were kept the same. M3 was then aligned by maximizing the idler power. Next, the fused silica intracavity attenuators were inserted in-between the Nd:YVO<sub>4</sub> crystal and the mode matching lens. There was adequate room for the attenuators to fit, none of the cavity dimensions were changed. Power vs. intracavity attenuator loss was measured at a number of currents and will be discussed in Section 4.5. Once these measurements were accomplished, M3 was replaced by the double HR mirror and realigned to optimize idler output. The fused silica windows were also removed. The PPLN oven was left on the entire time at a set point of  $155.0 \pm 0.3$  °C.

Although the threshold is higher in Fig. 23 (18.0 amps) compared to Fig. 21 (16.0 amps), most of the OPO powers measured at 30.0 amps are similar. The largest disagreement is between the measurements for signal 1. While signal clamping begins at similar currents, 23.0 amps for Fig. 21 and 24.0 amps for Fig. 23, signal 1 at 30.0 amps is

$241 \pm 5$  mW (Fig. 21) and  $163 \pm 11$  mW (Fig. 23), a difference of almost 80 mW. Since the other OPO powers are very similar, the disagreement between the signal 1 measurements may be due to the data collection, namely the position of the dielectric mirror. As mentioned before, the transmission across the face of the mirror is not uniform. Although every effort was made to take both data sets in an identical manner, the position of the dielectric mirror after M1 may have changed.

Note, clamping of the signal in Fig. 17 begins at 21 amps, when the pump begins to rise. The same comparison can be made between Figs. 21 and 22. At 23.0 amps the signal power begins to clamp while the pump which was clamped begins to rise. In both of these instances, the slope of the idler beam decreases when the signal beam begins to clamp. The clamping of the signal and idler may be attributed to the rollover of the intracavity pump power seen in Fig. 22 with the OPO off. In the region from 26.0 to 30.0 amps the intracavity pump power is constant at 29.0 watts.

Figures 21 & 23 were attempts at measuring the repeatability of the OPO performance keeping the cavity layout identical (Cavity IV). In these graphs, the performance, idler power, of the OPO was not as high as the results shown in Fig. 17. An explanation for this may be damage to the PPLN coatings as explained earlier.

Another reason for the decrease in performance is that the experiment was disassembled and rebuilt in the period between Figs. 17 and 21. This was necessary in order to pump the double pass OPO experiment. Although every effort was made to rebuild the laser to the same dimensions, there could easily be distances off by a few millimeters at certain locations which could have a large impact on the beam size within the cavity. It appears that the distance between the Nd:YVO<sub>4</sub> and the mode matching lens is the most critical parameter. This has the largest impact on the overall mode size of the pump beam within the cavity. Differences of a few millimeters can change not only the size of the pump beam at the crystal but also affect the overall stability of the laser. The distance between the Nd:YVO<sub>4</sub> and M3 appears to be the most insensitive to

position, relatively speaking. This distance can usually be varied by tens of millimeters with hardly any change to the performance of the OPO.

### Signal Investigation

Clamping of the signal has been observed in most of the OPO output power data collected. Since the idler powers continue to increase after the signal clamps, one thought was that perhaps the measurements of the signal power were being done incorrectly or the measurements were influenced by the other wavelengths. As a check, a measurement of the signal on the opposite side of the beamsplitter was done. While highly transmitting at the signal ( $T \sim 96\%$ ), a few percent of the signal beam is reflected each time it strikes the beamsplitter. The detector was located where the word "beamsplitter" in Fig. 10 is. This location measures pump leaking through the beamsplitter coming from the mode matching lens and signal first reflected from M2 and then from the uncoated surface of the beamsplitter. At this location, there is only pump and signal present, there is no idler since all the idler passing through the beamsplitter leaves through M2. This was verified by power measurements done with the Ge filter indicating the lack of idler present.

From the transmission curves supplied by the manufacturer, the transmission of the pump and signal for three different incidence angles is given in Table 5 below:

**Table 5 % Transmission of Beamsplitter at 1.064 and 1.57  $\mu\text{m}$  for Incidence Angles of 55, 57 and 60 deg.** These values were taken from the transmission curves of the beamsplitter supplied by the manufacturer.

Angle (deg)	% Transmission	
	1.064 $\mu\text{m}$	1.57 $\mu\text{m}$
55	0.45	96.08
57	0.61	96.58
60	0.76	95.12

By adjusting the incidence angle on the beamsplitter, the transmission at  $1.57\text{ }\mu\text{m}$  can be adjusted. Adjustment of the beamsplitter also changes the wavelength of maximum transmission. At an incidence angle of  $55\text{ deg.}$ , the transmission at  $1.609\text{ }\mu\text{m}$  is given as  $99.67\%$ . As the angle is increased, the transmission at  $1.609\text{ }\mu\text{m}$  decreases.

Figure 24 shows the signal power within the OPO cavity as a function of diode current measured at this location. The data in this figure was taken together with the data from Fig. 21. Note, a similar measurement could be performed on the opposite side of the beamsplitter but this measurement would have to be done after mirror M3.

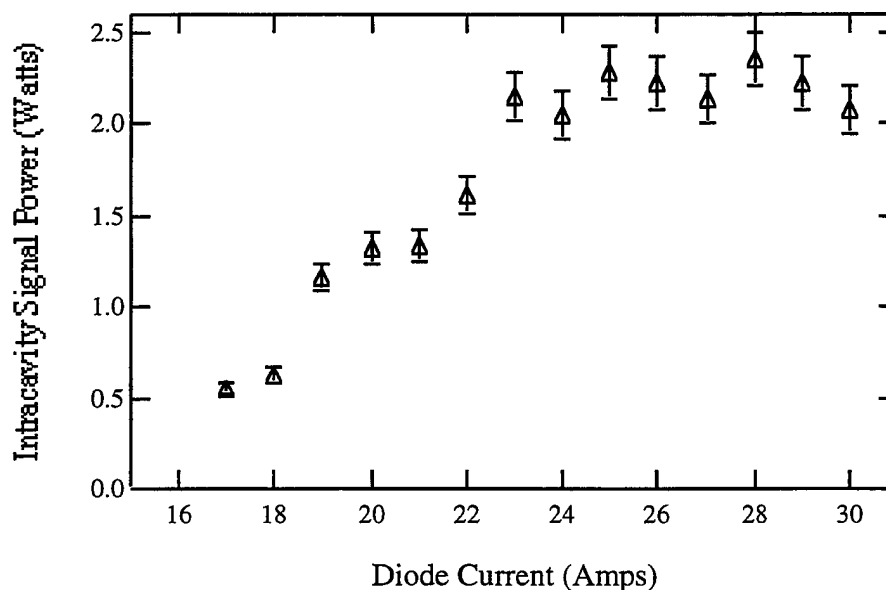


**Figure 24. Intracavity Signal Power vs. Current.** This plot shows the intracavity power measured from the signal reflected by the beamsplitter.

This plot agrees with the previous data showing the clamping of the signal. Measurements at this location are also better for calculating the intracavity signal power than measurements from either M1 or M2. The beamsplitter acts as a small percentage output coupler at the signal,  $\sim 4\%$ . This is a better method of determining the intracavity signal power than using the signal at either M1 or M2 where the transmission of the mirror is on the order of a tenth of a percent.

Another thought was that perhaps the signal clamping was an indication that a second OPO was operating. Perhaps the clamping signal was similar to a pump clamping. For a second OPO to phase match at this temperature (155 °C) and with the signal acting as the pump, the signal wavelength of the second OPO would be  $\sim 2.2 \mu\text{m}$  with a corresponding idler of  $\sim 5.5 \mu\text{m}$ . Unfortunately, none of the optics in the OPO cavity had significant reflectivity at either of these second signal or idler wavelengths, losses at these wavelengths appeared too great to sustain a second OPO. This is not necessarily the case in pulsed OPOs where pump energies tens of times above threshold with some reflectivity at the secondary signal wavelength lead to a cascading OPO effect [26, 27].

A survey scan with the Acton Research monochromator was done to search for a second signal. The scan ranged from 1.7 to 2.5  $\mu\text{m}$  and the detector used was an AlGaAs photodiode. This detector is sensitive in the 2  $\mu\text{m}$  region. The PMT is sensitive up to  $\sim 1 \mu\text{m}$  and the Ge sensitivity quickly dies off at 1.8  $\mu\text{m}$ . Before the spectral scan was done, a quick power out vs. current scan of the OPO was done to ensure that the signal was still clamping, which it was. The current was then left at a setting well into the clamping region of the signal. An initial scan showed a spectral line at 2.1  $\mu\text{m}$ , unfortunately this turned out to be a second order reflection of the pump beam. The 1  $\mu\text{m}$  HR dielectric mirror used earlier was inserted into the beam path to filter out the pump. The mirror was first inserted into the Lambda 9 spectrophotometer to check the transmission at 2  $\mu\text{m}$  ( $T \sim 60\%$ ). A second scan with the now filtered pump did not reveal a second OPO.

Since a second OPO was not present, the next thought was that perhaps the mode quality of the signal was deteriorating or that not all of the signal power was being measured. To verify this, beam profiles of the signal and idler beams were done in the region of signal clamping (at 28.0 amps). The pump was profiled at the same current but with the OPO off. These measurements were done by taking the beam from M1 and sending it through a  $\text{CaF}_2$  lens. The lens was uncoated, plano/convex and labeled as

having a +200 mm focal length. Beam profiles were taken symmetric about the waist location for each beam. The Ge and dielectric mirror were located after M1 and before the lens to filter the idler and signal beams, respectively. The PPLN was at  $155.0 \pm 0.3$  °C yielding a signal wavelength of  $1.5734 \pm 0.0001$   $\mu\text{m}$  and an idler wavelength of  $3.2893 \pm 0.0002$   $\mu\text{m}$ . These results are shown in Table 6.

**Table 6. Signal, Idler and Pump Beam Profiles at 28.0 amps (clamped).** Beam profiles of the signal, idler and pump beams done at 28.0 amps. The signal was clamped during these measurements. The pump measurements were done with the OPO off (M2 blocked).

Beam	Results	Horizontal	Vertical	Radial
Signal	$w_0$ ( $\mu\text{m}$ )	$41 \pm 6$	$51 \pm 5$	$48 \pm 6$
	$z_r$ (mm)	$2.6 \pm 0.4$	$3.2 \pm 0.4$	$3.0 \pm 0.4$
	$M^2$	$1.3 \pm 0.6$	$1.6 \pm 0.5$	$1.5 \pm 0.5$
Idler	$w_0$ ( $\mu\text{m}$ )	$43 \pm 5$	$71 \pm 8$	$71 \pm 7$
	$z_r$ (mm)	$1.6 \pm 0.2$	$1.8 \pm 0.2$	$2.0 \pm 0.2$
	$M^2$	$1.3 \pm 0.5$	$2.6 \pm 0.9$	$2.4 \pm 0.7$
Pump	$w_0$ ( $\mu\text{m}$ )	$27 \pm 2$	$30 \pm 3$	$30 \pm 3$
	$z_r$ (mm)	$2.0 \pm 0.2$	$2.2 \pm 0.2$	$2.2 \pm 0.2$
	$M^2$	$1.1 \pm 0.3$	$1.2 \pm 0.3$	$1.2 \pm 0.3$

Although the uncertainties are large, the  $M^2$  values of the pump and signal beams are reasonable. The  $M^2$  of the idler beam is large but this may be due to the idler not being resonated within the cavity. Since it leaves the cavity after being generated within the OPO, there is no direct control of the mode quality of the beam.

An attempt at profiling the signal beam before clamping was done but the amount of signal power available at the detector before clamping was too low. Beam profiles of the idler and pump were done before the signal was seen to clamp (24.0 amps). The pump measurements were done with the OPO off. These results are in Table 7 below:

**Table 7. Signal, Idler and Pump Beam Profiles at 24.0 amps (unclamped).** Beam profiles of the idler and pump beams done at 24.0 amps. The signal was not clamped during these measurements. The pump measurements were done with the OPO off (M2 blocked).

Beam	Results	Horizontal	Vertical	Radial
Idler	$w_0$ ( $\mu\text{m}$ )	$43 \pm 5$	$90 \pm 8$	$77 \pm 7$
	$z_r$ (mm)	$1.5 \pm 0.2$	$2.2 \pm 0.2$	$2.2 \pm 0.2$
	$M^2$	$1.1 \pm 0.4$	$3.5 \pm 0.9$	$2.6 \pm 0.7$
Pump	$w_0$ ( $\mu\text{m}$ )	$20 \pm 2$	$23 \pm 2$	$23 \pm 2$
	$z_r$ (mm)	$1.2 \pm 0.1$	$1.4 \pm 0.1$	$1.4 \pm 0.1$
	$M^2$	$1.0 \pm 0.3$	$1.1 \pm 0.2$	$1.1 \pm 0.3$

The results of the pump beam profile at 24.0 amps are comparable to the results at 28.0 amps. Neither of these indicate a problem with the quality of the pump beam. These results do show a slight ellipticity of the pump beam. The idler profile is also similar at the two currents except for the vertical  $M^2$  which appears worse at 24.0 amps. The idler measurements contain the largest uncertainty.

Since the beam profiles appear reasonable, the apparent clamping of the signal may be due to not all of the signal beam being collected at the detector. Since the idler power continues to increase in the signal clamping region, the signal power must be increasing as well. The signal beam within the cavity may be expanding and getting apertured within the cavity so that all the signal power does not reach the detector.

Another possibility is that signal photons generated, after the signal appears to clamp, may be recombining with the pump beam through SFG. This measurement could be done by separating the red,  $\sim 0.63 \mu\text{m}$ , from either end of the OPO and observing the SFG power as a function of current. Lastly, an IR camera sensitive to the signal wavelength may be used to observe the OPO cavity. The camera could be focused onto the ends of the PPLN oven to determine if the signal beam is being clipped by the oven aperture. The camera could also be pulled back to observe the entire laser cavity to see if

any signal photons are striking another part of the cavity so that they are not collected by the power meter.

### **Pump Clamping**

As seen previously with the Nd:YAG laser, Fig. 14, and in Refs. 4 and 12, once the pump reaches the OPO threshold, it should remain clamped at that level. This is not seen in the intracavity data with the Nd:YVO<sub>4</sub> laser. This may be due to poor overlap between the pump and signal beams. In an external OPO, the alignment of the signal beam does not affect the operation of the pump laser, which is not the case in this setup. Both the OPO and pump cavities share a common path, between the PPLN and M1. This path may not be optimized for both cavities leading to poor overlap between the pump and signal beams.

There may be three possible cases where the two cavities are not optimally overlapped. The first is where the beams are superimposed but the waist locations are longitudinally displaced. Figures 25 below show the case of optimum overlap between the pump and signal beams and the case where the signal beam is displaced along the axis.

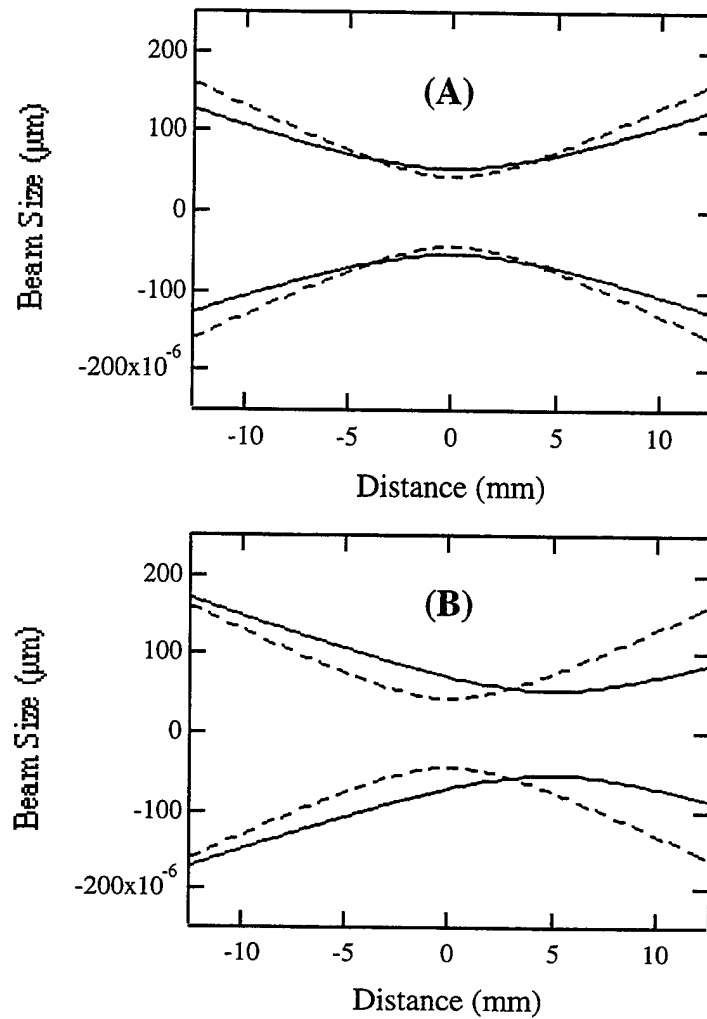


**Figure 25. Optimum and Displaced Overlap Between Pump (dashed) and Signal (solid) Beams.** A) Optimum overlap between the pump and signal beams in a 25 mm long, 0.5 mm thick sample of PPLN B) The unoptimized overlap between the pump beam focused at the crystal center and the signal waist displaced along the axis.

The misalignment in Fig. 25 can be corrected by adjusting the length of the OPO cavity to correctly overlap the waists.

A second misalignment condition is where the beams are parallel but separated transversely. A third poor overlap condition exists when the beams are not parallel to each other but intersect at an angle. Figure 26 below shows both of these misalignment conditions.

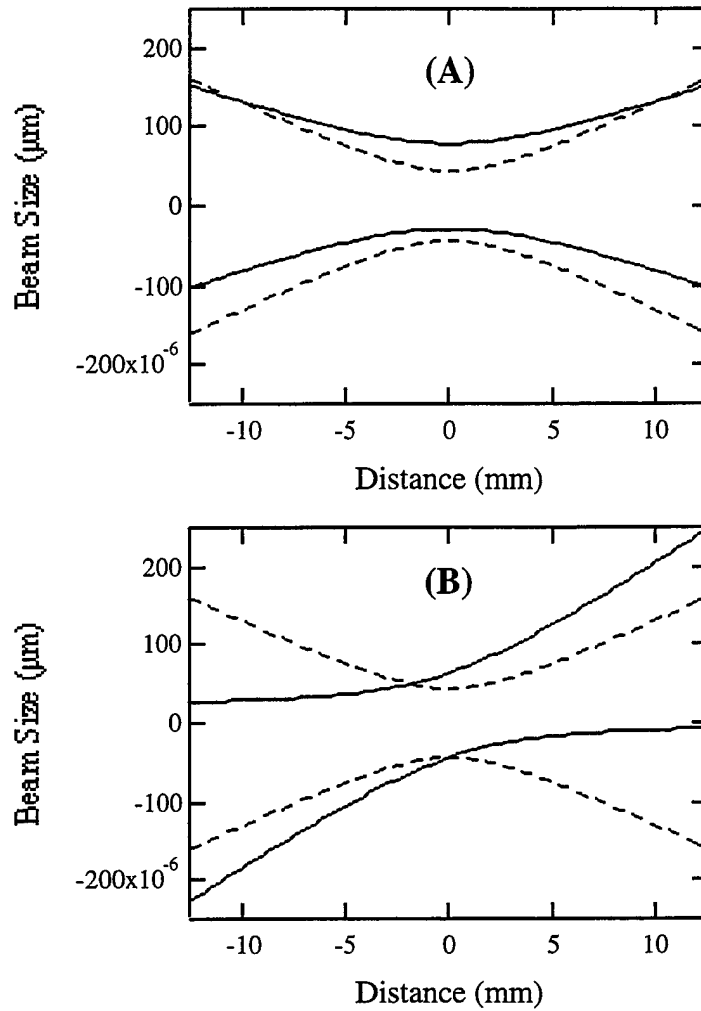


**Figure 26. Transverse and Angular Overlap Misalignment Between Pump (dashed) and Signal (solid) Beams. B) Signal parallel and shifted transverse to the pump beam C) Signal angularly misaligned to the pump beam**

Both of these misalignments in Fig. 26 can be corrected by adjusting both OPO end mirrors to change the angle and position of the signal beam. Unfortunately, in the instances where both end mirrors have to be adjusted, the pump laser is affected as well needing adjustment of M3 to compensate for misalignment of the pump. In addition to the misalignments shown in Figs. 25b and 26; there may also be combinations of these various cases.

The axes in Figs. 25 and 26 correspond to a 25 mm long PPLN crystal with a thickness of 0.5 mm. The minimum waists of the pump and signal beams each correspond to  $L/b = 1$ .

In the cavity configuration for the data presented so far, Cavity IV, the waist of the pump beam within the crystal is calculated to be  $\sim 80 \mu\text{m}$  and remains this size over most of the length of the crystal. The signal waist created by the OPO cavity is  $107 \mu\text{m}$ . Note, this cavity setup is not optimal in terms of pump beam waists; the cavity is mainly optimized in terms of pump beam size at the Nd:YVO<sub>4</sub> crystal.

In this setup, the optimum idler power was found by translating both M1 and M3 along the OPO axis and realigning each time until the OPO cavity giving the maximum idler power was found. This cavity created a signal waist of  $107 \mu\text{m}$ . Note, for a pump beam of  $80 \mu\text{m}$  and setting the  $L/b$  parameters of the pump and signal equal, the optimum signal waist is  $98 \mu\text{m}$  and the optimum crystal length would be 82 mm. For this cavity, the beam sizes, pump and signal waists are optimized for each other but not for the use of this PPLN sample.

For proper mode matching of the pump to the PPLN ( $L_c = 25 \text{ mm}$ ) crystal, the pump waist needs to be  $44 \mu\text{m}$  within the PPLN. A cavity layout which gives this spot size is as follows: the distance from M3 to the Nd:YVO<sub>4</sub> is 175 mm. The distance from the Nd:YVO<sub>4</sub> to the modematching lens remains the same, 150 mm. From the modematching lens to the PPLN is 63.5 mm and from the PPLN to M1 is 43 mm.

While this cavity provides good modematching at the PPLN, the power extracted from the Nd:YVO<sub>4</sub> laser crystal is less. The radius of the pump beam at the Nd:YVO<sub>4</sub> is now ~ 150  $\mu\text{m}$ , about 50  $\mu\text{m}$  less than the cavity in use. The volume of the pump beam at the Nd:YVO<sub>4</sub> crystal has decreased by about 44%. This cavity was briefly tried but the idler power was less than what has been reported. Also no clamping of the pump beam was observed but this may have been due to misalignment between the beams as stated earlier. As the pump waist is decreased within the PPLN, the alignment tolerance between the beams increases since there is less overlap area.

### **Optimum Output from the Laser**

In the period between the data shown in Figs. 21 and 23, a determination of optimum output from the laser was made. This was done by varying the loss within the cavity and observing the change in output power from the laser. These measurements were done at a number of currents to determine the optimum output power for each current setting. In an intracavity OPO, the total down converted power from the OPO should approach the optimum output power from the laser [12].

The method used to vary the loss was to insert two fused silica windows within the cavity to act as intracavity attenuators, Fig. 10. They were positioned between the Nd:YVO<sub>4</sub> crystal and the mode matching lens (Cavity IV). These windows were 25.4 mm diameter, 3 mm thick plane/plane windows with  $n = 1.45$  at  $\lambda = 1.0643 \mu\text{m}$ . They are inserted to mirror each other such that translation of the beam by one window is compensated for by the second. In this manner, the alignment of the pump laser is unaffected. The windows were aligned to the laser cavity by first inserting one window at normal incidence to the beam. With ~3 % loss per surface at normal incidence the laser will continue to operate. Next, the angle is slightly varied while observing the pump power. When the pump power is a maximum, the position of the window is marked as zero degrees. The second window is then inserted and aligned in the manner described.

As the angle of the windows is varied from 10 to 70 degrees the loss within the laser cavity changes in the manner shown in Figure 27 below:

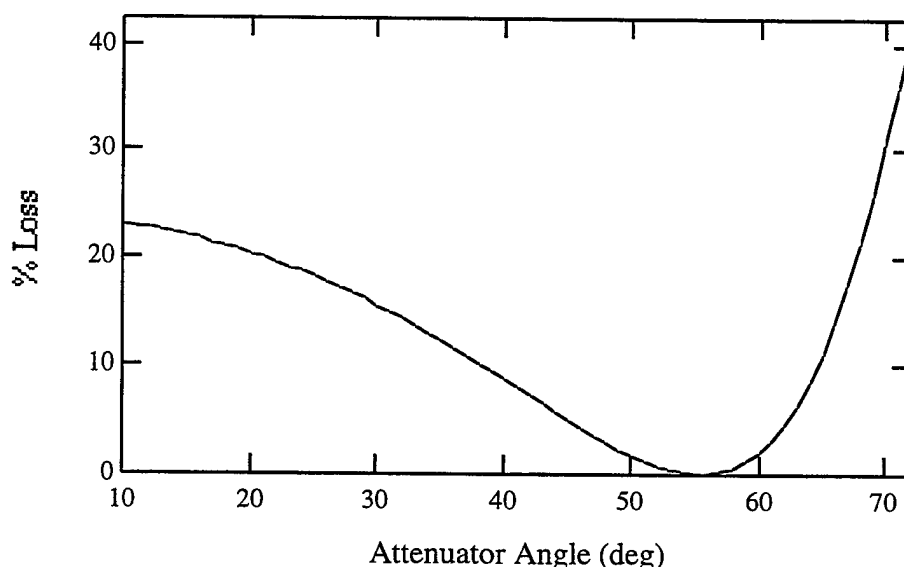


**Figure 27. Loss Due to Attenuators vs. Angle.** Intracavity loss for *p*-polarized light varies as a function of the incidence angle on the intracavity attenuators (fused silica windows). Minimum loss is at the Brewster angle of 55.4°.

This graph shows the loss for *p*-polarized light as a function of the incidence angle upon the intracavity attenuators in a linear optical cavity. The loss is a minimum at Brewster's angle, which for these windows occurs at 55.4 degrees and reaches 42 % at 72 degrees.

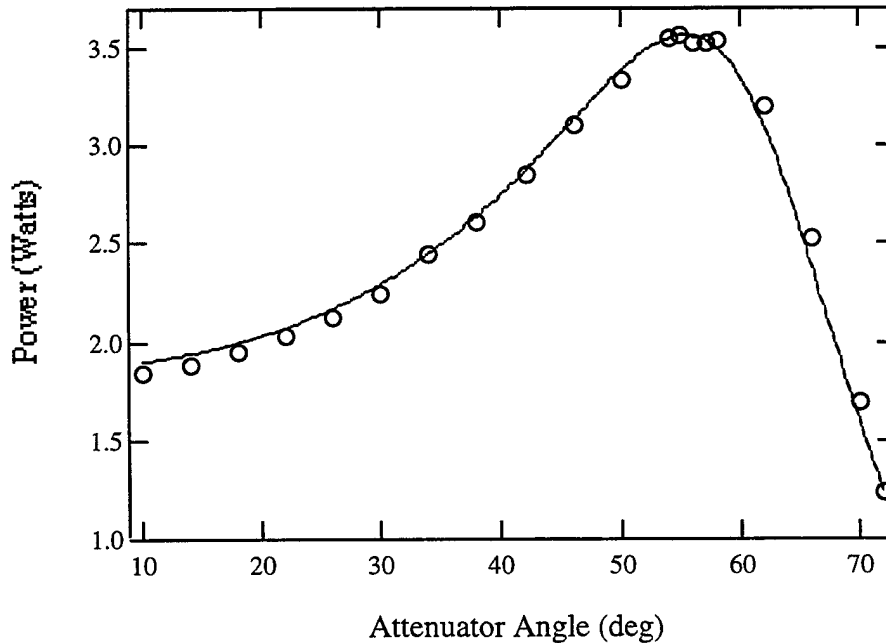
After insertion of the intracavity attenuators, M3 was replaced with an OC (80% R). After swapping mirrors, the angular alignment was adjusted to give the maximum idler output. After that, no mirrors were adjusted. Note, although the double HR mirror at M3 was removed, the base was left in place and the same mirror mount was used so that the OC was in the same location as the double HR mirror. Both mirrors had a ROC of 150 mm. There was a slight change in distance between the Nd:YVO<sub>4</sub> and M3 since these mirrors had different substrate thicknesses.

Figure 28 shows a typical plot of the laser output vs. intracavity attenuator angle. The theoretical line is the best fit to:

$$I_{out} = \delta_e \left[ \frac{2\alpha_m L_g}{\delta_e + \delta_o + \delta_{att}} - 1 \right] I_{sat} \quad (4.5.1)$$

where the intensities are replaced by powers.  $I_{out}$  corresponds to the power measured after the OC,  $\delta_e, \delta_o$  are losses due to external coupling (OC) and internal losses,  $\delta_{att}$  is the loss due to the intracavity attenuators.  $L_g$  is the length of the gain medium (4 mm),  $2\alpha_m$  ( $m^{-1}$ ) is the unsaturated gain coefficient and  $I_{sat}$  is the saturated intensity (power).  $I_{out}$ ,  $L$  and  $P_m$  are known and the rest of the parameters,  $2\alpha_m$ ,  $\delta_o$  and  $I_{sat}$  are free parameters in the fit.

Figure 28 below shows a typical trace of power measured after the OC as a function of the incidence angle on the intracavity attenuators for a fixed current. This data was taken at 26.0 amps and the uncertainty in the power measurements are within the size of the markers.



**Figure 28. Typical Power Out vs. Intracavity Attenuator Angle.** These measurements were done at 26.0 amps. Peak power was  $3.56 \pm 0.01$  W.

These measurements were done at six currents and a fit to Eqn. 4.5.1 was done at each current. The results of the fits are given in Table 8 below. From these values the optimum output power at each current was determined. The value of optimum output power corresponds to the most power that can be extracted from the pump laser in the current cavity configuration. This includes having the PPLN as part of the pump laser cavity but with the OPO off (Cavity IV).

**Table 8. Results of Intracavity Loss Fit.** These are the results from the fits to Eqn. 4.4.1 using the data of power out vs. intracavity attenuator angle.

Amps ( $\pm 0.1$ )	$2\alpha_m$	$\delta_o$	$I_{sat}/2$
10.0	$189 \pm 6$	$0.13 \pm 0.04$	$1.04 \pm 0.16$
14.0	$270 \pm 5$	$0.17 \pm 0.03$	$2.10 \pm 0.27$
18.0	$370 \pm 66$	$0.13 \pm 0.06$	$2.33 \pm 1.06$
22.0	$440 \pm 94$	$0.14 \pm 0.05$	$2.84 \pm 1.23$
26.0	$470 \pm 90$	$0.19 \pm 0.06$	$4.75 \pm 1.85$
30.0	$448 \pm 2$	$0.35 \pm 1.74$	$8.97 \pm 0.08$

The values for internal losses,  $\delta_o$ , should remain constant since the data is plotted as a function of the intracavity attenuator loss and the other internal losses are not changing. Ignoring the last point, 30.0 amps, the values for  $\delta_o$  all lie within each others uncertainty. Redoing the fit with the data from 30.0 amps but holding the value of  $\delta_o$  fixed at 0.15 (which is the average value of  $\delta_o$  from the 10.0 to 26.0 amps data sets) yields  $2\alpha_m$  of  $834 \pm 1$  and  $I_{sat}/2$  of  $2.45 \pm 0.43$ .

The optimum output coupling at each current can be determined by differentiating Eqn. 4.5.1 with respect to  $\delta_e$  yielding:

$$\delta_{e,opt} = \sqrt{2\alpha_m P_m L_g} - \delta_o \quad (4.5.2)$$

This can then be substituted back into Eqn. 4.5.1 to give the maximum output intensity/power at each current:

$$I_{\text{out,opt}} = \left[ \sqrt{2\alpha_m L_g} - \sqrt{\delta_o} \right]^2 \frac{I_{\text{sat}}}{2} \quad (4.5.3)$$

Figure 29 shows the results from Eqn. 4.5.3 as well as the total down converted power from the OPO. Total down converted power from the OPO was determined by summing the idler from M1 and M2 from Fig. 21 and using the signal leaking from the beamsplitter, Fig. 24, to determine the signal power within the OPO.

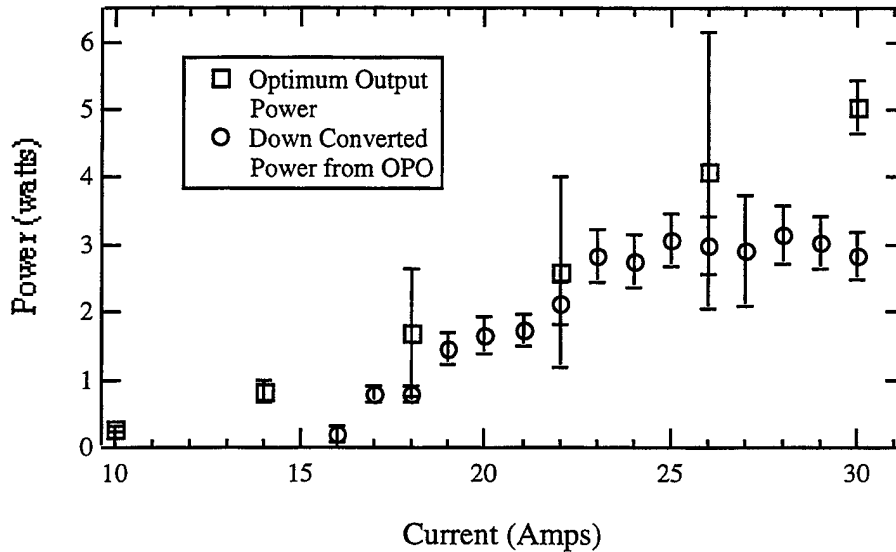


**Figure 29. Optimum Output Power and Total Down Converted Power vs. Current.** The optimum output power was determined from the data of the intracavity attenuator fits. Total down converted power was determined from the idler power of Fig. 21 and the intracavity signal from Fig. 24.

Optimum output power at 30.0 amps was taken from the fit data holding the intracavity loss fixed. Note, the optimum power at 30.0 amps using the data from Table 7 gives  $5.01 \pm 5.38$  W. The value from the fit holding  $\delta_o$  constant is  $5.06 \pm 0.39$  W.

As expected, the total power converted by the OPO appears to approach the optimum power available from the laser. The intracavity OPO should act as an optimum output coupler for the laser. Unfortunately the apparent clamping of the signal limits the down converted power at the higher currents.

### Intracavity OPO Experiment with 50 mm PPLN

The final experiment done with this laser was to replace the 25 mm sample of PPLN with a longer crystal. The new sample used was number 29.75-2 # 9 and was 51.75 mm in length, 0.5 mm thick and 5 mm wide with a grating period of 29.75  $\mu\text{m}$ . Figure 30 below shows the idler power measured from both ends of the OPO cavity (Cavity V). Maximum idler power was  $746 \pm 14$  mW measured at 30.0 amps after mirror M1.

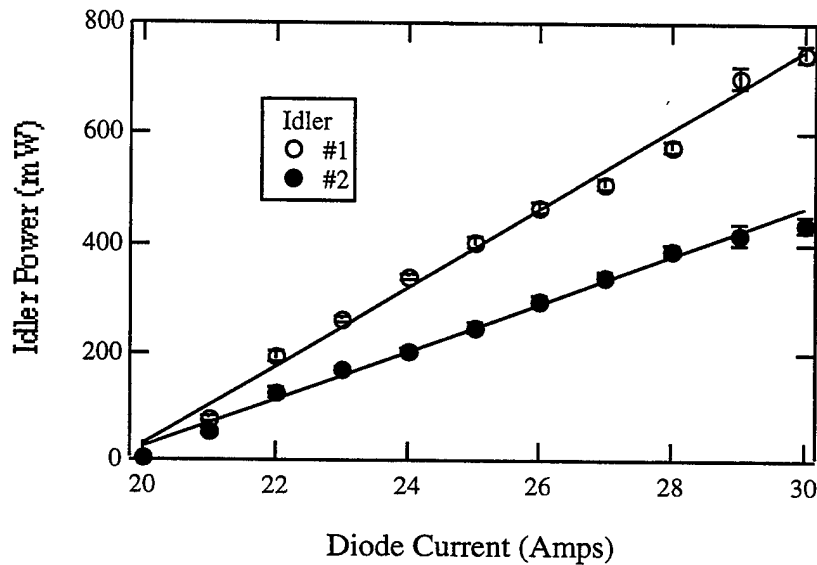


**Figure 30. Idler Power from 50 mm PPLN:** Idler power from both ends of the OPO cavity using the 51.75 mm length PPLN. Maximum idler power was  $746 \pm 14$  mW measured after M1

The slope efficiency of the idler after M1 was  $73 \pm 2$  mW/amp or 1 % wallplug efficiency. At 30.0 amps drive current, the voltage across the diodes was 5.5 V. At 20.0 amps the voltage was 4.6 V. The slope efficiency of the idler from M2 was  $44 \pm 1$  mW/amp or 0.6 % wallplug efficiency.

A reason why the slope efficiency and power from M1 is greater may be due to a large percentage of the pump being depleted after the first pass through the PPLN. As the length of the PPLN is increased, the interaction length between the beams increases and the single pass pump depletion should begin to dominate the interaction.

With this cavity, no clamping of the signal was observed as seen previously. Figure 31 shows the signal powers measured from both ends of the OPO cavity.

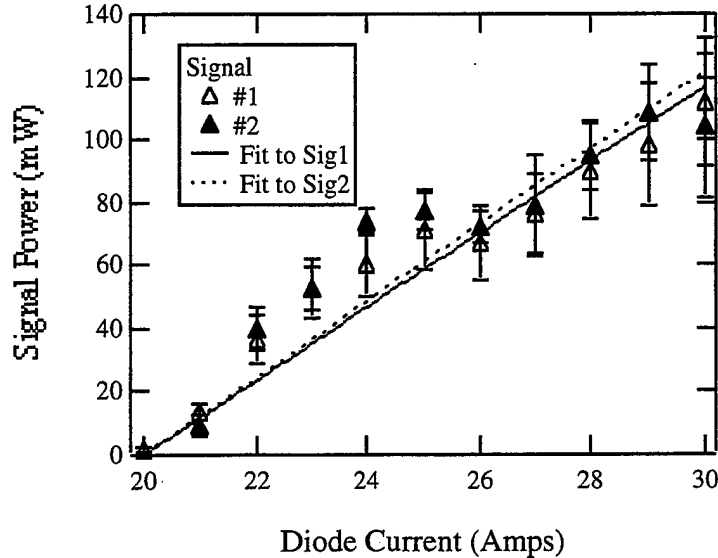


**Figure 31. Signal Powers from 50 mm PPLN** Signal power from both ends of the OPO cavity. No clamping of the signal is observed.

Maximum signal power was  $112 \pm 20$  mW measured after M1. The signal power after M2 was determined by measuring the idler power with a Ge filter and subtracting it from the filterless measurement. The signal at M1 was determined using the dielectric mirror mentioned previously.

The cavity dimensions were as follows (Cavity V): the distance from M3 to the Nd:YVO<sub>4</sub> was 100 mm. From the Nd:YVO<sub>4</sub> to the mode matching lens was not changed (150 mm). The distance from the lens to the beamsplitter was 40 mm and from the beamsplitter to the PPLN was 33 mm. Distance from the PPLN to M1 was 8 mm. The OPO cavity had mirror M1 41 mm from the beamsplitter. This gave a pump waist of 91  $\mu\text{m}$  within the PPLN and a signal waist of 111  $\mu\text{m}$ . The value of  $L/b$  for both the pump and signal was 0.5.

These cavity dimensions were determined by varying the positions of M1 and M2 until the maximum idler power was found. The distance between M3 and the Nd:YVO<sub>4</sub>

was calculated after the distances of M1 and M2 were measured . After the optimum idler power was found, the cavity dimensions were remeasured. These values give a pump cavity with poor stability at weak thermal lensing (low currents). Stability improves with thermal lensing. This may explain the trend of the intracavity pump power with the OPO off shown in Fig. 32 below. The pump powers were measured after mirror M3 with both the OPO on and off:

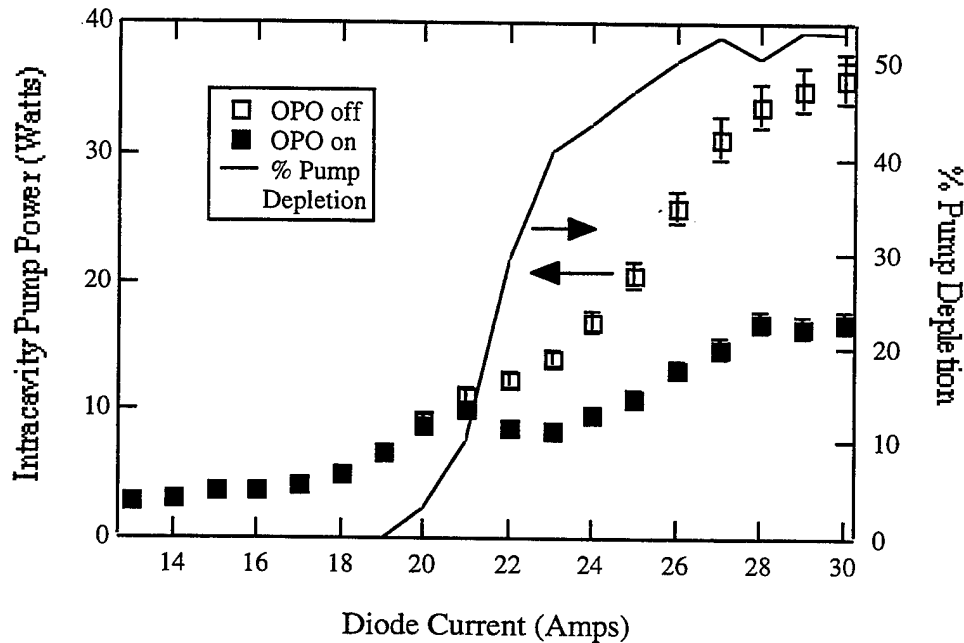


**Figure 32. Intracavity Pump Power and Depletion:** Intracavity pump power determined by measurements of the pump beam after M3. Maximum pump depletion was 54%. Threshold of the OPO was at ~9 W of circulating pump power.

The open squares represent the intracavity power with the OPO off, mirror M2 blocked. The filled squares show the intracavity pump power with the OPO running. Threshold of the OPO was ~9 W of circulating intracavity pump power at 20.0 amps. The threshold from Eqn. 4.2.1 is 6.5 W with  $w_p$  of 91  $\mu\text{m}$  and  $w_s$  of 111  $\mu\text{m}$  (using a value for  $h_{SM}$  of 0.385 [Refs. 10, 29, 30]). Maximum pump depletion was 53 % at 30.0 amps and

corresponds to double pass pump depletion since the measurement was done at mirror M3. Single pass pump depletion, measured after M1, was not investigated due to time constraints.

## Conclusion

This chapter presented the results from the intracavity OPO experiment using the Nd:YVO<sub>4</sub> laser as the pump source. Output power, idler stability and OPO tunability data was presented from a 25-mm sample of PPLN. Figures 21 and 23 showed the reproducibility of the laser performance with data taken on two separate dates. All of the data in Section 4.2 was taken with the same 25-mm PPLN crystal, sample 29.75-1 # 10.

A method for calculating the optimum output power from the laser was shown in Section 4.5. Figure 29 showed how the optimum output power from the laser varied with current and how the total down converted power from the OPO approached the optimum output power limit. Finally, data with a 50 mm PPLN crystal, number 29.75-2 # 9, was presented in Section 4.6. The data from this sample has shown the most one-way idler power extracted to date from the intracavity OPO.

The advantage of the intracavity OPO experiment with the Nd:YVO<sub>4</sub> laser is that it is small and compact. The entire experiment is situated on a 1' x 2' breadboard simplifying the mounting of most of the components and improving the overall mechanical rigidity. This was a major improvement over the Nd:YAG laser since the OPO would now consistently turn on, day to day, allowing improvements to be done to the previous day's work.

## 5. Conclusion and Future Research

This thesis has described the design, construction and results of the first CW intracavity singly resonant optical parametric oscillators using periodically poled LiNbO<sub>3</sub>. Output power, tunability, and power stability of the system was investigated. Maximum idler power of  $746 \pm 14$  mW was recorded with a 50 mm PPLN crystal using the Nd:YVO<sub>4</sub> laser. Tuning of the intracavity OPO was from 1.56 to 1.60  $\mu\text{m}$  for the signal and 3.33 to 3.18  $\mu\text{m}$  for the idler. The idler power stability was  $\pm 5\%$  over a period of 30 minutes. The main emphasis during the research of this thesis has been getting the device to operate reliably

Compared to an external OPO, an intracavity system has some advantages and disadvantages. One of the main advantages is the amount of pump power available within the cavity. Tens of watts of pump are readily available within the cavities of most lasers. An intracavity system allows a relatively inexpensive laser with modest output power to produce ample powers at the signal and idler wavelengths. While there is sufficient intracavity power to reach SRO thresholds, alignment difficulties must be addressed.

For the intracavity system, it was quite difficult to align the OPO to the signal beam while not adversely affecting the alignment of the pump laser cavity. With both the pump and OPO laser cavities partially coupled together, alignment can be a time consuming process. An advantage of an external OPO is that once the pump laser is turned on and optimized, its alignment is left as-is. The OPO alignment can be adjusted with no effect on the pump laser. This is a degree of freedom lacking in an intracavity system.

External OPOs have also operated with pump depletion exceeding 90 % [3], while the most pump depletion seen in the intracavity OPO to date is just over 50 %. There is still room for improvement with the intracavity system, with the main emphasis in

lowering the OPO threshold to be able to reach multiple times above threshold. Efficiency of the OPO quickly increases as threshold is surpassed.

While the reliability of the system has been demonstrated, there are still many improvements that can be made as well as new directions for the intracavity OPO research to take. One of the improvements that can be made to the system is better characterization of the thermal lensing properties of the Nd:YVO<sub>4</sub> crystal. At low currents, the weak thermal lensing of the crystal appears to have some astigmatism. At higher currents, the stronger thermal lensing appears less astigmatic. This impacts the design of the pump cavity over a large current/pumping range. The main requirements of the pump cavity are a large mode volume, few 100  $\mu\text{m}$ 's radius, at the gain medium and a small beam size,  $\sim 40 - 60 \mu\text{m}$ , at the nonlinear crystal. A strong variable lens within the cavity may not keep the pump beam at an optimum size over a large current range.

A possible method of meeting both pump beam size requirements could be to use a telescope system within the pump laser cavity [22]. These systems can compensate for thermal lensing over a large pumping range, helping to maintain a fixed mode size at the gain media and nonlinear crystal. Another possible cavity design involves changing the coupling optics which focus the diode lasers from the fibers into the Nd:YVO<sub>4</sub>. In most of the cavity designs to date, a cavity with a tight pump waist within the PPLN usually produces a small pump waist at the Nd:YVO<sub>4</sub>, in comparison to the size of the pump beam from the diode lasers. If the pump light from the diode lasers is focused to a tighter beam, then there will be better extraction of available power from the Nd:YVO<sub>4</sub>, assuming the Nd:YVO<sub>4</sub> can handle the increased power density.

An investigation should also be made into the thermal lensing properties of PPLN. Thermal lensing of the PPLN has not been addressed in this thesis but researchers have recently seen cases of thermal lensing in PPLN, due to generation of frequency doubled Nd:YAG [27]. If thermal lensing due to the PPLN is significant, then this may need to be modeled to correctly design both the pump and OPO cavities. This may be of greater concern in an intracavity OPO because of the higher pump powers/intensities seen by the PPLN compared to an external OPO.

Another possible cavity design could involve nonresonantly reflecting the idler from only one end of the OPO cavity. This will have a similar effect as pump double passing in that the threshold of the OPO can be lowered by up to an additional factor of two [11]. The problem in this case is that the phase of the reflected idler beam may need to be compensated for, to obtain optimum threshold reduction. If mirror M2 in Fig. 10 was highly reflecting at both the signal and idler beams, then it could be mounted on a piezo actuated mount so that small changes to the OPO cavity length could be made. The authors in Ref. 2 have tried a similar approach in an external OPO, yielding good results. The advantage to this setup, in addition to a lower threshold, is that all of the idler power can be collected from one end of the OPO cavity.

A list of possible optics to purchase for future intracavity experiments should include a better filter for the signal. This could possibly be a silicon based filter so that the pump and signal can be separated. Much of the noise in the signal data presented is mainly due to the use of the dielectric mirror which transmitted only a portion of the signal. Transmission across the face of the mirror is not uniform. While attempts were made to ensure the reproducibility of the results with this mirror, there are still instances where the positioning of the mirror is suspect.

Other possible optics are an improved beamsplitter. The beamsplitter purchased was optimized for high reflectivity at the pump wavelength with the second priority being high transmission at the signal. A different approach may be to optimize signal

transmission first followed by reflection at the pump. An additional approach may be to transmit the pump and reflect both the signal and idler. End mirrors for the OPO may be purchased that reflect both the signal and idler, as mentioned earlier, or that allow some of the signal to be coupled out. This research has concentrated on the idler wavelengths,  $\sim 3.3 \mu\text{m}$ , but there may be applications where a source at the signal wavelength is necessary.

The use of longer PPLN samples, 50 mm, allows looser focusing of the pump beam within the cavity as well as providing a longer interaction length between the beams. The data presented in Section 4.6 was taken over 4 days. In this time, the 50 mm PPLN was inserted into the cavity and slight changes in the cavity layout were made. The cavity changes made were the simplest alterations which could be done in the available time. This was the last data collected before printing of this thesis. While the maximum idler power was reported as 746 mW, the maximum power seen during alignment was approximately 870 mW. If more time is spent optimizing this setup, idler powers approaching 1 W from one end of the OPO cavity are reasonable. An investigation of single pass pump depletion vs. double pass pump depletion can also be accomplished in this setup. As shown in Fig. 30, the idler power after M1 is almost twice the idler power measured after M2. While there is some additional loss for the M2 data due to the beamsplitter, the large discrepancy in powers could be due to greater single pass depletion with the longer PPLN.

Intracavity frequency doubling may be a different research area for the intracavity setup. Recent results with short grating periods,  $<10 \mu\text{m}$ , show promising results for the use of PPLN in converting a pump wavelength of  $1.06 \mu\text{m}$  to its second harmonic,  $0.532 \mu\text{m}$ , visible green [28]. These second harmonic generation (SHG) experiments have shown conversion efficiencies exceeding 40%. This SHG experiment was conducted by focusing the output from a CW Nd:YAG laser, 6.5 W output, into the short period PPLN.

Maximum power at  $0.532\text{ }\mu\text{m}$  was 2.7 W. By trying intracavity doubling, higher pump powers would be made available.

As a final note, researchers from St. Andrews University in Scotland have teamed with Edinburgh Instruments to develop and sell a commercial CW intracavity singly resonant OPO marketed as the "OPOTune." This system is based on the recent Optics Letter, Ref. 12, using potassium titanyl arsenate (KTA) as the nonlinear media. Output powers are on the order of a few 100 mW at both the signal and idler wavelengths.

## **Appendix A**

### **Design, Setup and Alignment of an Intracavity Optical Parametric Oscillator**

#### **A1 Design**

Design of an intracavity singly resonant optical parametric oscillator (OPO) begins with the OPO cavity, most importantly the length of the crystal. By knowing the length of the crystal, one knows the optimum spot sizes of the pump and signal beam within the crystal [16].

First begin with the OPO cavity. Taking into account the availability of optics, an OPO cavity needs to be designed so that the signal waist defined by the cavity is in the center of the crystal and satisfies the criteria that  $L/b=1$ , see Eqns. 2.2.1 and 2.2.2. Optimally one wants to use the shortest radius of curvature mirrors possible. This keeps the overall cavity length short which eases alignment and improves stability.

Typical mistakes in designing the OPO cavity are incorrectly defining the signal wavelength or defining the index of refraction of  $\text{LiNbO}_3$  for the wrong wavelength. These are subtle points which are easily overlooked. Once the OPO cavity has been designed, examine the cavity stability. A good rule of thumb is to not exceed a stability value of 0.9. This will likely involve some tradeoff between cavity stability and optimum size of the beam waist. Keep in mind that a cavity with a perfect size waist may be right on the edge of stability and will be extremely sensitive to alignment.

Another issue to keep track of is that a portion of this OPO cavity will be within the laser cavity. This implies that there will be a beamsplitter in one leg of the OPO cavity resulting in an asymmetric cavity. One end mirror of the OPO will be close to the PPLN, this will also be the end mirror shared by the pump beam. The other end mirror will most likely have a larger ROC such that it can be placed farther away from the PPLN allowing room for the beamsplitter. The beamsplitter within the OPO cavity can be considered as acting as a Brewster plate since it will be transmitting the *p*-polarized signal and idler.

To summarize, the main issues in the design of the OPO are crystal length and separation of the end mirrors. A shorter cavity will usually be much more stable and less sensitive to misalignment but may not give the optimal beam waist. One arm of the OPO cavity must also be long enough to accommodate placement of the beamsplitter.

Next, the cavity for the pump laser needs to be determined. The main constraint is the arm of the pump cavity containing the PPLN and double HR end mirror. The distance between the two has already been determined by the OPO cavity. The second constraint is the mode size of the pump beam in the PPLN and within the gain media. Within the PPLN, the ideal pump waist is located in the center of the crystal and has a waist such that  $L/b = 1$ . For a 25 mm long crystal this is a pump waist of 44  $\mu\text{m}$ . The pump size at the gain media depends on the crystal used and the method it is pumped.

In the case of the Nd:YAG rod, there is thermal birefringence induced by heating from the arc lamp. Minimal birefringence is found along the center of the rod, so the best case for good beam quality and polarization would be a small beam waist along the center of the crystal. Unfortunately, the power extracted from the rod depends on the volume of the rod used. One technique is to try to reproduce the beam within the Nd:YAG to the same size as when the system was a simple two mirror 10W laser. Ideally if the laser originally produces 10 W and the cavity is changed, one should still be able to extract 10 W from the laser.

In the case of the Nd:YVO<sub>4</sub> laser, the optimum mode size of the pump is one which completely overlaps the light from the diodes. This gives the most power extraction and helps the beam quality. In the optimum case, if the pump and diode light completely overlap at the crystal, the laser will naturally operate as a TEM<sub>00</sub> beam without the use of intracavity apertures. For the laser used in this experiment, the value from the manufacturer for the beam size from the diodes at the Nd:YVO<sub>4</sub> is a diameter of ~ 380  $\mu$ m over the length of the crystal.

The next step is the choice of the lens for mode matching between the pump and OPO cavities. A focal length of +50 mm seems to work best in our experimental arrangements. This gives an adequate pump waist at the crystal and provides enough room between the lens and the crystal for insertion of the beamsplitter. The beamsplitter needs to be placed as close as possible to the PPLN but allowing room for the crystal to be manipulated within the cavity. Keeping the beamsplitter close is mainly to allow the OPO cavity to be as short as possible. Fortunately, the beamsplitter has no affect on the pump cavity other than redirecting it. A longer focal length lens doesn't provide a tight enough focus. A stronger lens provides a good focus but doesn't allow enough room to insert the beamsplitter.

The last consideration is the thermal lensing of the gain media, be it Nd:YAG or Nd:YVO<sub>4</sub>. In the case of the Nd:YAG rod, the thermal lensing is circularly symmetric, unlike the lensing in the Nd:YVO<sub>4</sub>. One of the problems with Nd:YVO<sub>4</sub> is that it does not dissipate heat as well as Nd:YAG and its rate of heat transfer is different along each axis and it is only attached to the heatsink by the top and bottom faces. These factors cause an astigmatic thermal lensing from this Nd:YVO<sub>4</sub> crystal.

Thermal lensing of the gain media has been modeled as one of two possible ABCD matrices. The Nd:YAG rod has been modeled as a Gaussian duct, a region where the index of refraction  $n$  is radially varying. The approximations are shown in Eqns. 3.1.1 and 3.1.2. The Nd:YVO<sub>4</sub> crystal (4 mm length) has been modeled as two regions of  $n =$

2.168 each 2 mm long with a positive lens in-between. Both of these thermal lens approximations, the Gaussian duct and the lens centered in the crystal, yield comparable results in the cavity models.

With all of these constraints in mind, the layout of the cavity can follow figure 9. The variables are the distance between M3 and the rod, between the rod and the lens and the lens and the PPLN. The curvature of M3 is determined by the availability of 1  $\mu\text{m}$  HR optics. For a starting point, the distance from M3 to the gain media can be on the order of the ROC of the mirror. The distance from the lens to the PPLN can be close to the focal length of the lens. The final distance, from the gain media to the lens, can be varied until the cavity becomes stable. Once a stable cavity is found, then the distances can be adjusted until the proper pump beam sizes within the crystals are found.

Once a cavity design has been found, remove the PPLN from the design and replace it with air. The cavity will most likely go unstable, in which case bring in mirror M1 until the cavity is stable again. Next, reinsert the PPLN keeping the distance to M1 short until the cavity is stable with and without the PPLN. This in-between cavity will allow the laser to run with and without the PPLN making the initial alignment easier. Trying to align the laser for the first time having the PPLN within the cavity may be difficult.

## **A2 Cavity Setup**

Once a cavity design has been found, set up of the cavity begins with a helium neon laser (HeNe). The HeNe is aligned parallel to the table at the height and direction desired for the laser cavity. The HeNe now defines the optical path of the laser. Next the lasing media is inserted, either Nd:YAG or Nd:YVO<sub>4</sub>. The crystal is inserted such that the HeNe laser passes through the center and the reflections from the front and back surfaces are retro-reflected onto themselves. The HeNe should enter the gain media from the side of M3. Next, the pumping source, either arc lamp or diodes, is powered up. As

the current is increased, the beam which passes through the crystal is observed on a distant target. The spot should change size as the current changes indicating that the crystal is acting as a variable lens. The positioning of the crystal needs to be aligned such that the HeNe spot does not translate in position as the current is varied. Note, once the positioning of the gain media, or of any other component is determined, its base and any set-screws or clamps must be properly secured before insertion and alignment of the next component.

After the gain media is aligned, insert the mode matching lens. While the lens is being inserted, two issues must be kept in mind, distance and centration. The lens must be positioned at the proper distance and orientation from the gain media. Once the position is located, the lens must be aligned normal and centered to the HeNe to reduce off-axis aberrations. This can be accomplished through the use of a screen with a pinhole. The screen is located after the gain media but before the lens with the pinhole centered about the HeNe beam. After insertion of the lens, there should be two reflections from the lens evident on the screen. These will be due to reflections from both surfaces of the lens. These must be superimposed on each other and onto the pinhole. This ensures that the lens is normal and centered to the optical axis defined by the HeNe.

Next, the beamsplitter is inserted. The beamsplitter should be mounted on a rotating stage so that the incidence angle can be measured. Also, the location of the beamsplitter must be calculated so that it is relatively close to the PPLN, yet not interfering with the oven. The beamsplitter is first inserted normal to the beam path with the coated surface facing the lens. The optic is aligned until the HeNe laser is reflected onto itself. This position is marked as 0 degrees. Next, the angle is adjusted to between 56 and 57 degrees. Once it is at the proper incidence angle, check the location of the HeNe striking the coated surface. The HeNe should be centered, if not, reposition the beamsplitter to center the HeNe and then check if normal incidence still corresponds to

the zero degree mark. This process is repeated until the beamsplitter is at the proper angle and the HeNe is correctly centered.

Next, mirror M1 is inserted at the calculated distance such that the laser will operate without the PPLN in the cavity. M1 is aligned in the same method as the lens such that any surface reflections are superimposed on each other and the pinhole. Before insertion of the last mirror, M3, ensure that either the laser cavity is physically blocked or that the lamp/diodes are off. This will prevent any inadvertent lasing from occurring. Mirror M3 is aligned in the same manner as M1 and the mode-matching lens. Once all of the elements are in the cavity and secured the lamp/diode current is slowly brought up.

### **A3 Cavity Alignment**

As the current is increased, the laser should begin operating on its own assuming the distances are correct and all of the elements are properly aligned to the cavity. In the case that the laser does not come on, then either M1 or M2 must be adjusted. Chances are that the misalignment is due to M1 since any misalignment in the lens or beamsplitter will continue on to M1 causing it to be mispositioned. A good method of getting the laser to turn on is to do a systematic raster-like scan of M1. This is done adjusting one axis of the mirror and sweeping through the range of motion of the other axis. Once the sweep is completed, the first axis is adjusted again and then another sweep is done. If the laser still does not operate, then decrease the distance from M1 to the lens and retry to raster scan.

Once the laser is operating, power must be optimized by adjustment of both M1 and M3. A power meter should be placed after the OC or after either of the end mirrors if both are HRs. Ideally, M3 should be an OC and the power measured in this setup should be close to the power measured from the laser when it was just a two-mirror cavity. This ensures that the gain media is being properly used. This is easy to do if the OC and the HR which will be at position M3 are both the same ROC.

The method to accomplish this alignment is by adjusting each mirror independently for power. This process is repeated until the power is peaked. Next, one of the mirrors is very slightly adjusted, then the second mirror is adjusted to try and bring the power back up. If the power increases to a greater value than before, this means the beam must be translated within the cavity by the manner just described, misaligning one mirror and re-optimizing with the second. This is also done in a raster-like method until the optimum pump power is found. There is no need yet to deal with the spatial mode structure of the beam, that will be done after the PPLN is inserted.

Once the optimum alignment for power has been accomplished, then the lamp/diode current is lowered until the laser is off. Next, the PPLN is inserted into the pump cavity and aligned with the HeNe. Since the PPLN is long and thin, the angular adjustment is critical. The PPLN is aligned by observing the HeNe passing through it as the crystal is translated perpendicular to the beam. If the spot moves then the PPLN is not parallel to the optical axis, the HeNe is reflecting from either the top or bottom of the crystal. This is corrected by making an angular adjustment and retranslating the crystal. This process is repeated until the spot does not shift while the PPLN is translated. This is done in both of the crystal directions which are transverse to the optical axis. Once the PPLN is normal to the optical axis, it should be adjusted along the width of the crystal until the HeNe is near one edge of the crystal. This is done such that if the coatings or other damage to the crystal occurs, then the crystal can be systematically translated away from that edge and onto a clean location.

Once the PPLN is aligned to the HeNe, then the current is slowly increased until the laser turns on. If the laser does not turn on at maximum current, then the PPLN is misaligned since the laser was operating previously without it. Lower the current to about half its maximum value (or to the threshold value if this cavity has been built before). Next, slowly adjust the PPLN in angle and translation until the laser comes on. Once the laser is operating, adjust the position of the PPLN for maximum pump power.

With the laser running again, the next step is to optimize the pump waist within the PPLN by increasing the distance between M1 and the crystal. Recall there should be a cavity design already at hand giving the optimum pump beam within the crystal and this differs from the cavity just built by the location of M1. To reposition M1, turn the current down until the laser is barely at threshold. Next, loosen the base of M1 and keeping the laser aligned, pull back mirror M1 until it is at the proper distance. It may help to have a rail as a guide while moving the mirror away from the PPLN.

Once the mirror is at the proper distance, the next step is to adjust the alignment of M1 to re-optimize the pump power. Next, the location of an intracavity aperture must be determined, if necessary. First observe the far field pump beam coming from either M1 or M3. If the beam is not Gaussian, then a intracavity aperture must be inserted. If the Nd:YVO<sub>4</sub> laser is used and the pump mode is properly matched to the diodes, then the laser may run TEM<sub>00</sub> without the need of an aperture.

To determine the location and size of the aperture, go back to the cavity model and observe the pump beam at strong and weak thermal lensing. Find the location where the beam is similar in size at both cases, this will be the location of the pinhole assuming the size of the pump beam is not too large for the apertures at hand. The initial aperture size should be about 1.5 - 2 times as large as the calculated size of the pump beam [22]. If the beam is larger than the available apertures then it will be necessary to find a balance between the location of an adequate size beam at both strong and weak thermal lensing. The pinhole must be mounted such that it can be finely adjusted in both axes perpendicular to the beam. Once the aperture is inserted and the laser is running, the aperture position must be adjusted to optimize the power. Next, re-examine the spatial beam quality to see if the beam is TEM<sub>00</sub>. If the beam still has higher order modes, then a smaller aperture is needed.

After the pump beam power and mode have been optimized, the OPO alignment is next. Mirror M2 should be positioned after the beamsplitter. There should be green

generated by the OPO to aid in the alignment of this mirror. Use the green to center and align the mirror. The green should be incident on the center of the mirror and should be retroreflected back onto itself. A white screen should be placed after M1. There should be two main green spots and weaker secondary reflections visible on the screen. The stronger green spot will be from the green generated by the first pass of the pump through the crystal and leaving the cavity after reaching M1. The weaker green is due to reflection from M2. M2 should be adjusted until the green beams are superimposed in both axis. The OPO should come on once the green beams are aligned onto each other.

If the OPO does not come on, then a more thorough alignment must be done. This will involve the use of both OPO end mirrors. The method is basically to slightly adjust M1 in one axis in one direction. Next, M2 is scanned horizontally and vertically. M1 is then moved again in the same direction; for each "step" with M1, a scan with M2 is done. The problem with adjusting M1 is that the pump laser becomes misaligned, but for now leave M3 alone. Once the pump laser power has significantly decreased, then bring back M1 but along a different path. This means that once one end of travel is reached, then slightly adjust the second axis. Next, go back to the first axis but make adjustments in the opposite direction in order to bring the mirror back. The OPO should come on after this systematic scan.

If the OPO still doesn't come on, then recheck all the cavity distances as well as the angle on the beamsplitter. Another way to find the OPO is to shorten the cavity. This can be done by moving M2 closer to the beamsplitter. This will increase the size of the signal beam defined by the cavity, and while it may help the OPO to turn on, it may not give the best performance.

Once the OPO is running, then the performance must be optimized. The main issue is overlap of the pump and signal within the PPLN. The relative location of the waists can be optimized by moving M2. With the OPO running, M2 can be used to adjust the length of the cavity. By varying the cavity length and realigning the OPO each

time, there should be a location of M2 which gives the best power. The PPLN can also be translated along the axis. Once these adjustments for power have been made, the angle between the pump and signal beams must be optimized. This is done in the same step-like method of aligning the OPO mentioned earlier but now the pump laser will be scanned as well. This is done by using M3. Slight adjustments are done with M3, followed by scans with the OPO end mirrors.

After all of these adjustments, the OPO should be running reasonably well. Once running, it is best to leave the PPLN oven continuously on. When the oven is on and at temperature, the PPLN adheres to the oven. If the oven is turned off each day and then turned on the next, it may cause the position of the PPLN to shift, disrupting the alignment. Leaving the oven on also helps the coatings by minimizing the stresses on the crystal. If the oven is cycled on and off, this causes the crystal to expand and contract which stresses the coatings on the faces. Keeping the crystal at a constant temperature minimizes the stresses on the coatings. Also, when heating/cooling the crystal, it is recommended to change the temperature by a rate of no more than  $\pm 5\text{ }^{\circ}\text{C/min}$ , again to minimize stressing of the coatings.

## **Appendix B**

### **Transmission Curves of Dual High Reflecting OPO Mirror**

This section contains the transmission curves of the double high reflecting (HR) OPO end mirrors used. These traces were taken with a Lambda9 Spectrophotometer. Figure B1 is the overall transmission plot and is an expanded plot of the high reflectivity region.

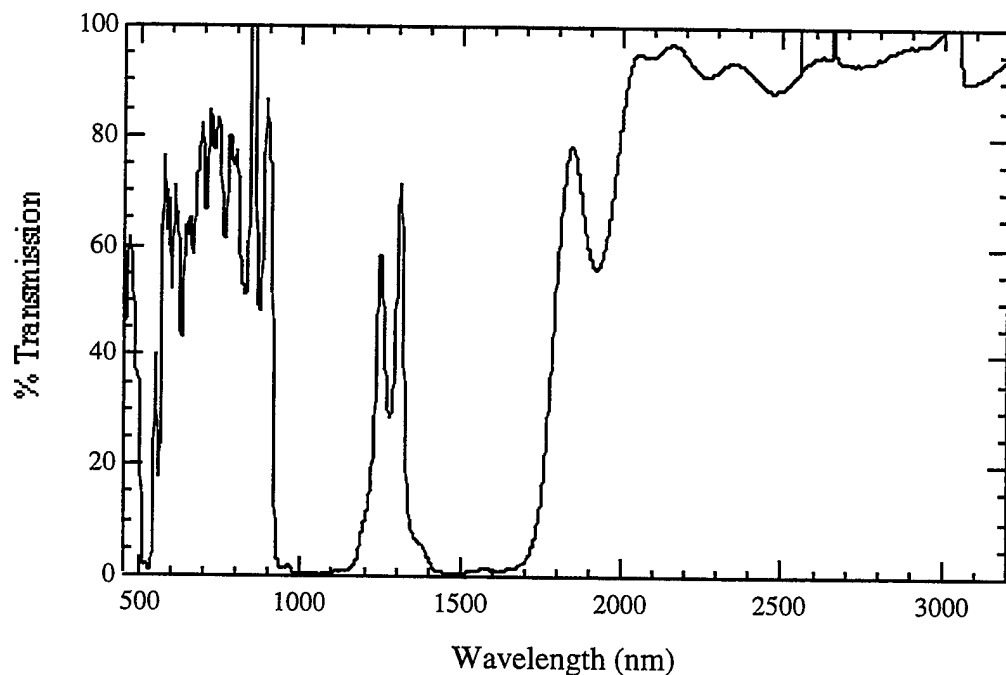


**Figure B1. Broadband Transmission Spectra of Double HR OPO End Mirrors.** This plot was produced by measuring the transmission of a plano/plano double HR coated optic using the Lambda9 Spectrophotometer. The plot shows the regions of high reflectivity around 1.06  $\mu\text{m}$  and 1.57  $\mu\text{m}$ . The plot ends at 3.2  $\mu\text{m}$  due to the operating limit of the Lambda9 Spectrophotometer

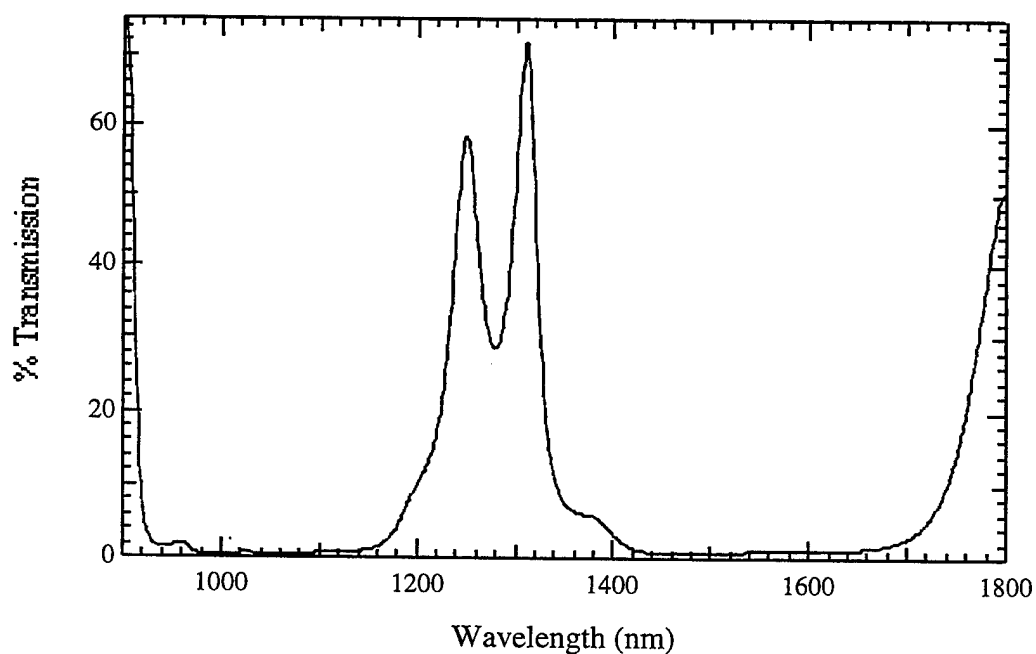
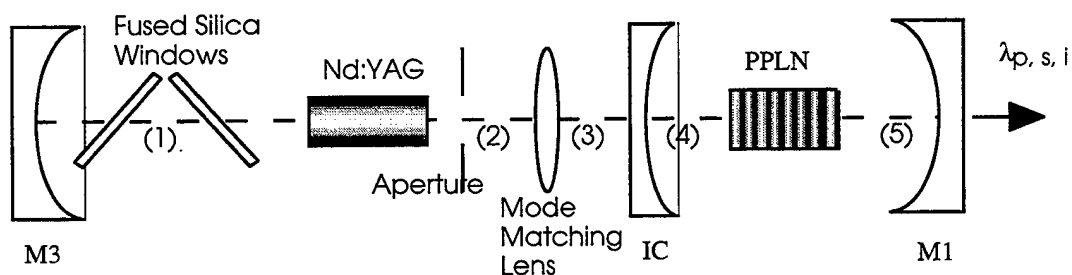


**Figure B1. Expanded Plot of HR Region.** This plot shows the HR regions in greater detail.

## Appendix C

### Intracavity OPO Layouts

#### Cavity I: Linear Intracavity OPO (Nd:YAG)

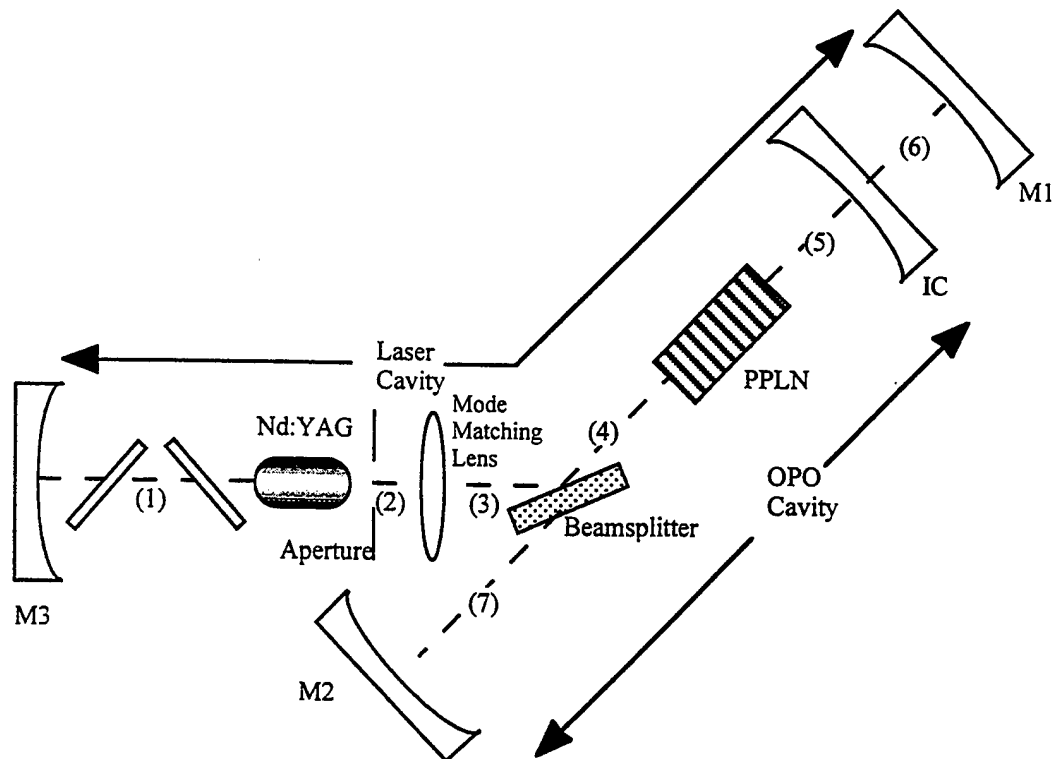


Position	Distance (mm)	Description
(1)	150.0	M3 to Nd:YAG
(2)	330.0	Nd:YAG to lens
(3)	40.0	lens to IC
(4)	30.0	IC to PPLN
(5)	94.0	PPLN to M1

#### Component Description

- M3 is 600 mm ROC, HR coated for 1.06  $\mu\text{m}$
- Nd:YAG rod length is 80 mm
- lens is plano/convex (25.8 mm ROC), BK7 substrate AR coated at 1.06  $\mu\text{m}$ ,  $t_c$  is 5.1 mm
- IC is plano/concave (37.5 mm ROC),  $\text{CaF}_2$  substrate, HT @ 1.06 & 3.3  $\mu\text{m}$ , curved surface is HR at 1.5  $\mu\text{m}$
- PPLN length is 25 mm
- M1 is 100 mm ROC HR @ pump & signal, HT @ idler

## Cavity II: Intracavity (Nd:YAG) with beamsplitter and IC

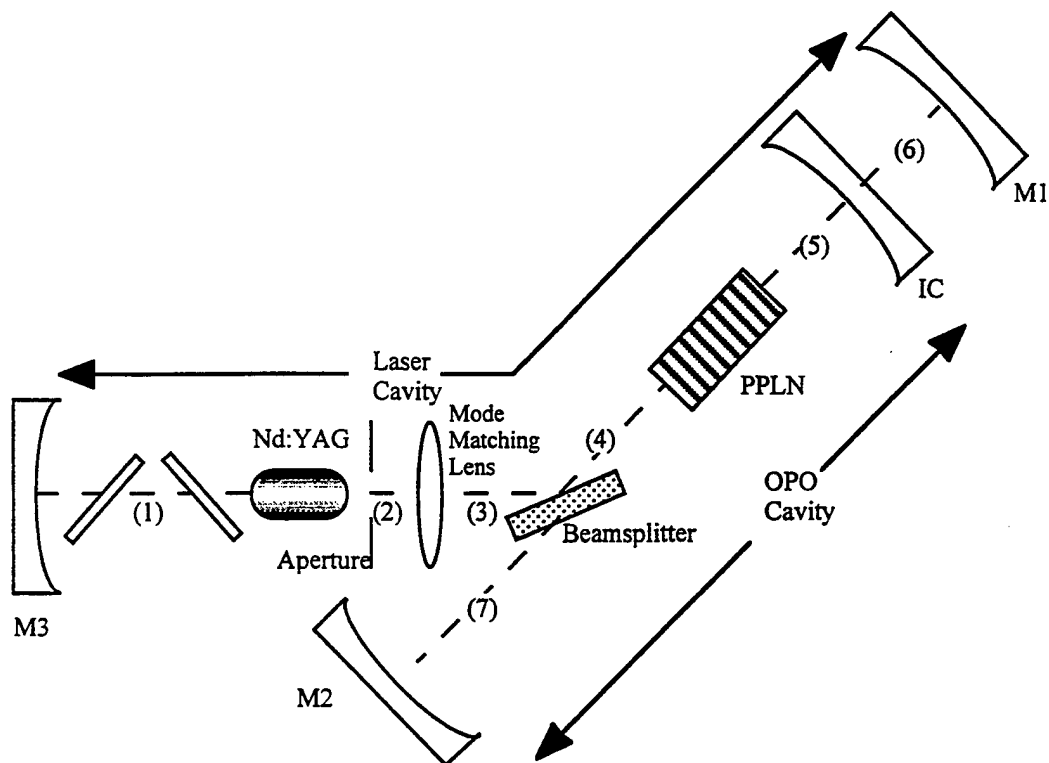


Position	Distance (mm)	Description
(1)	375.0	M3 to Nd:YAG
(2)	215.0	Nd:YAG to lens
(3)	47.0	lens to beamsplitter
(4)	30.0	beamsplitter to PPLN
(5)	31.0	PPLN to IC
(6)	71.0	IC to M1
(7)	72.0	M2 to beamsplitter

### Component Description

- M3 is 600 mm ROC, HR coated for 1.06  $\mu\text{m}$
- Nd:YAG rod length is 80 mm
- lens is plano/convex (25.8 mm ROC), BK7 substrate AR coated at 1.06  $\mu\text{m}$ ,  $t_c$  is 5.1 mm
- IC is plano/concave (37.5 mm ROC),  $\text{CaF}_2$  substrate, HT @ 1.06 & 3.3  $\mu\text{m}$ , curved surface is HR at 1.5  $\mu\text{m}$
- PPLN length is 25 mm
- M1 is 100 mm ROC HR @ pump & signal, HT @ idler
- M2 is 100 mm ROC HR @ pump & signal, HT @ idler
- beamsplitter is HR for  $p$ -polarized pump and HT @  $p$ -polarized signal and idler

**Cavity III: Intracavity (Nd:YAG) with beamsplitter and IC  
(modified Cavity II)**

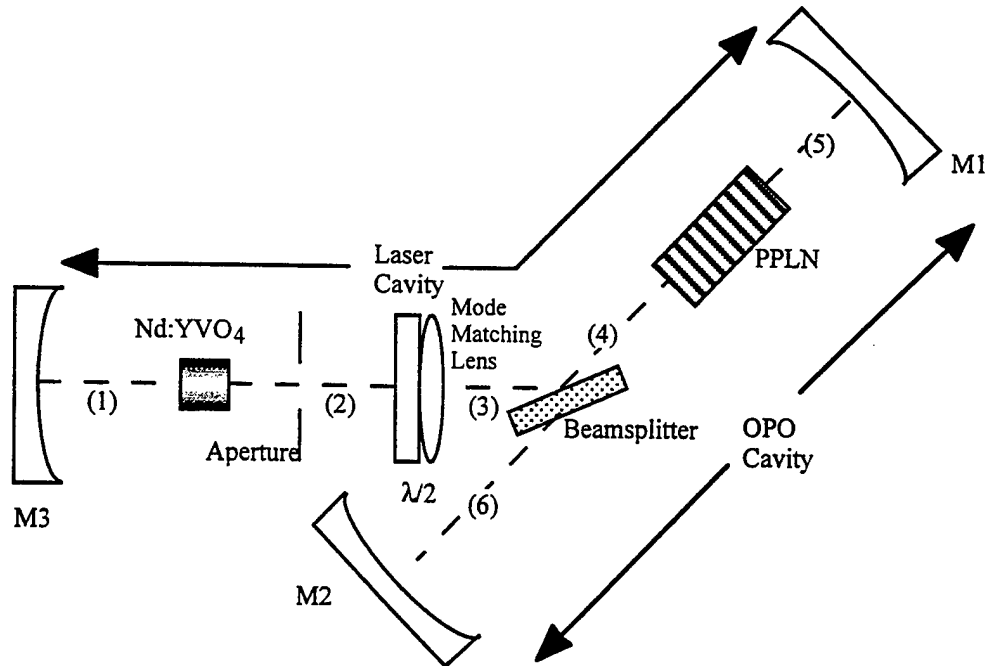


Position	Distance (mm)	Description
(1)	365.0	M3 to Nd:YAG
(2)	450.0	Nd:YAG to lens
(3)	19.5	lens to beamsplitter
(4)	30.0	beamsplitter to PPLN
(5)	31.0	PPLN to IC
(6)	71.3	IC to M1
(7)	72.0	M2 to beamsplitter

**Component Description**

- M3 is 600 mm ROC, HR coated for 1.06  $\mu\text{m}$
- Nd:YAG rod length is 80 mm
- lens is plano/convex (25.8 mm ROC), BK7 substrate AR coated at 1.06  $\mu\text{m}$ ,  $t_c$  is 5.1 mm
- IC is plano/concave (37.5 mm ROC),  $\text{CaF}_2$  substrate, HT @ 1.06 & 3.3  $\mu\text{m}$ , curved surface is HR at 1.5  $\mu\text{m}$
- PPLN length is 25 mm
- M1 is 100 mm ROC HR @ pump & signal, HT @ idler
- M2 is 100 mm ROC HR @ pump & signal, HT @ idler
- beamsplitter is HR for  $p$ -polarized pump and HT @  $p$ -polarized signal and idler

#### Cavity IV: Intracavity (Nd:YVO<sub>4</sub>) with beamsplitter

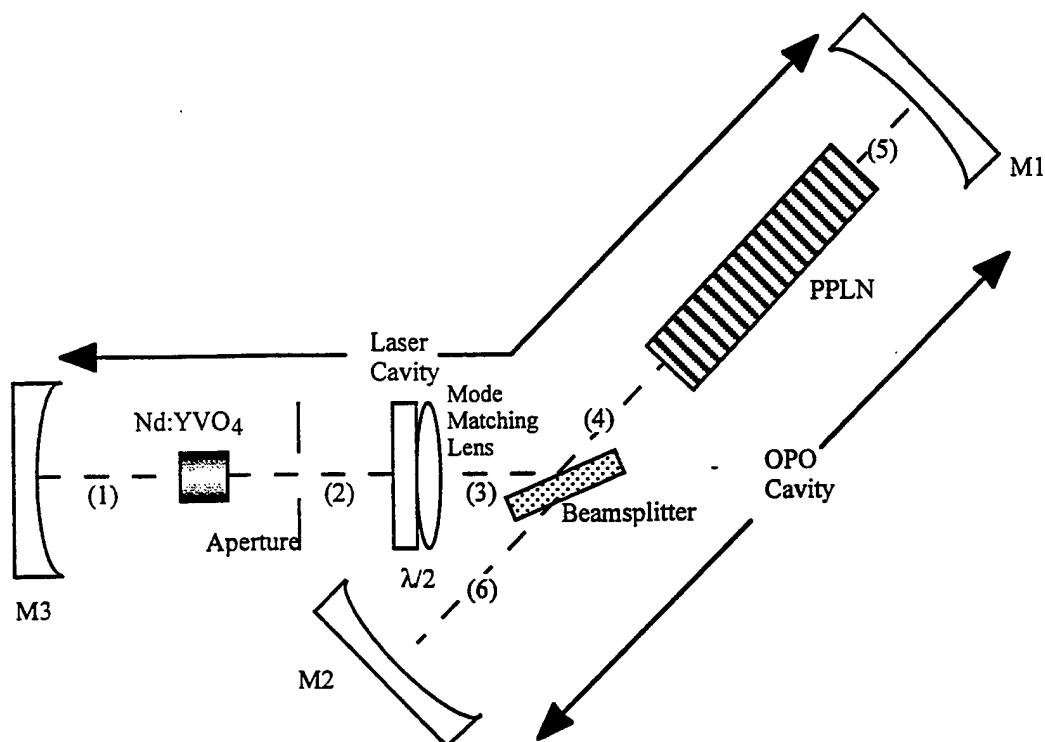


Position	Distance (mm)	Description
(1)	70.0	M3 to Nd:YVO <sub>4</sub>
(2)	150.0	Nd:YVO <sub>4</sub> to lens
(3)	40.0	lens to beamsplitter
(4)	29.75	beamsplitter to PPLN
(5)	23.75	PPLN to M1
(6)	62.0	M2 to beamsplitter

#### Component Description

- M3 is 150 mm ROC, HR coated for 1.06  $\mu\text{m}$
- Nd:YVO<sub>4</sub> cube length is 4 mm
- lens is plano/convex (25.8 mm ROC), BK7 substrate AR coated at 1.06  $\mu\text{m}$ ,  $t_c$  is 5.1 mm
- PPLN length is 25.5 mm
- M1 is 50 mm ROC HR @ pump & signal, HT @ idler
- M2 is 100 mm ROC HR @ pump & signal, HT @ idler
- beamsplitter is HR for  $p$ -polarized pump and HT @  $p$ -polarized signal and idler

### Cavity V: Intracavity (Nd:YVO<sub>4</sub>) with beamsplitter & 50 mm PPLN



Position	Distance (mm)	Description
(1)	100.0	M3 to Nd:YVO <sub>4</sub>
(2)	150.0	Nd:YVO <sub>4</sub> to lens
(3)	40.0	lens to beamsplitter
(4)	33.0	beamsplitter to PPLN
(5)	8.0	PPLN to M1
(6)	41.0	M2 to beamsplitter

#### Component Description

- M3 is 150 mm ROC, HR coated for 1.06  $\mu\text{m}$
- Nd:YVO<sub>4</sub> cube length is 4 mm
- lens is plano/convex (25.8 mm ROC), BK7 substrate AR coated at 1.06  $\mu\text{m}$ ,  $t_c$  is 5.1 mm
- PPLN length is 51.75 mm
- M1 is 50 mm ROC HR @ pump & signal, HT @ idler
- M2 is 100 mm ROC HR @ pump & signal, HT @ idler
- beamsplitter is HR for *p*-polarized pump and HT @ *p*-polarized signal and idler

## REFERENCES

1. J. A. Giordmaine and R. C. Miller, "Tunable Coherent Parametric Oscillation in  $\text{LiNbO}_3$  at Optical Frequencies," *Phy. Rev. Lett.* **14**, 973 (1965)
2. S. T. Yang, R. C. Eckardt and R. L. Byer, "Continuous-wave singly resonant optical parametric oscillator pumped by a single-frequency resonantly doubled Nd:YAG laser," *Opt. Lett.* **18**, 971 (1993)
3. W. Bosenberg, A. Drobshoff, J. I. Alexander, L. E. Myers and R. L. Byer, "93% pump depletion, 3.5-W continuous-wave, singly resonant optical parametric oscillator," *Opt. Lett.* **21**, 1336 (1996).
4. M. K. Oshman and S. E. Harris "Theory of Optical Parametric Oscillation Internal to the Laser Cavity," *IEEE J. of Quantum Elec.* **QE-4**, 491 (1968).
5. E. O. Ammann, J. M. Yarborough, M. K. Oshman and P. C. Montgomery "Efficient Internal Optical Parametric Oscillation," *Appl. Phys. Lett.* **16**, 309 (1970).
6. R. W. Boyd, Nonlinear Optics, Academic Press, New York (1992).
7. A. Yariv, Quantum Electronics, 3rd edition, Wiley & Sons, New York (1989).
8. L. E. Myers, R. C. Eckardt, M. M. Fejer, R. L. Byer and W. R. Bosenberg, "Multigrating quasi-phase-matched optical parametric oscillator in Periodically Poled  $\text{LiNbO}_3$ ," *Op. Lett.* **21**, 591 (1996)
9. L. E. Myers, "Quasi-Phasematched Optical Parametric Oscillators in Bulk Periodically Poled Lithium Niobate," PhD. Dissertation, Stanford Univ., Dec 1995
10. G. D. Boyd and D. A. Kleinman, "Parametric Interaction of Focused Gaussian Light Beams," *Journal of Applied Physics*, **39**, 3597 (1968)
11. J. E. Bjorkholm, "Improvement of Optical Parametric Oscillators by Nonresonant Pump reflection," *IEEE J. of Quantum Elec.* **QE-6**, 797 (1970).
12. A. Yariv, W. H. Louisell, "Theory of the Optical Parametric Oscillator," *IEEE J. of Quantum Elec.* **QE-2**, 418 (1966)

13. F. G. Colville, M. H. Dunn and M Ebrahimzadeh, "Continuous-wave singly resonant intracavity parametric oscillator," *Opt. Lett.* **22**, 75 (1997)
14. A. E. Siegman, "Nonlinear Optical Effects: An Optical Power Limiter," *Appl. Opt.* **1**, 739 (1962)
15. M. Lawrence and G. J. Edwards, "A temperature-dependent dispersion equation for congruently grown lithium niobate," *Optical and Quantum Electronics* **16**, 373 (1984).
16. Y. S. Kim, R. T. Smith, "Thermal Expansion of Lithium Tantalate and Lithium Niobate Single Crystals," *Journal of Applied Physics*, **40**, 4637 (1969).
17. A. E. Siegman, "New Developments in laser resonators," *Laser Resonators*, D. A. Holmes Ed., *Proc. Spie*, vol. 1224.
18. B. E. A. Saleh and M. C. Teich, Fundamentals of Photonics, Wiley & Sons, New York (1991).
19. L. E. Myers R. C. Eckardt, M. M. Fejer, R. L. Byer W. R. Bosenberg and J. W. Price, "Quasi-phase matched optical parametric oscillators in bulk periodically poled LiNbO<sub>3</sub>," *J. Opt. Soc. Am. B* **12**, 2102 (1995).
20. W. R. Bosenberg, A. Drobshoff, J. I. Alexander, L. E. Myers and R. C. Eckardt, "Continuous-wave singly resonant optical parametric oscillator based on periodically poled LiNbO<sub>3</sub>," *Opt. Lett.*, **21**, 713 (1996)
21. D. Chen, "Single-frequency low-threshold cw 3- $\mu$ m PPLN OPO," paper CMD6, Conference on Lasers and Electro-Optics, 1997, Baltimore, MD.
22. W. Koechner, Solid State Laser Engineering, 4th edition, Springer-Verlag, NY (1996).
23. H. J. Eichler, A. Haase, R. Menzel and A. Siemoneit, "Thermal lensing and depolarization in a highly pumped Nd:YAG laser amplifier," *J. Phys. D: Appl. Phys.* **26**, 1884 (1993).
24. Technical Brief, Nd: Yttrium Vanadate, Litton Airtron SYNOPTICS div, 4/93
25. L. DeShazer, "Vanadate crystals exploit diode-pump technology," *Laser Focus World*, Feb 1994
26. M. Vaidyanathan, L. E. Myers and T. P. Grayson, "Dual optical parametric oscillations in 1  $\mu$ m pumped periodically poled lithium niobate", paper CThY5, Conference on Lasers and Electro-Optics, 1997, Baltimore, MD.

27. M. Vaidyanathan, R. C. Eckardt, V. Dominic, L. E. Myers, and T. P. Grayson, "Cascaded optical parametric oscillations," *Optics Express* **1** (2), 49-53 (1997).
28. G. D. Miller, R. G. Batchko, W. M. Tulloch, D. R. Weise, M. M. Fejer and R. L. Byer, "42% efficient single-pass second harmonic generation of CW Nd:YAG laser output in a 5.3 cm length PPLN," paper CTuB2, Conference on Lasers and Electro-Optics, 1997, Baltimore, MD.
29. S. Guha, F. J. Wu, and J. Falk, "The effects of focusing on parametric oscillation," *IEEE J. of Quantum Elec.* **QE-18** (5), 907-912 (1982).
30. R. Fisher, C. Tran-ba, and L. W. Wiczorek, "Optimum focusing in a singly resonant parametric oscillator," *Sov. J. Quantum Electron.* **7** (12), 1455-1458 (1978).